POLYMER LIGHT EMITTING DIODES AND ORGANIC SOLAR CELLS TOWARDS ITO FREE DEVICES AND HIGH EFFICIENCY DEVICES USING ELECTROCHEMICALLY SYNTHESIZED POLYMERS

A THESIS SUBMITTED TO
THE GRADUATE SCHOOL OF NATURAL AND APPLIED SCIENCES
OF
MIDDLE EAST TECHNICAL UNIVERSITY

BY

GÖNÜL HIZALAN ÖZSOY

IN PARTIAL FULFILLMENT OF THE REQUIREMENTS
FOR
THE DEGREE OF DOCTOR OF PHILOSOPHY
IN
CHEMISTRY

SEPTEMBER 2017

Approval of the thesis:

POLYMER LIGHT EMITTING DIODES AND ORGANIC SOLAR CELLS TOWARDS ITO FREE DEVICES AND HIGH EFFICIENCY DEVICES USING ELECTROCHEMICALLY SYNTHESIZED POLYMERS

submitted by **GÖNÜL HIZALAN ÖZSOY** in partial fulfillment of the requirements for the degree of **Doctor of Philosophy in Chemistry Department, Middle East Technical University** by,

Prof. Dr. Gülbin Dural Ünver
Dean, Graduate School of **Natural and Applied Sciences**

Prof. Dr. Cihangir Tanyeli
Head of Department, **Chemistry**

Prof. Dr. Levent Toppare
Supervisor, **Chemistry Dept., METU**

Examining Committee Members:

Prof. Dr. Ali Çırpan
Chemistry Dept., METU

Prof. Dr. Levent Toppare
Chemistry Dept., METU

Assoc. Prof. Dr. Yasemin Udum
Advanced Technologies, Gazi University

Assoc. Prof. Dr. İrem Erel Göktepe
Chemistry Dept., METU

Prof. Dr. Ertuğrul Şahmetlioğlu
Chemistry and Chemical Processing Technologies Dept.,
Erciyes University

Date: 08.09.2017

I hereby declare that all information in this document has been obtained and presented in accordance with academic rules and ethical conduct. I also declare that, as required by these rules and conduct, I have fully cited and referenced all material and results that are not original to this work.

Name, Last name: GÖNÜL HIZALAN ÖZSOY

Signature :

ABSTRACT

POLYMER LIGHT EMITTING DIODES AND ORGANIC SOLAR CELLS TOWARDS ITO FREE DEVICES AND HIGH EFFICIENCY DEVICES USING ELECTROCHEMICALLY SYNTHESIZED POLYMERS

Hızalan Özsoy, Gönül
PhD, Department of Chemistry
Supervisor: Prof. Dr. Levent Toppare,

September 2017, 145 pages

In this study, polymer based solar cells and polymer based light emitting diodes were constructed. In the third and fourth chapters of this study, effect of terminal units and effect of molecular weight on electroluminescence and photovoltaic properties were investigated. Triphenyl end capped polymer P1 based PLED shows luminance value of 10411cd/m^2 at 8.5V whereas benzene end capped polymer P2 based PLED has the peak luminance value of 14583cd/m^2 at 8V. P2 based photovoltaic devices exhibited superior performance. The best performance device based on P2 achieved a power conversion efficiency (PCE) of 4.11 % with a current density (J_{sc}) of 6.59 mA/cm^2, an open-circuit voltage (V_{oc}) of 0.99 V, and a fill factor (FF) of 0.63.

In the fifth chapter, electrochemically synthesized polymers were used in polymer solar cell applications for the first time in literature. P3HT, P3EHT, P3OT, P3DecT and P3DHT were synthesized via electrochemical means. P3EHT based solar cells showed the highest performance. PCE of 2.03% was obtained with a J_{sc} value of 5.10mA/cm^2, V_{oc} value of 0.83V, FF value of 0.48 Ternary solar cells comprising

P3EHT, PTB7 and PC$_{71}$BM was fabricated. PCE value of 6.50 % were achieved with a V$_{OC}$ of 0.72V, J$_{SC}$ of 14.60 mA/cm^2 and a FF of 0.62.

In the last part of this study, ITO free polymer solar cell and PLED characterizations were carried out. Instead of ITO, Ag nanowires were used as the anode materials in polymer solar cell and polymer light emitting diode applications. 1.13% PCE value was achieved with a V$_{OC}$ of 0.53V, J$_{SC}$ of 4.99mA/cm^2 and FF of 0.43 with the device structure of glass/Ag nanowire /P3HT:PC$_{71}$BM/ LiF /Al. 2625cd/m^2 luminance value was obtained with P2 incorporated electroluminescent device with a lower turn on voltage than the one for the ITO based device.

Keywords: Conjugated polymers, polymer solar cells, polymer light emitting diodes, electropolymerization

ÖZ

POLİMER IŞIK YAYAN DİYOTLAR, ELEKTROKİMYASAL YÖNTEMLERLE ÜRETİLEN POLİMERLER KULLANILARAK ÜRETİLEN YÜKSEK VERİMLİ CİHAZLAR VE ITO İÇERMEYEN CİHAZLAR

Hızalan Özsoy, Gönül
Doktora, Kimya Bölümü
Supervisor: Prof. Dr. Levent Toppare

Eylül 2017, 145 sayfa

Bu çalışmada polimer tabanlı güneş pilleri ve polimer tabanlı ışık yayan diyotlar üretilmiştir. Bu çalışmanın üçünü bölümünde terminal unitenin ve polimer molekül ağırlığının elektoluminesans özelliklerine etkisi incelenmiştir. Dördüncü bölüm bu parametrelerin fotovoltaik özelliklere olan etkisini kapsamaktadır. Trifenilamin ünitesi ile sonlandırılmış polimer (P1) 8.5 voltta 10411cd/m^2 luminans değeri göstermiştir. Benzen ünitesi olan sonlandırılmış polimer (P2) 8 voltta 14583cd/m^2 luminans değeri göstermiştir. P2 kullanılarak üretilen güneş gözelerinde % 4.11 güç çevirim verimine ulaşılmıştır. Açık devre voltajı 0.99V, kısa devre akımı 6.59 mA/cm^2, dolum değeri 0.63 bulunmuştur.

Bu çalışmanın beşinci bölümünde elektrokimyasal yöntemelerle üretilen polimerler polimer güneş pili uygulamalarında kullanıldı. Bu özelliğiyle bu çalışma literatürde bir ilktir. P3HT, P3EHT, P3OT, P3DecT ve PDHT elektrokimyasal yöntemlerle sentezlenmiştir. P3EHT kullanılarak üretilen güneş gözeleriyle en yüksek verime ulaşılmıştır. % 2.03 güç çevirim verimine, 5.10mA/cm^2 kısa devre akım değeri, 0.83V açık devre voltaj değeri ve 0.48 dolum faktörü ile ulaşılmıştır. Ayrıca P3EHT, PTB7 ve $PC_{71}BM$ içeren üçlü güneş pilleri üretilmiştir. Bu güneş pilleri ile % 6.50 güç çevirim verimine ulaşılmıştır.

Bu çalışmanın altıncı ünitesi ITO bulundurmayan güneş gözeleri ve ışık yayan diyotlar üretilmesine ayrılmıştır. ITO yerine, gümüş ve bakır nanoteller OLED ve organik güneş pili uygulamalarında kullanılmıştır. Cam/Ag nanotel / P3HT:$PC_{71}BM$/ LiF/Al cihaz mimarisine sahip güneş gözesiyle %1.13 güç çevirim verimine ulaşılmıştır. Açık devre voltajı 0.53V, kısa devre akımı 4.99 mA/cm^2, dolum değeri 0.43 bulunmuştur. P2 kullanılarak üretilen ışık yayan diyotlarla 2625cd/m^2 luminans değeri elde edilmiştir.

Anahtar Kelimeler: Konjuge polimerler, polimer güneş pilleri, polimer ışık yayan diyotlar, elektropolimerizasyon

To Kaan

ACKNOWLEDGMENTS

I would like to express my gratitude to my supervisor Prof. Dr. Levent Toppare for his guidance, support, encouragement and advice. I always feel his trust to me. I became more passionate with his trust. During weekends we worked together for electrochemical polymerizations, it was a great experience.

I would like express my gratefulness to Prof. Dr. Ali Çırpan for valuable discussions and support. In the masters studies I was in the organic synthesis lab and moved to organic solar cell lab with his advice to Prof. Toppare. Afterwards OSC lab became my home. I appreciate his trust.

I gratefully acknowledge the funding from European Union Project (ECOPIX).

I would like to thank to TÜBİTAK National Scholarship Program (2211) for PhD Students.

This work is also partially supported by Scientific and Technological Research Council of Turkey (TÜBİTAK) (Project No: 113Z269 and Project no:115M036) and Ministry of Technology, Science and Industry, (SAN-TEZ Project No: 1294.STZ.2012-1). I would like to thank to Ozan Erlik and Emre Ataoğlu for working for these projects and synthesizing polymers.

I would like to thank to Assoc. Prof. Dr. Yasemin Arslan Udum for valuable discussions and for her help in the electrochemical characterizations.

I would like to thank to Assoc. Prof. Dr. Emrah Ünalan and Ece Alpuğan for their collaboration.

I would like to thank to Asisst. Prof. Dr. Görkem Günbaş for valuable discussions.

I would like to thank to my dear friend Emine Kaya for her support in all stages of PhD.

I would like to thank to Gözde Öktem for friendship and help in GPC analyses.

Here it comes to the family and friends who shape us, who makes life amazing!

I would like to thank to my friends Nurdan Başaran, Özge Karakaş for their friendship

I would like to thank to Ahmet Hakan Koç, Esen Çevik, Zeliha Fırat Cüylan, Gökhan Cüylan, Görkem Şimşek Şenel and Sinan Şenel for their friendship and their support.

I would like to thank all my friends from high school and university years whose names are not mentioned here, but always been in my heart. I love all!

I would like to thank to Mine Özsoy and Cengiz Özsoy for their support and love.

Words fail to express my eternal gratitude to my family Erdinç Hızalan, Nihal Hızalan, Zeynep Hızalan for always believing in me, giving me endless support and unconditional love. I also thank to my brother in law Oğuzhan Arslan.

I would like to thank to Kubilay Kaan Özsoy, for his patience, understanding and love. Words fail to explain my gratefulness. PhD was a long journey full of up and downs, Kaan was the one who made me laugh most. He not only cooked delicious food, but also helped me in OLED characterizations after work.

TABLE OF CONTENTS

CHAPTERS

APPENDICES

LIST OF FIGURES

FIGURES

LIST OF TABLES

TABLES

LIST OF ABBREVIATIONS

ACN	Acetonitrile
AM1.5G	Air Mass 1.5 Global
BHJ	Bulk-heterojunction
CT	Charge Transfer
CP	Conducting polymer
CV	Cyclic Voltammetry
D-A	Donor Acceptor
J-V	Current Density- Voltage
EL	Electroluminescence
E_{el}	Electronic band gap
EQE	External Quantum Efficiency
FF	Fill Factor
GPC	Gel Permeation Chromatography
HOMO	Highest Occupied Molecular Orbital
IPCE	Incident Photon-to-Electron Conversion Efficiency
IQE	Internal Quantum Efficiency
IPA	Isopropylalcohol
LUMO	Lowest Unoccupied Molecular Orbital
MeOH	Methanol

V_{OC}	Open circuit voltage
Eopt	Optical Band Gap
OLED	Organic Light Emitting Diode
OPV	Organic Photovoltaic
OSC	Organic Solar Cell
P3HT	Poly(3-hexylthiophene-2,5-diyl)
PCE	Power conversion efficiency
PEDOT:PSS	Poly(3,4 ethylenedioxythiophene):poly(styrenesulfonate)
PL	Photoluminescence
PF	Polyfluorene
PSC	Polymer Solar Cell
R_s	Series Resistance
SQ	Shockley and Queisser
R_{sh}	Shunt Resistance
Jsc	Short-Circuit Current Density
$TBAPF_6$	Tetrabutylammonium hexafluorophosphate
VB	Valence Band
$PC_{61}BM$	[6,6]-phenyl C61 butyric acid methyl ester
$PC_{71}BM$	[6,6]-phenyl C71 butyric acid methyl ester
o-dcb	1,2-dicholorobenzene
DIO	1,8-diiodooctane

CHAPTER 1

INTRODUCTION

1.1 Photoelectric Effect: Photons in Electrons out

The photoelectric effect was first observed in 1839 by Edmund Becquerel while working on silver coated platinum electrodes which were immersed in electrolyte solution. It was observed that in the presence of light, current running between anode and cathode was higher. The reason behind this fact is when light shines the metal surface, electrons are emitted from the surface of the metal.[1] In 1887, Hertz observed the photoelectric effect while working on a spark gap generator which is the early form of a radio receiver.

Robert Millikan reported that no matter how bright the light is, light with lower frequency than threshold value did not eject electrons from the metal surface. This observation cannot be explained with classical physics which predicts higher intensity of light would eject more electrons from the surface of the metal. Figure 1 explains the results of photoelectric experiment.

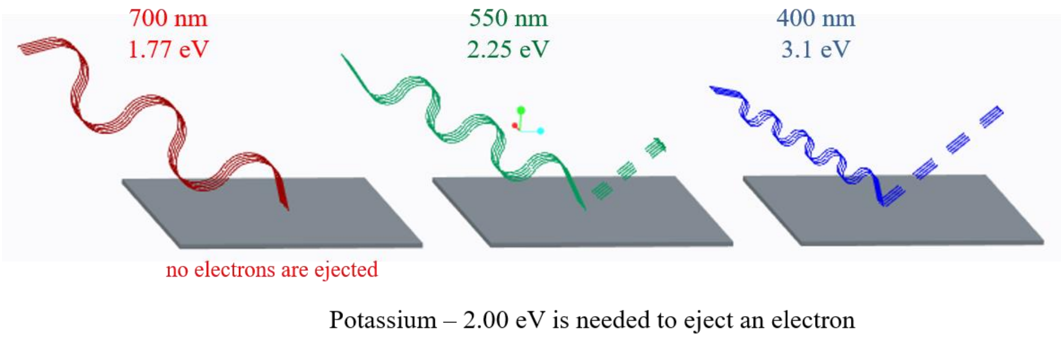

Figure 1 Results of photoelectric experiment

In 1905, Einstein reported that light behaves as tiny particles; quanta or photons. He proposed that the energy of these particles are proportional to the frequency of the electromagnetic radiation. He was awarded with Nobel Prize in 1921 for the detailed explanation of photoelectric effect.

Einstein described the photoelectric effect using a formula that relates the maximum kinetic energy (K_{max}) of the photoelectrons to the frequency of the absorbed photons (ν) and the threshold frequency (ν_0) of the photoemissive surface.

$$K_{max} = h\,(\nu - \nu_0) \tag{1}$$

where $h\nu$ is the energy of the absorbed photon which stands for E, and $h\nu_0$ is the energy needed to eject an electron from the surface of a metal which is the work function of metal (ϕ).

$$K_{max} = E - \phi \tag{2}$$

Energy of the absorbed photon is

$$E = h\,\nu = \mathrm{hc}/\lambda \tag{3}$$

Threshold frequency and wavelength of light depends on the work function of the metal.

$$\phi = h\,\nu_0 = \frac{hc}{\lambda_0} \tag{4}$$

Detailed explanation of photoelectric effect was very important for the development many technologies and also for understanding how nature works. It is the basis for photosynthesis, which is very similar to a very efficient solar cell where sunlight is absorbed by plants to make them grow. Thus this discovery opened new research eras such as photovoltaic devices. First solar cell was constructed in Bell laboratories in 1950. 6% power conversion efficiency was achieved with a silicon (Si) solar cell. [2]

1.1.1 Types of Solar Cells and Current Situation

Solar cells are divided into three generations. First generation solar cells are Crystalline Silicon solar cells. Second generation solar cells are amorphous silicon, CIGS ($CuI(Ga)Se_2$) and CdTe/CdS which are also known as thin film solar cells. Third generation solar cells includes efficiency record holder multijunction solar cells, dye synthesized solar cells, perovskite solar cells and organic solar cells. [3]

Figure 2 demonstrates the chart showing the best research cell efficiencies. It was prepared by National Renewable Energy Laboratory (NREL). These results were all certified by NREL. [4]

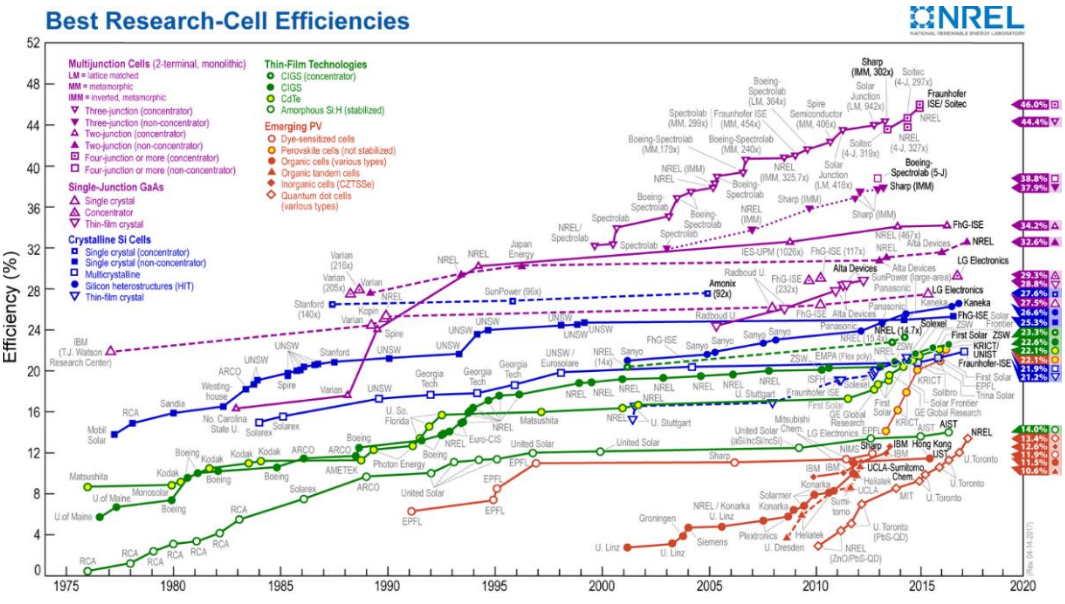

Figure 2 Best research cell efficiencies chart [4]

1.1.2 Organic Solar Cells

After the discovery of conducting polymers [5], new research areas are opened and conducting polymers have been used in many electronic applications like organic photovoltaics and organic light emitting diodes, organic field effect transistors. Especially the interest towards organic photovoltaics are growing and make low cost photovoltaic technology promising. Organic materials have several advantages like low cost, application to flexible substrates and easy manufacture by solution processing such as printing and spin coating. In addition to these, organic materials are good chromophores with absorption coefficients around 10^{-5}cm^{-1} [6]. Most importantly electronic and optical properties of these materials can be tuned via chemical modifications using versatility of organic chemistry.

First organic solar cell was constructed by Tang in 1986. In that study, Indium tin oxide (ITO) was used as the anode material. On top of ITO, copper phtalocyanine was evaporated which acted as the donor material. Perylene derivative which acted as the acceptor material was evaporated on donor material. Silver metal was evaporated as the cathode material. With this device structure which is known as bilayer device architecture, 1% power conversion efficiency was achieved.[7]

Due to short diffusion lengths and short lifetimes of excitons in organic materials bilayer device architecture has some drawbacks. 70 - 100nm thickness is needed for substantial amount of absorption of light. In bilayer devices, only the excitons in 10-20 nm distance to the D-A interface can reach the interface.

To annihilate this drawback bulk heterojunction device architecture was realized in which donor and acceptor moieties are blended to form the active layer. This architecture was first realized by Hiramoto group by the co-evaporation of donor and acceptor molecules.[8] First bulk heterojunction PSCs were constructed by Heeger [9] and Friend [10] groups, independently. Figure 3 demonstrates the bilayer and bulk heterojunction device geometries.

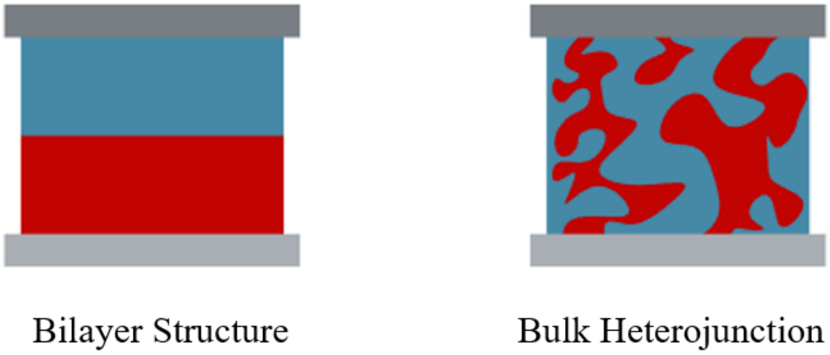

Figure 3 Bilayer vs. bulk heterojunction device geometries

Although device processing innovations, interfacial engineering efforts and synthetic efforts have been made there is still absorption limit of a material and Shockley Quessier limit which is a trade-off between photo- current and photovoltage in single-junction OSCs. With the efficiency of broad spectrum absorbers thermalization losses are reduced. To annihilate these limitations tandem device geometry was realized. It is composed of two sub cells with complementary absorption profiles. It not only improves absorption but also decreases thermalization losses. However fabrication and optimization of sub cells are hard. Therefore, ternary device geometry was realized. Ternary solar cells are composed of D- A moieties and the third component which can be polymer, nanoparticle, small molecule or dye. Structures of binary, tandem and ternary solar cells are depicted in Figure 4.

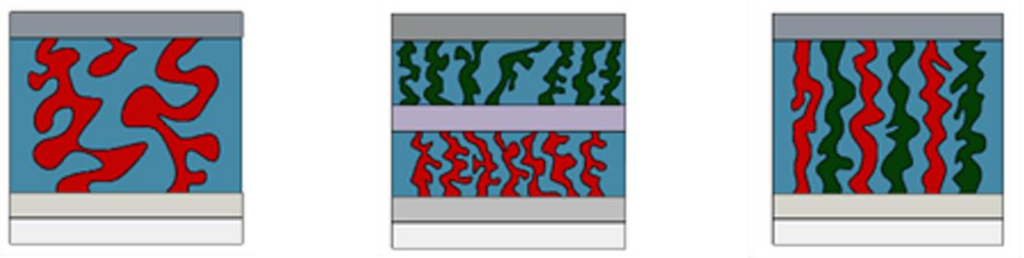

Binary Organic Solar Cell Tandem Organic Solar Cell Ternary Organic Solar Cell

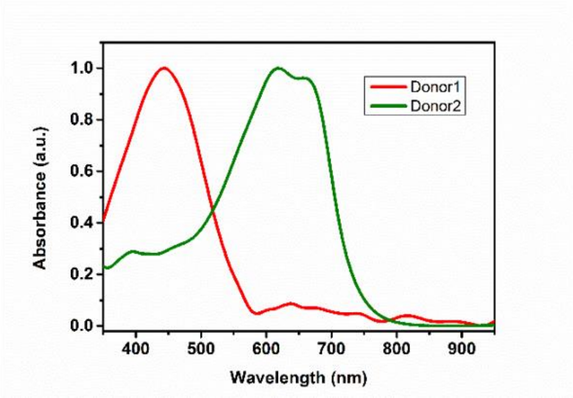

Figure 4 Binary, tandem and ternary solar cells

1.1.3 Operation Principles of Organic Solar Cells

Working principle of an organic solar cell is summarized in four main steps. (1) Upon absorption light, coulombically bound electron and whole pair (exciton) is formed. (2) Exciton diffuses to donor (D) acceptor (A) interface. (3) Exciton dissociates into free charge carriers. (4) Free charge carriers are transported and collected at the respective electrodes.

1.1.4 Absorption of Light

Due to the large band gap of organic molecules only the limited portion of solar light is harvested. A polymer with a band gap of 2 eV, absorbs the sunlight up to 620 nm, which means that 70% of the solar photons are wasted.[11] Fortunately, absorption coefficients of organic molecules are high compared to those of inorganic counterparts, 100 nm thick active layer is enough if reflective back contact is used.[11] Upon sunlight absorption, through photo excitation process, coulombically bound electron and hole pair which is called singlet (Frenkel) exciton is generated. The ratio of the generated excitons to the energy of incident light is called absorption efficiency (η_A). Organic materials have low dielectric permitivity values around 3-4, therefore they exhibit large exciton binding energies (hundreds of meV). Thermal energy (kT) at room temperature (at 298 K) is 0.025eV is not enough for the dissociation of excitons. There is a need for driving force for dissociation of excitons. In organic solar cells polymers and small molecules are used as donor materials which is analogous to p type materials in inorganic solar cells. There is a need for second material which has higher affinity to electrons. Mostly fullerene derivatives are used as the acceptor materials in organic solar cells which are analogous to n type materials in inorganic solar cells. Fullerene derivatives are the most commonly used acceptor materials due to several reasons. They have high electron mobilities up to 1cm^2 V^{-1} s^{-1}. [12] They can be reduced up to 6 electrons thus negative charges are stabilized. Most importantly photoinduced charge transfer to fullerene derivatives takes place ultrafast (ca. 45fs) with a not favorable back transfer rate.[13]

1.1.5 Exciton Diffusion and Dissociation

The electric field built in donor acceptor interface is a driving force the separation of excitons. Therefore excitons must diffuse to the D-A interface within their diffusion length which is 10-20 nm in organic materials. Therefore, exciton diffusion length limits the thickness of the layers in the bilayer device geometry in which donor acceptor are coated on top of each other. Due to this limitation bulk heterojunction device geometry where donor acceptor is mixed have been realized. In this geometry diffusion length of excitons limits the donor acceptor phase separation length. Excitons decay radiatively or nonradiatively before reaching the interface. The ratio of the number of excitons that reach the D–A interface to the total number of excitons formed with photoexcitation is defined as the exciton diffusion efficiency (η_{ED}).

After excitons reach to D-A interface, charge transfer process takes place. Electrons which are still coulombically bound to holes are transferred from LUMO of the donor to the LUMO of the acceptor. The energy difference between the LUMO levels of donor and acceptor is the driving force for electron transfer. Empirical studies showed that 0.3 eV energy difference is needed and a higher energy difference is not advantageous.

1.1.6 Charge Collection

As a result of electric field built, excitons dissociate into free charge carriers and collected by the respective electrodes. Efficiency of this process is called charge collection efficiency η_{CC}. Finally, free holes and electrons drift to anode and cathode respectively. For the highly efficient charge extraction, bicontinuous phase separated donor acceptor pathways are crucial. Discontinuous routes lead charge carriers to encounter oppositely charged carriers which is called non geminate recombination. There are three main driving forces that help the holes and electrons to reach respective electrodes. The energy difference between HOMO of the donor and LUMO of the acceptor which determines the V_{OC}, creates internal electric field and aids field induced drift of carriers. Second, using asymmetric electrodes (high work function electrode for collection of holes and low work function electrode for electrons) will contribute to the drift of charge carriers. Third, concentration difference of charges will be the driving force for diffusion of charge carriers. Figure 5 demonstrates the working principle of an organic solar cell.

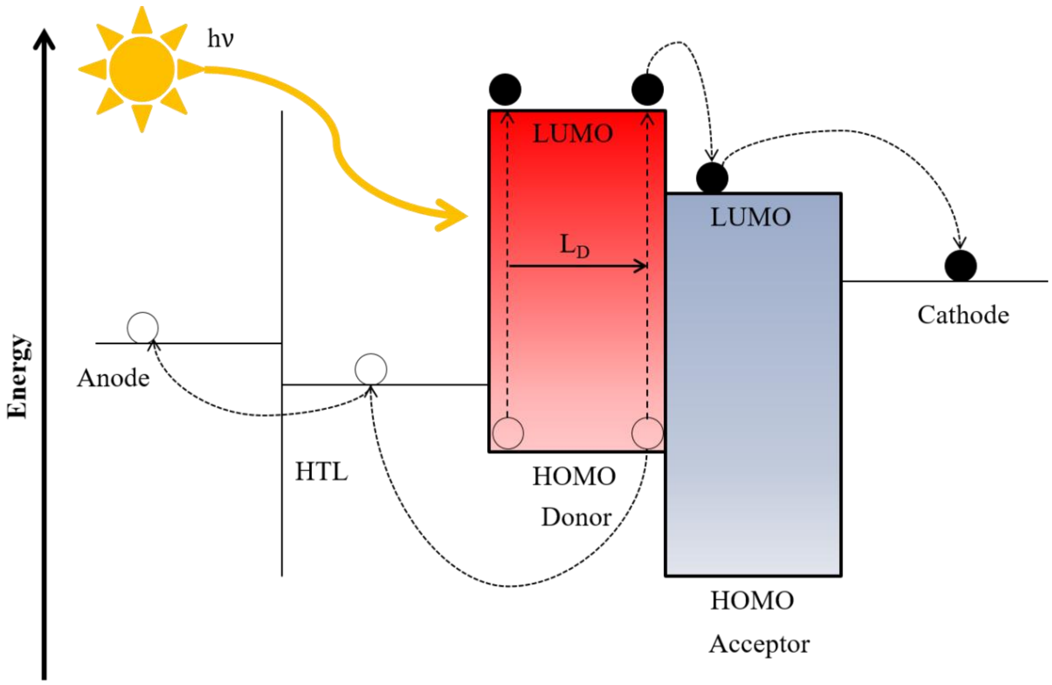

Figure 5 Working principle of an organic solar cell

1.1.7 Characterization of Organic Solar Cells – Important Parameters

Current density (J) vs voltage (V) characteristics of a solar cell is tested under illumination. Illumination is standardized at 100mW/cm^2 with a distribution of incoming light which matches sun's spectral distribution on the earth's surface at an incident angle of 48.2°. By varying the applied voltage to the solar cell, current values are recorded. Typical J-V curve is shown under illumination in Figure 6. Under dark, there is no current passing through the device, solar cell obeys the diode characteristics. Upon applied reverse bias no current passes since charge carrier drift to electrodes is high. As the applied voltage increases (when voltage reaches to turn on voltage) diffusion current over rules the drift current and voltage increase results in exponential current rise.[14]

As opposed to the processes taking place in dark, under illumination excitons are formed and charge carriers are transported to the respective electrodes. Therefore, upon illumination, J-V curve becomes superposition of the dark J-V curve, shifted to fourth quadrant with the solar light induced current.

From the J-V curve under illumination, open circuit voltage (V_{OC}), short circuit current (J_{SC}), fill factor (FF), power conversion efficiency (PCE), shunt resistance (R_{SH}) and series resistance (R_S) values can be extracted. Short circuit current value is the current value when there is no applied external field. It depends on the absorption of light, morphology of the active layer. High absorption coefficients and broad absorption range is advantageous for high J_{SC} values. V_{OC} is the voltage value when there is no net current flowing through the cell. It depends on the energy level difference between the HOMO of the donor moiety and the LUMO of the acceptor moiety and limited by the intermolecular charge transfer state. Solar cells based on donor moieties having deep HOMO energy levels and/or acceptor moieties having high lying LUMO energy levels are usually show high V_{OC}. Fill factor value defines the degree of power produced by the solar cell compared to the power that can be delivered ideally. As depicted from Figure 6 and eqn 5, FF is a degree of rectangularity of the J-V curve. It is the ratio of the product of V_{MP} and J_{MP} to the product of V_{OC} and J_{SC}. For high fill factor devices charge carriers could be flow out under the electric field. Parasitic resistances, shunt and series resistances affect fill factor values significantly.

$$FF = \frac{V_{MP} \times J_{MP}}{V_{OC} \times J_{SC}} \tag{5}$$

Rs is calculated by taking the slope of J-V curve around V_{OC}. It is affected by the bulk resistances of layers, bulk resistance of electrodes and contact resistance of interfaces. It is reported that if the series resistance increases per 0.1%, the FF of an inorganic solar cell declines about 2.5%.[15] In the case of copper phtalocyanine and C_{60} incorporated organic solar cell FF is improved from 52% to 60% when Rs is dropped from 6.2 to $0.1\Omega.cm^2$.[16]

Another important factor that affect the rectangularity of the J-V curve is the shunt resistance. R_{SH} is estimated by taking the slope of J-V curve around J_{SC}. It is affected by the current losses in the solar cell. Current leakage from the pinholes in the film or by the traps are the possible current losses in the cell. Ideal R_{SH} should approach infinity, which means there is no current loss in the device. If R_{SH} is small, current passing through the cell will not be constant while potential is swept as a result J-V curve will deviate from rectangularity hence fill factor value decreases. [3]

Maximum power generated in the cell is the product of V_{OC}, J_{SC} and FF as depicted in Equation 6. Power conversion efficiency is the ratio of the power output of the cell to the power of incoming light.

$$PCE = Pmax / Psolar = V_{OC} \text{ x } J_{SC} \text{ x } FF / Psolar \tag{6}$$

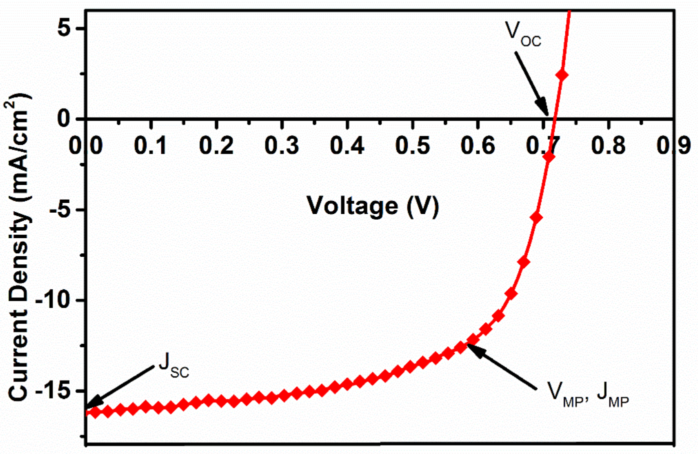

Figure 6 Typical J-V curve for a solar cell under illumination

Another important characterization parameters for solar cells are internal and external quantum efficiencies (IQE and EQE) or incident photon to current / charge carrier efficiency (IPCE) which is a measure of how absorbed photons are efficiently converted to charge carriers and collected at electrodes. Therefore it can be expressed as given by Equation 7. In this method monochromatic light with certain intensity is shined onto the device and response of the device is measured by scanning the whole spectrum.

$$\mathrm{EQE} = \eta_A \times \eta_{ED} \times \eta_{CS} \times \eta_{CC} \text{ for a particular wavelength} \qquad (7)$$

1.1.8 Historical Development and Current Status of Organic Solar Cells

As mentioned before first organic solar cell was constructed by Tang by the evaporation of copper phtalocyanine as the donor material and the perylene derivative as the acceptor material. [7]

First bulk heterojunction polymer solar cell was constructed by Heeger and Wudl in 1995. In this study, MEH-PPV was used as the donor material whereas C_{60} was used as the acceptor material. Via blending donor and acceptor a bicontinuous network of donor-acceptor heterojunctions were formed. [9] MEH-PPV [17] and PCBM [18] were developed by Wudl.

After that MDMO-PPV was developed, it has similar electronic properties with MEH-PPV. However MDMO-PPV has better miscibility with PCBM which is advantageous for better morphology. 3% PCE was achieved with MDMO-PPV comprising solar cells with a V_{OC} value of 0.77V, J_{SC} value of 7.6mA/cm^2, and FF of 0.51. [19]

Reynolds and coworkers reported a novel PPV polymer where cyano (-CN) group is introduced to vinylene moiety. Due to electron withdrawing nature of –CN groups resulting polymer has 0.5eV lower HOMO and LUMO energy levels than MEH-PPV. LUMO energy level of the CN-PPV is -3.8eV which matches the LUMO energy level of PCBM (-4.1eV). However improvement of power conversion efficiencies with PPV derivatives is limited by the narrow absorption of these polymers. Structures of PPV polymers are depicted in Figure 7.

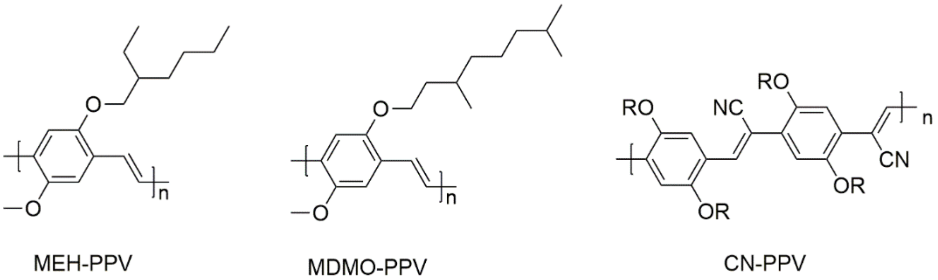

Figure 7 Structures of representative PPV polymers

Poly (3-hexylthiophene) showed better performance due to higher hole mobility and broader absorption compare to PPV polymers. Regioregular P3HT based devices showed the average power conversion efficiency of 3%. [20] Record efficiency of P3HT incorporated solar cells belongs to P3HT: ICBA (indene-C60-bisadduct) solar cells. Without any additive, PCE of 4.12% was obtained with a V_{OC} of 0.87V, J_{SC} of 7.76mA.cm^{-2} and a FF of 0.61. With the addition of 1-chloronaphtalene (CN) additive, 7.4% PCE value was achieved with a V_{OC} value of 0.87V, J_{SC} value of 11.35 mA.cm^{-2} and FF value of 0.75.[21] With non- fullerene acceptors P3HT based solar cells had the record PCE of 6.4% [22]. Structure of P3HT is shown in Figure 8.

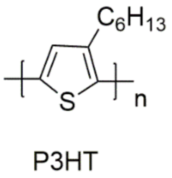

Figure 8 Structure of P3HT

Although with P3HT promising photovoltaic results were obtained, due to its limited absorption range, research interest shifted to polymers having broader absorption. For that matter poly[2,6-(4,4-bis-(2-ethylhexyl)- 4H-cyclopenta[2,1-b;3,4-b']dithiophene)-alt-4,7-(2,1,3-benzothi-adiazole)] (PCPDTBT) was synthesized. It absorbs light up to 890 nm with a maximum at 775nm. Without any optimization, PCPDTBT:PC61BM comprising solar cells showed 2.67 % PCE value. PCE value was improved to 3.16% when $PC_{61}BM$ was replaced with $PC_{71}BM$. [23] Absorption contribution of $PC_{71}BM$ results in 35% EQE and 11mA/cm^2 J_{SC} value. With the addition of 1,8-octanedithiol to the PCPDTBT, $PC_{71}BM$ solution, absorption maxima shifts to 800nm due to improved interaction of polymer chains and enhanced structural order. [24] 5.5 % PCE value was obtained with Jsc of 16.2mA/cm^2, FF of 0.55 and a Voc of 0.62V. 1,8-Octanedithiol addition strongly affects absorption and the morphology of the active layer implying that physical interactions between the polymer chains and /or between the polymer and PCBM are affected. [25]

Park et al introduced TiO_2 layer in between active layer ($PCPDTBT:PC_{71}BM$) and Al electrode as an optical spacer and hole blocking layer. With this device geometry 100% IQE was achieved meaning that all absorbed photons form a separated pair of charge carriers and all carriers reach to the electrodes. A 5.96 % PCE value was achieved and certified by NREL. It was the record efficiency in 2009.[26] Structure of PCPDTBT is depicted in Figure 9.

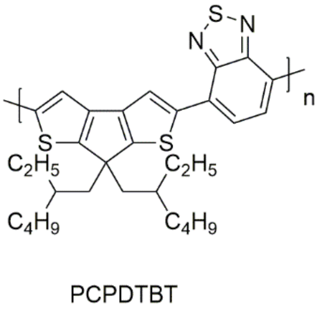

Figure 9 Structure of PCPDTBT

Yu et al synthesized polymers bearing thienothiophene and benzodithiophene moities. This study was yet another milestone in polymer design. PTB1 has absorption maximum at 694nm with an onset value of 784nm which covers the maximum photon flux region of solar light. With PTB1:PC61BM comprising solar cells 4.8% PCE value was obtained whereas PTB1:PC71BM comprising solar cells reach 5.6% PCE with a V_{OC} of 0.58V. [27]

To anhilate the low V_{OC} problem, PTB3, a derivative of PTB1 with less electron-donating alkyl chains and PTB4 with fluorine substitution which acts as an electron withdrawing group were synthesized. With PTB3 and PTB4 based polymer solar cells, 5.85% PCE and 5.90% PCE values were achieved with V_{OC} values of 0.72V and 0.74V, respectively. Chen et al reported 7.73% PCE value with modification of alkyl chain and introduction of fluorine on thienothiophene unit. [28]Different scientists reported (thieno[3,4- c]pyrrole-4,6-dione) – benzodithiophene (TPD – BDT) copolymer, independently.

Leclerc group synthesized TPD- BDT copolymer namely PBDTTPD and reached PCE value of 5.5% with the device area of 1cm^2. [29]

While Frechet group was also working on TPD-BDT copolymers, Leclerc group published above mentioned work. Frechet group synthesized three polymers with the ethylhexyl, dimethyloctyl and octyl side chains on TPD moiety. Polymer with octyl side chain showed better photovoltaic performance. With PSCs based on polymer with octyl side chain, 6.8% PCE value with J_{SC} of 11.5mA/cm^2, V_{OC} of 0.85 V and FF of 0.70. Authors attributed superior performance to reduction of the side-chain bulkiness, which leads to the crystallization of polymer.[30]

Zhang et al also reported PSC based on TPD-BDT units with dodecyl and branched ethylhexyl side chains on BDT units. Polymer with dodecyl side chain showed PCE value of 1.95% and with the addition of 2% DIO PCE was improved to 3.42% through rise in current values. Whereas PSC based on polymer with ethylhexyl side chain had 1.49% PCE value and with the addition of 2% DIO it was improved to 4.79%. Authors attributed performance difference to the fact that different alkyl chains had an influence on solubility of the polymer, packing of chains and morphology of the active layer. [31]

Jen group also synthesized TPD – BDT based copolymer. 4.1% PCE value was achieved with a V_{OC} of 0.84V, J_{SC} of 9.8 mA/cm^2 and FF of 0.50. [32] Structure of TPD-BDT polymer is shown in Figure 10.

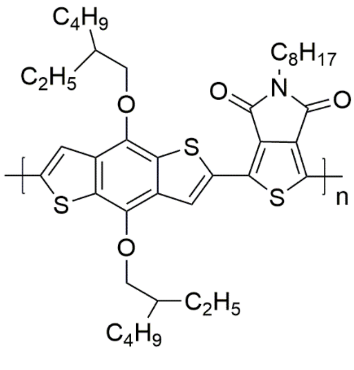

PBDTTPD

Figure 10 Structure of TPD – BDT based polymer

Next world record efficiency was from PSCs based on a PTB (thienothiophene and benzodithiophene comprising polymer) derivative. As mentioned before PTB4 showed promising photovoltaic properties. Liang et al replaced octyl side chain on thienothiophene unit in the structure of PTB4 with a branched ethylhexyl side chain and called this polymer as PTB7. Alkyl chains are very important for the solubility of the polymer in common organic solvents. However, intermolecular packing, crystallinity degree of polymers also influence device performance. Branched alkyl chains improve the solubility of the resulting polymer but preventing the order of chains and charge transport as proven in this literature example. Hole mobility of this polymer was calculated as 5.8 x10 $^{-4}$cm^{2} V^{-1} s^{-1}. PTB7:PC$_{71}$BM incorporated solar cells exhibited an efficiency of 7.4% when processed with DIO and chlorobenzene.[33]

Liu et al synthesized PTB7 derivatives with different molecular weights (Mn=18, 40, 128 kDa). Power conversion efficiencies of the PSCs were found as 5.41%, 6.27% and 8.50% based on PTB7 with molecular weights of 18, 40, 128 kDa, respectively. Authors attributed enhancement of PCE values to the improvement of light absorption and mobility of charge carriers. Polymer with the highest molecular weight has the lowest PDI value which facilitates a more ordered structure.The relation between the morphology of the active layer and the molecular weight proved with the TEM images indicating the enhanced phase separation with the increasing molecular weight.[34]

He et al constructed inverted solar cells with the device structure of ITO/PFN/ PTB7:$PC_{71}BM$/ MoO_3 /Al. With this structure 9.15% PCE value was achieved with V_{OC} value of 0.74V, J_{SC} value of 17.2mA/cm^2 and FF value of 0.72. PTB7 based inverted devices showed better performance mainly through an improvement in JSC values which was attributed to increased absorption of light due to decreased reflectance. [35]

Hou and coworkers further improved the BDT and thienothiophene based polymers via incorporation of thiophene side groups on BDT moiety in order to increase the 2-D orbital delocalization and thus improving charge transport properties. Resulting polymer was called as PTB7-Th where it had a narrower band gap (1.59eV) which is very close to the optimum band gap value (1.1 -1.5ev) [36] hence, quite lower than that of PTB7. Efficiency of devices based on PTB7-Th was 9.0% a with V_{OC} value of 0.78V, J_{SC} value of 16.86 mA/cm^2 and FF value of 0.68.[37] Polymers with narrow band gaps are suffering from low VOC values which depend on the difference between the LUMO energy level of the acceptor and the HOMO energy level of the donor. It was shown that the PCE of PTB7-Th based PSCs were improved to 10.61% with a V_{OC} value of 0.825V by increasing the amount of $PC_{71}BM$ loading. The increase in V_{OC} and PCE was attributed to improved domain purities of $PC_{71}BM$. [38] Structures of PTB derivatives are demonstrated in Figure 11.

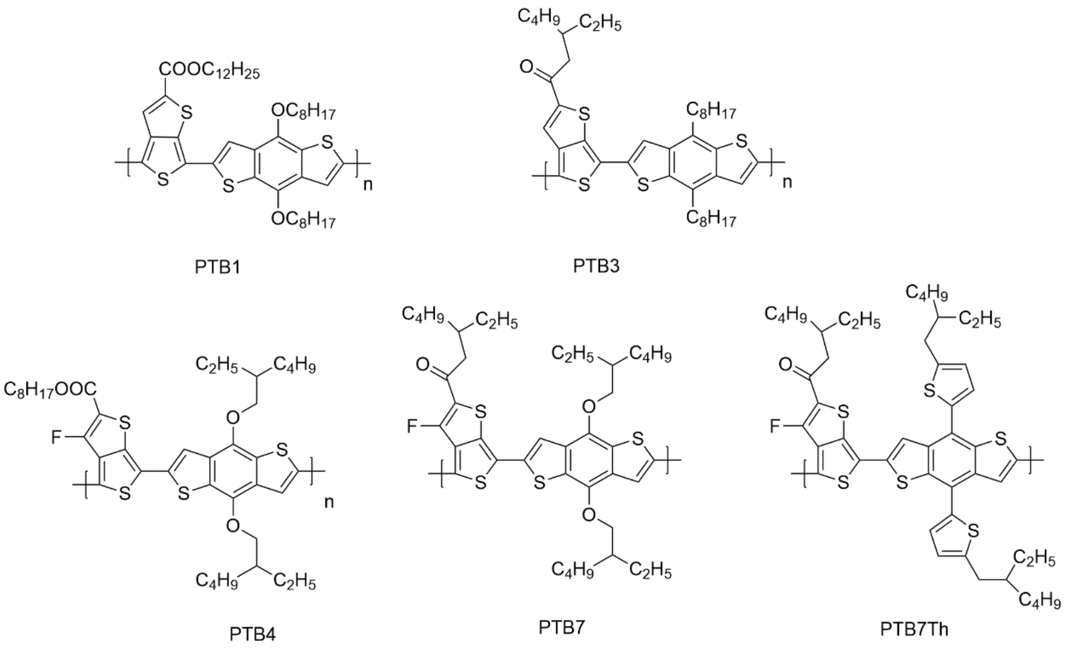

Figure 11 Structures of PTB derivatives

Li and coworkers reported that PTFB-O based polymer solar cells with non-fullerene acceptors. 10.88% PCE value was achieved which was one of the highest PCE value in 2016 for single junction solar cells. [39] Structure of PTFB-O is depicted in Figure 12.

Yan and coworkers achieved record efficiency of 11.7% with single junction organic solar cells. This achievement was certified by NREL and placed in NREL chart of best research cell efficiencies. Poly[(5,6-difluoro-2,1,3-benzothiadiazol-4,7-diyl)-alt -(3,3‴- di(2-nonyltridecyl)-2,2′;5′,2″;5″,2-quaterthiophen-5,- diyl)] (PffBT4T-C9C$_{13}$) PC$_{71}$BM comprising solar cells processed from 1,2,4-trimethylbenzene (TMB), 1-phenylnaphthalene (PN) exhibited PCE value of 11.7%. [40] Structure of PffBT4T-C$_9$H$_{13}$ is shown in Figure 12.

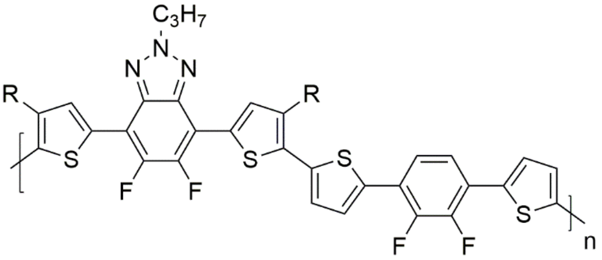

R: 2-decyltetradecyl
PTFB-O

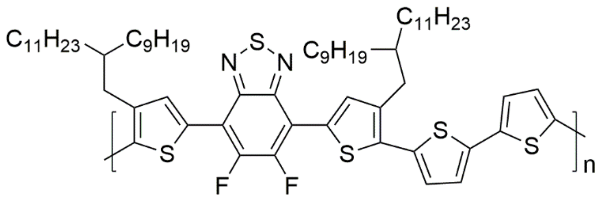

PffBT4T-C_9H_{13}

Figure 12 Structures of PTFB-O and PffBT4T-C_9H_{13}

1.2 Electroluminescence of Organic Materials

1.2.1 Photoluminescence

Photoluminescence, chemiluminescence, triboluminescence, and bioluminescence are several forms of luminescence. Luminescence is the energy release by the emission of light. If the stimuli is a chemical reaction, mechanical action or absorption of a photon luminescence is called chemiluminescence, triboluminescence and photoluminescence, respectively. Fluorescence and phosphorescence are the forms of photoluminescence. Fluorescence is basically emission of light upon absorption of photons. Emitted light usually has lower energy than absorbed photon, therefore emission takes place at longer wavelengths. If emitted light has the same energy and the wavelength with the absorbed photon, this is called resonance fluorescence.

In the case of phosphorescence, emission does not take place immediately after the absorption of photon. Excitation of electrons to a higher state is accompanied with the change of the state of the spin. Once in a different spin state, electrons cannot relax into the ground state readily since the reemission involves quantum mechanically forbidden energy state transitions. Figure 13 explains the fluorescence and phosphorescence phenomena.

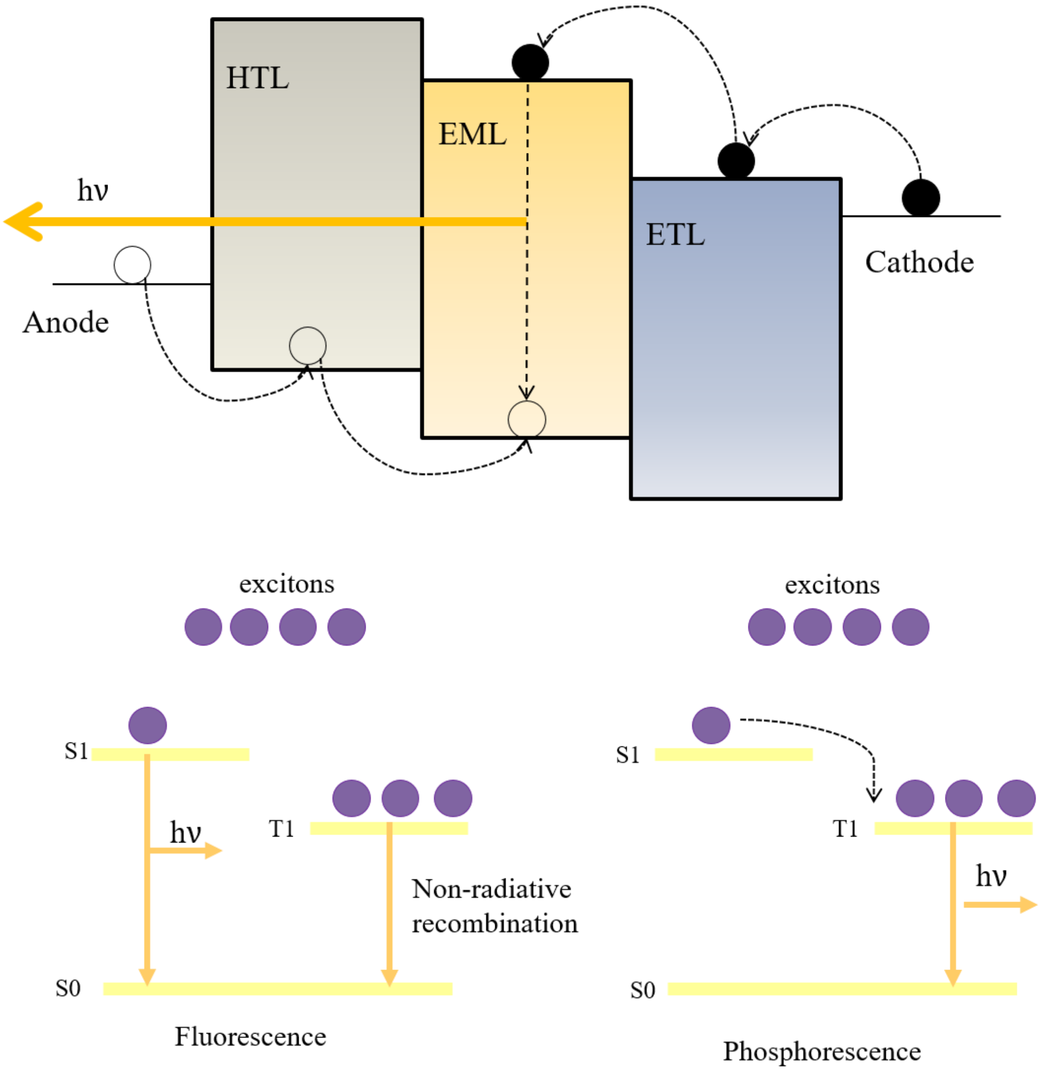

Figure 13 Energy diagram for fluorescence and phosphorescence

1.2.2 Electroluminescence

Electroluminescence is defined as the generation of light upon electrical stimuli. This phenomenon is realized in most of the semiconductor materials including organic semiconductors. It was first reported for anthracene single crystal in 1960.[41] However it is not significantly improved until 1980s. Tang and Van Slyke constructed electroluminescent devices comprising 8-hydroxyquinoline aluminum as the emissive material and diamine derivative as the hole transport material.[42] With the discovery of conducting polymers in 1977[5], advances in this research era took place fast. In 1990, first polymer based electroluminescent device was constructed by R.H. Friend. In this study, poly(p-phenylene-vinylene) was used as the emissive material.[43]

1.2.3 OLED Fabrication

OLED fabrication can be made by thermal evaporation and wet coating techniques.

Small molecule based OLEDs are usually constructed by thermal evaporation technique. With this technique, it is possible to coat multilayers on top of each other with high thickness control. OLED display of the Motorola cell phone was fabricated using Kodak small molecule evaporator. Fraunhofer Institute produces white OLEDs via thermal evaporator for lightning purposes.

However thermal evaporation techniques cannot be used for polymer coating since polymers decompose or cross link upon heating. Therefore polymers are coated by wet coating techniques. Wet techniques are spin coating, doctor blade, inkjet printing, screen printing, hot microprint contact and micro stamping. All these solution based coating techniques require soluble materials and additionally different layers should have mutual insolubility in each other. Doctor blade is useful for coating thick (thicker than 100nm) uniform films over the substrates with the precision tool “blade”. [44]

Polymer comprising light emitting devices have several advantages like efficient light generation and low manufacturing costs. The main interest towards polymer based LEDs lies in the room for lower cost due to no need for expensive vacuum systems. Whereas inorganic materials and small molecules require vacuum deposition systems which does not meet the requirements of low cost and large area coating.

1.2.4 Device Structure

In basic device structure of PLEDs, electroluminescent layer; a small molecule or a polymer, is sandwiched between two electrodes. Cathode material is usually calcium and aluminum. For the emission of light at least one electrode must be transparent. Indium tin oxide serves as an excellent anode material due to high conductivity and transparency. Structure of an PLED is depicted in Figure 14.

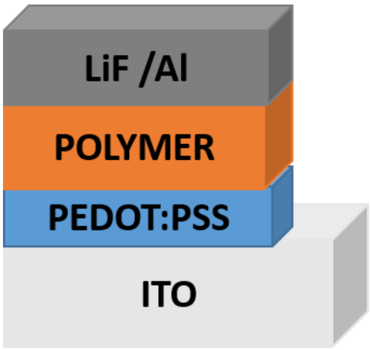

Figure 14 OLED stack

As an alternative to ITO, polyaniline (PANI) [45], silver nanowires [46] and graphene [47] were used as anode materials in literature. Work function of ITO is around 4.5eV and it increases to 5.1eV with the oxygen content. As the work function of the ITO increases charge injection process becomes easier and brightness and efficiency of the OLED increases. Ozone treatment, etching ITO with aquaregia and etching with plasma are utilized for oxygen saturation.

PEDOT:PSS is the most commonly used hole transport layer. HOMO energy level of the hole transport layer lies in between HOMO of the emissive layer and the work function of the anode material. Incorporation of this layer reduces the injection barrier of holes. As an alternative to PEDOT:PSS, platinum (Pt) [48], copper phthalocyanine (CuPc) [49], N,N′-Bis(3-methylphenyl)-N,N′-diphenylbenzidine (TPD) [50,51], N,N′-Di(1-naphthyl)-N,N′-diphenyl-(1,1′-biphenyl)-4,4′-diamine (NPB or NPD) [50,52,53] were also used as the hole transport materials in literature.

Phosphorescent small molecules and/or fluorescent polymers were used in the emissive layer of OLEDs. Since phosphorescent molecules generate light both from singlet and triplet excitons, internal quantum efficiencies can quadrapole the efficiencies of OLEDs based on fluorescent molecules which can only generate light from singlet excitons.[44]

Low to medium work function metals are used as cathode materials. Calcium /aluminum, lithium fluoride / aluminum, cesium fluoride / aluminum and magnesium /silver are commonly utilized cathode materials.

1.2.5 Working Principle of Oleds

Upon applied electrical field across the device, electrons are injected from the cathode to LUMO of the polymer. Holes are injected from the anode into the highest occupied molecular orbital (HOMO) of the polymer. Holes and electrons recombine and decay radiatively to form a light emission. Operation principle of OLEDs is outlined in Figure 15.

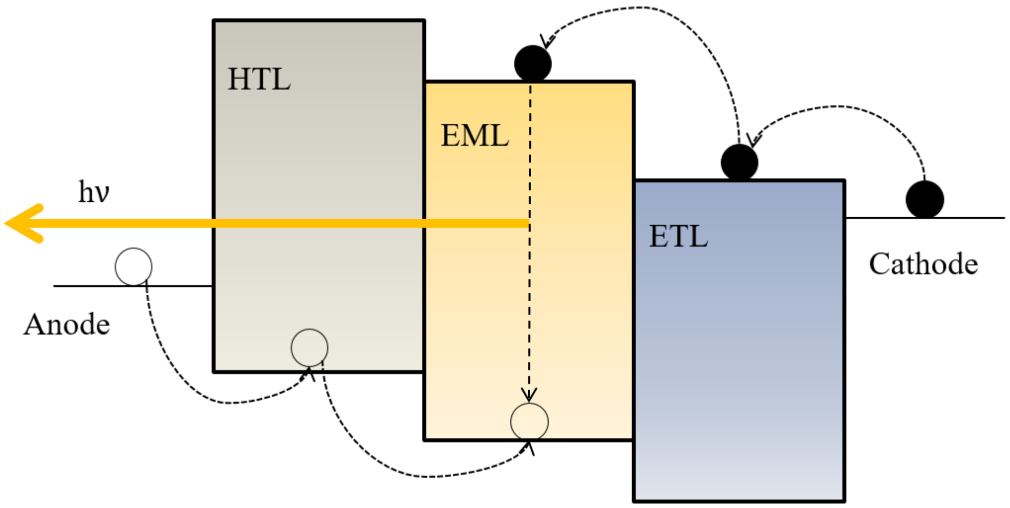

Figure 15 Operation principle of OLEDs

Using versatility of organic chemistry and knowledge of structure property relation of polymers, it is possible to control the electronic and optical properties of polymers. Figure 16 demonstrates the snapshots of the PLEDs that are fabricated in our laboratories with different polymers.

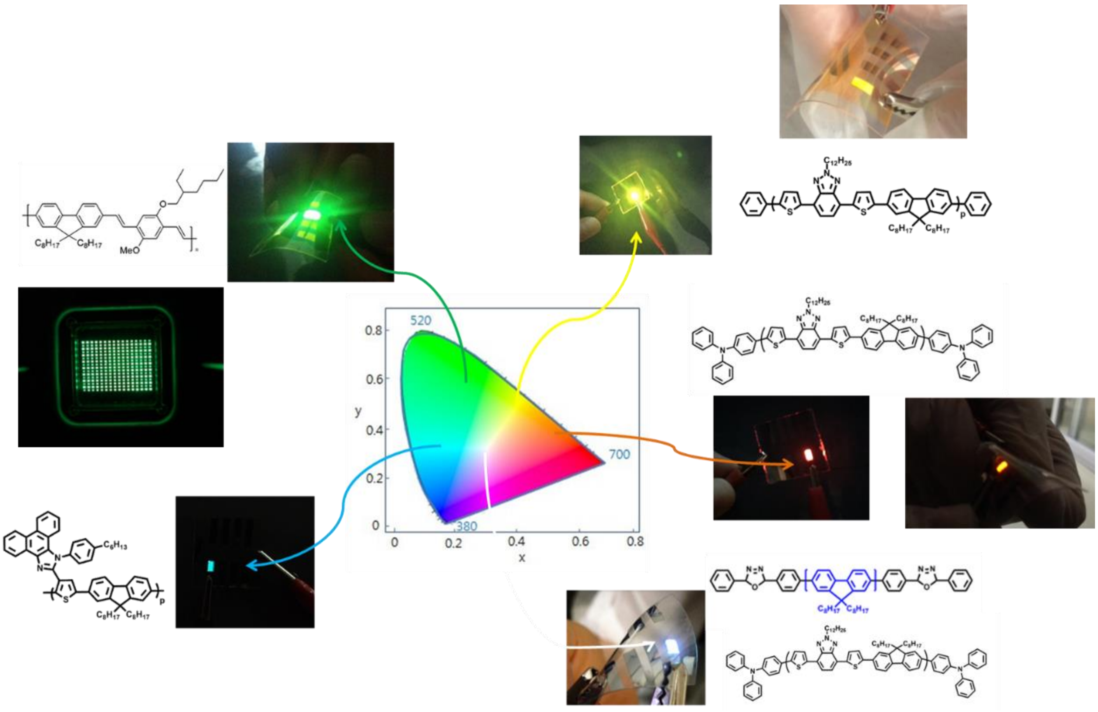

Figure 16 Snapshot of PLEDs constructed in our research group

1.3 Outline of the Thesis

In the first chapter of this thesis dissertation, introductory information and current status of polymer solar cells and polymer based OLEDs are emphasized.

In Chapter 2, fabrication steps of polymer solar cells and PLEDs are mentioned. Details of characterization methods are introduced.

Third chapter is about effect of terminal structure and molecular weight on electroluminescence behaviors. Benzene and triphenylamine end capped fluorene, benzotriazole and thiophene bearing polymers are synthesized. Their electroluminescence properties are investigated.

In chapter 4, effects of end capper and molecular weight on photovoltaic performance is investigated.

Chapter 5 is devoted to the electrochemical synthesis of polymers and their photovoltaic studies. To the best of our knowledge, **this is the first study in literature** where electrochemically synthesized polymers are used in organic photovoltaic applications. Works on ternary solar cells based on electrochemically synthesized polymers are also covered in this chapter.

Chapter 6 covers ITO free polymer solar cells and PLEDs. Instead of ITO, Ag nanowires are used as the anode materials in polymer solar cell and polymer light emitting diode applications.

This chapter also covers preliminary studies on semitransparent organic photovoltaic devices. Transparent Ag nanowires are used as top contacts and semitransparent P3HT based polymer solar cells are fabricated.

CHAPTER 2

EXPERIMENTAL

2.1 Materials

For electrochemical characterizations ITO coated glass slides (8ohm/square) were purchased from Delta Technologies. Supporting electrolytes, solvents (acetonitrile, nitromethane, dicholoromethane) were obtained from Sigma Aldrich. For UV-Vis, and photoluminescence analyses, glass slides from Sigma Aldrich were used.

ITO coated glass substrates for device fabrication were purchased from Visiontek. All chemicals and solvents used for etching, cleaning of substrates and active layer preparation were purchased from Sigma Aldrich. For active layer preparation anhydrous solvents were used. PCBM[60] and PCBM[70] were purchased from Solenne. Active layer solutions were prepared in vials (Sigma Aldrich) and filtered through PTFE syringe filters (Ossila) with a pore size of 0.22μm or 0.45μm.

For evaporation of metals a system equipped with a deposition controller was used. High purity metals were purchased from Kurt J. Lesker. The tungsten boats used for evaporation were obtained from R.D. Mathis Company. Thicknesses of the coated metals were controlled with QCM sensors.

2.2 Polymer Solar Cell Fabrication

ITO coated glass substrates (15ohm/square) were purchased from Visiontek. They were cut into small pieces (12.5cm x 2.45cm). ITO sites were protected with Scotch tape and immersed into HCl and HNO_3 mixture at 75ºC for 3 minutes. For neutralization, etched ITO substrates were immersed into K_2CO_3 solution and distilled water. Tape residues were removed with toluene. After cutting the substrates into smaller pieces (2.45cm x 2.45cm), substrates were cleaned using toluene, detergent (Hellmanex) – water mixture (2 vol %), water and isopropyl alcohol sequentially in an ultrasonic bath for 15 minutes. Subsequently, oxygen plasma cleaning was performed in Harrick Plasma Cleaner for 5 minutes to remove organic impurities. PEDOT:PSS (Heraeus V P Al 4083) was filtered through 0.45 µm pore sized PVDF filter. It was spin coated at 3500 rpm for 45 seconds resulting in 40 nm thick hole transport layer using Specialty Coating Systems G3P spin coater outside the glove box. In order to remove residual water, substrates were dried on hot plate at 130ºC for 15 minutes. Polymer PCBM blends were prepared in different weight ratios. These blends were filtered through 0.22 µm pore sized PTFE filter. On top of PEDOT:PSS layer, active layer was spin coated in moisture and oxygen free MBraun glove box (H_2O< 0.1ppm, O_2 <0.1ppm) using Sawatec SM-180 spin coater. Figure 17 shows the photograph of oxygen and moisture free glove box system.

LiF (lithium fluoride) or Ca (calcium) and Al (aluminum) metals were evaporated with average deposition rates of 0.08 Å /s, 0.2 Å/s and 1 Å/s, respectively. Resulting device configuration was ITO/PEDOT:PSS/ polymer:PCBM/LiF or Ca /Al.

Figure 17 Photograph of oxygen and moisture free glove box system

2.3 Polymer Light Emitting Diode Fabrication

For the construction of polymer light emitting diodes etching, cutting and cleaning procedures were followed as mentioned in Section 2.2. Right after cleaning, PEDOT:PSS was coated using G3P spin coater. Polymer solutions were dissolved in chloroform ($CHCl_3$), toluene or tetrahydrofuran (THF) with a w/w concentration in between 1 to 2.5%. Polymer solutions were filtered through 0.22µm or 0.45µm pore sized PTFE filters and spin coated on PEDOT:PSS layer. Figure 18 shows the illustration for spin coating. LiF or Ca and Al metals were evaporated with average deposition rates of 0.08 Å /s and 1 Å/s, respectively. Resulting device configuration was ITO/PEDOT:PSS/ light emitting polymer /LiF or Ca /Al.

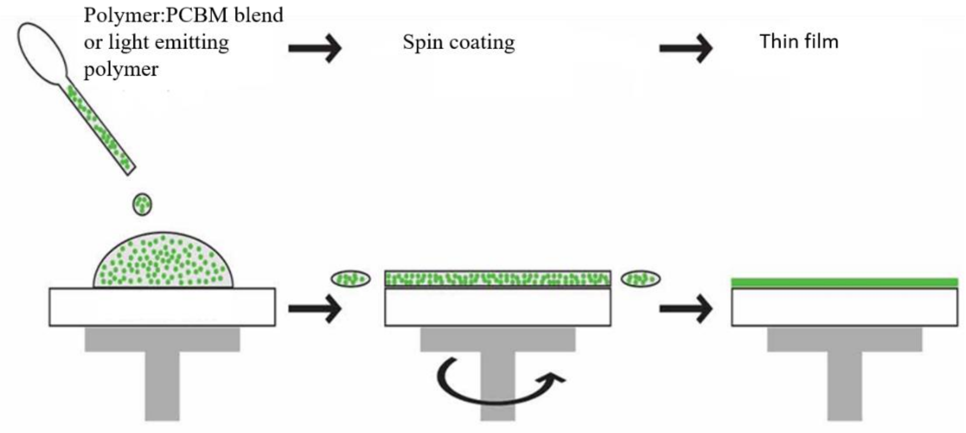

Figure 18 Illustration for spin coating of polymer PCBM blend or light emitting polymer

2.4. Characterizations

2.4.1 Gel permeation Chromatography (GPC)

GPC is a type of size exclusion chromatography used for molecular weight analyses of polymers. Molecular weight of polymers is not a discrete value, it is a distribution of different molecular weight chains. Number of chains and weight of the chains at every distribution should be determined to estimate the number average (Mn) and weight average (Mw) molecular weights of the polymers. Schematic diagram of a GPC is shown in Figure 13. Polymer is first dissolved in a solvent with a known concentration and injected to flowing stream of solvent which is called mobile phase. Column of GPC is made up of silica or polymer beads having uniform pores. Low molecular weight polymer chains are more strongly retained in the column than high molecular weight polymer chains. Whereas high molecular weight polymers do not suffer from retention in the column. The time that is spent in the column is called the retention time.

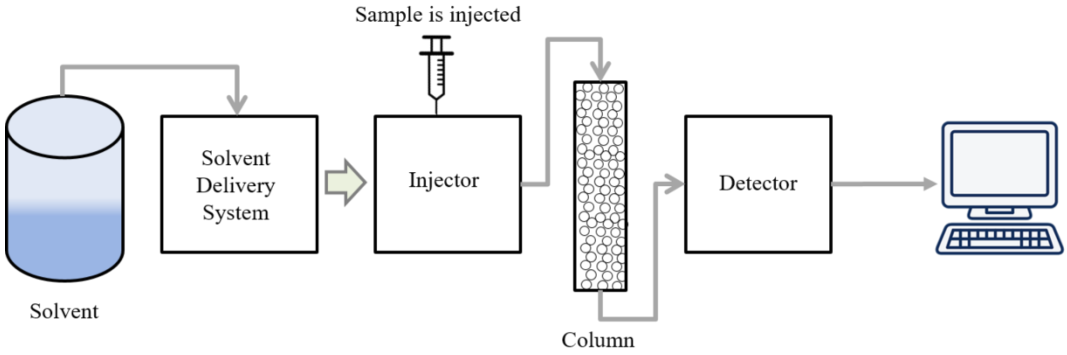

Figure 19 Schematic diagram of Gel Permeation Chromatograph

2.4.2 Cyclic Voltammetry (CV)

Cyclic voltammetry is a very useful tool to investigate electroactivity of the monomers, to convert monomers into corresponding polymers and to determine the oxidation potential of the monomer and the redox potentials of the polymers. In this study, electrochemistry experiments were conducted both for electrochemical characterization and electrochemical polymerization. Electrochemistry experiment set up is demonstrated in Figure 20.

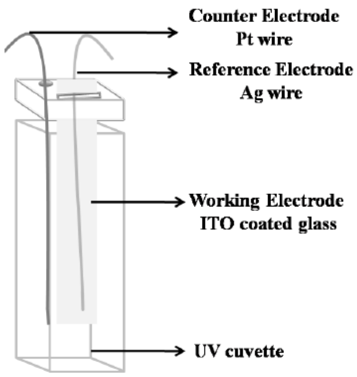

Figure 20 Demonstration of electrochemistry experiment set up

For the electrochemical synthesis of polymers, platinum (Pt) electrodes were used as the working and counter electrodes and a silver (Ag) wire was used as the reference electrode. Tetrabutylammonuium hexafluorophosphate was used as the supporting electrolyte. As the solvent nitromethane was used. Potential sweep technique was utilized and details of this experiment will be mentioned in Section 5.2.

For electrochemical characterization of chemically synthesized polymers cyclic voltammetry experiments were also carried out. Polymers were dissolved in $CHCl_3$ with a weight concentration of 1mg/ml and filtered through 0.45µm pore sized PTFE filter. Then polymer solution was spray coated on ITO glass electrodes. Counter, working and reference electrodes were connected to the Gamry potentiostat (Reference 600) which applies a potential between working and reference electrodes. Acetonitrile was used as the solvent due to its inertness in a wide range of potential.

Potential was swept with a constant rate (100mV/sec or 250mV/sec) current values were recorded. Current density vs voltage relation was obtained. From this graph, doping and dedoping potentials for p doping and n doping regions and oxidation and reduction onset values can be determined. Figure 21 demonstrates the oxidation and reduction onset values obtained from CV.

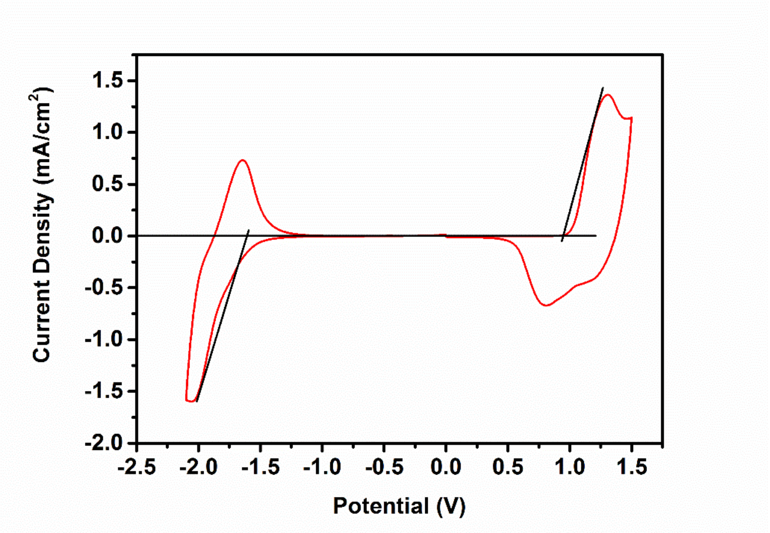

Figure 21 Demonstration of oxidation and reduction onset values obtained from CV

2.4.3 Uv-Vis Spectroscopy

With UV-Vis spectroscopy, absorption or transmittance of a solution in a cell with a path length b is measured. In this study, absorption of thin films and polymer solutions were investigated with Agilent Technologies 8453 UV-Vis Spectrophotometer.

From absorption onset values optical band gaps of the polymers were calculated using Equation 8 where Planck’s constant is 6.626 x 10^{-34} Joules/sec, speed of light is 3.00 x10^{8} meter/sec and λ is the cut off wavelength. For conversion 1eV is equal to 1.6 x 10^{-19} Joules.

$$E = h \times \frac{c}{\lambda} \qquad (8)$$

2.4.4 Photoluminescence Spectroscopy

In photoluminescence spectroscopy, light is directed to a sample, photoexcitation takes place. After that energy is released with an emission of photon called photoluminescence. Figure 22 demonstrates the schematic diagram of a fluorometer or spectrofluorometer. In fluorometer, excitation source is usually a mercury (Hg) lamp and as excitation and emission wavelength selector, absorption and interference filters are used. In spectrofluorometer, excitation source is usually a xenon (Xe) lamp and as the excitation and emission wavelength selector, a monochromator is utilized. Sample and detector are at right angle to each other to minimize scattering from the sample and cell wall.

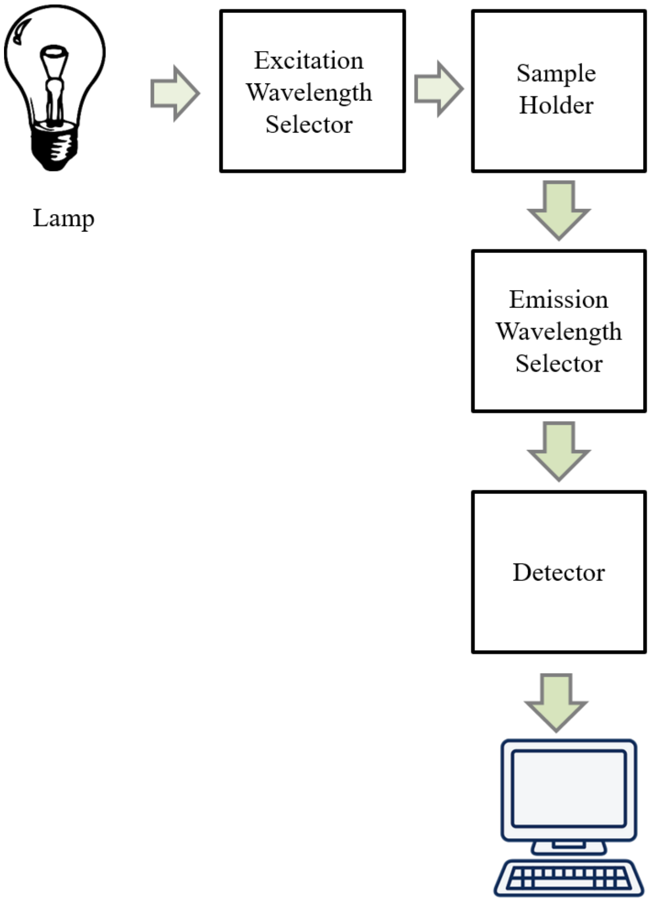

Figure 22 Schematic diagram of a fluorometer / spectrofluorometer

2.4.5 Transmission electron Microscopy (TEM)

Operation of transmission electron microscope (TEM) is similar to the optical microscope. In the case of TEM electrons are used as the light source. At the top of the microscope there is an electron gun that produces electron beams. Column of the microscope is in vacuum. Electrons are travelling to the condenser which is composed of electromagnetic lenses which focuses electrons into a beam. Then the beam focus on the sample and unscattered electrons hit the fluorescent screen. An image with darker and lighter areas is obtained. Darker areas correspond to electron rich areas whereas lighter areas correspond to electron poor areas. Figure 23 depicts the schematic diagram of TEM instrument.

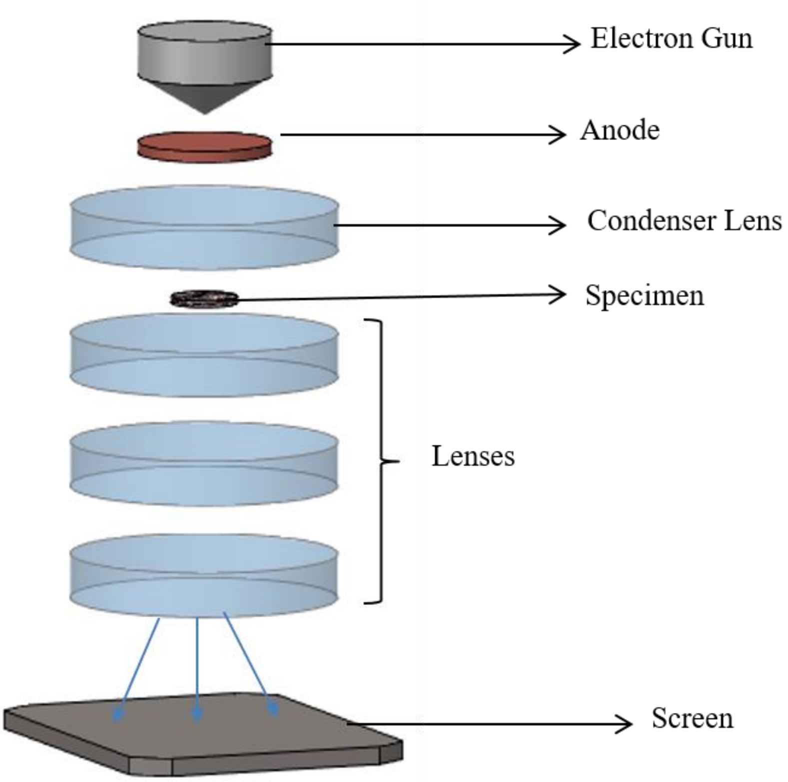

Figure 23 Schematic diagram of TEM

2.4.6 Atomic Force Microscopy (AFM)

Atomic Force Microscopy is a powerful technique for examining the topography of the samples at nanoscale and it is also used for lithographic purposes.

Cantilever equipped with a tip scans the surface of the sample. When the tip is close to the surface, attractive forces are dominant and lead cantilever to deflect towards the surface. If the tip approaches the surface more, repulsive forces become dominant and lead cantilever to deflect away from the surface. A laser beam is directed to the cantilever and cantilever deflections lead reflected beam to change its direction. These movements are tracked by a position sensitive photodiode and sent to the detector.

2.4.7 Organic Solar Cell Characterization

For the characterization of OSCs, current density vs voltage characteristics of the devices are tested under illumination of solar simulator with a power of 100mW/cm^2. The Committee Internationale d'Eclaraige (CIE) and the American Society for Testing and Materials (ASTM) declared standard testing conditions for solar panels. Standard test conditions include intensity of light, temperature and spectrum. Standard spectra are prefixed as AM and it is followed by a number. AM stands for Air Mass and the number depends on the path through the atmosphere normalized to the shortest path. Figure 24[54] demonstrates the definition of various global (G) air mass (AM) conditions.

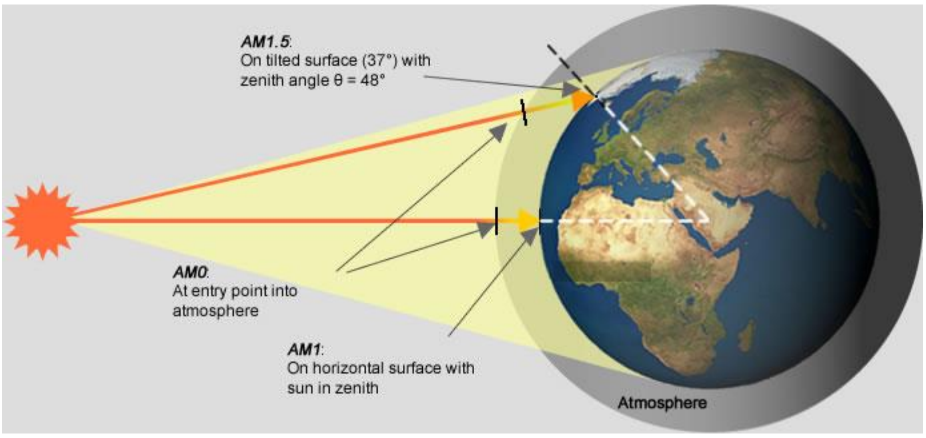

Figure 24 The definition of various global (G) air mass (AM) conditions [54]

Solar cells were tested under illumination of AM 1.5G solar simulator (Atlas Material Testing Solutions) using Keithley 2400 source meter controlled by LabTracer program. J-V (Current density vs voltage) relations of the devices were plotted using program Origin.

After J-V measurements, IPCE /EQE characterizations were carried out. EQE measurements were performed to determine how efficiently a solar cell converts sunlight into electricity. For this purpose, a calibrated Si photodiode (Newport) was used as the reference, and the cell’s photocurrent response was measured under illumination. IPCE measurement set up is shown in Figure 25. IPCE curve resembles the absorption spectrum of polymer PCBM blend. From the curve it is possible to estimate J_{SC} values of the solar cells.

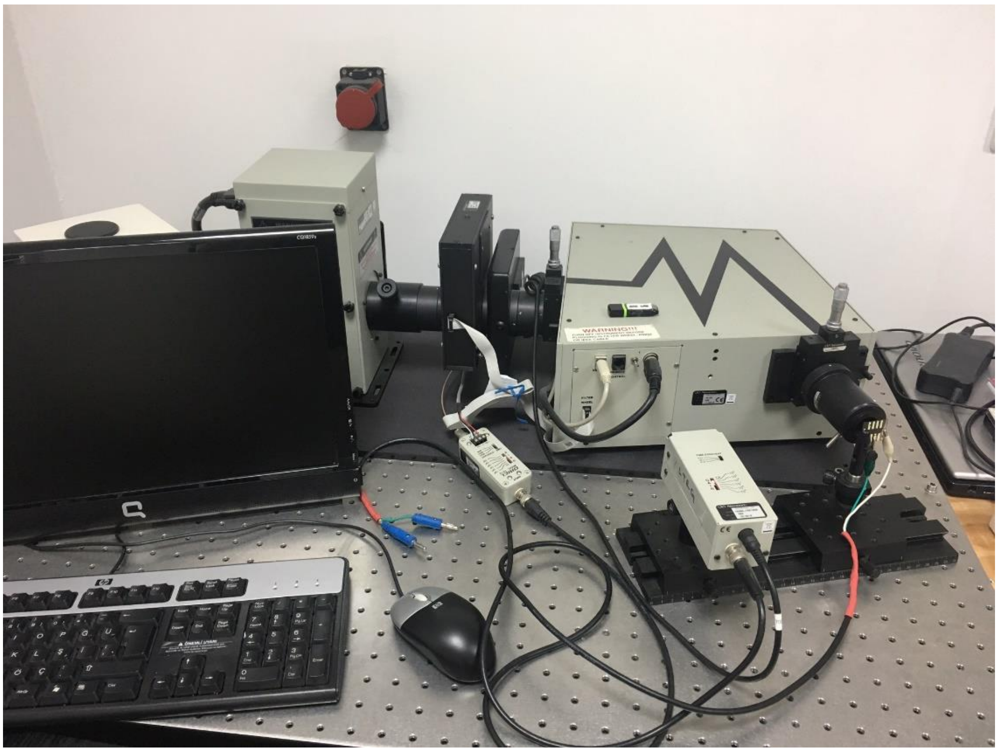

Figure 25 IPCE set up

2.4.6 Polymer Light Emitting Diode Characterization

In the characterization of PLEDs, while potential is swept, current and luminance data are collected simultaneously. Current density vs. voltage relation is collected by Keithley 2400 which is controlled by LabTracer. Luminance is detected by Maya spectrophotometer equipped by a fiber optic with a diameter of 100µm. Data is processed by SpectraSuit program.

CHAPTER 3

EFFECTS OF TERMINAL STRUCTURE AND MOLECULAR WEIGHT ON ELECTROLUMINESCENCE PROPERTIES OF POLYMERS

3.1 Introduction and Aim of Work

Polymer based light emitting diodes have attracted great interest both from academia and industry. They have some advantages such as ease of fabrication, low operating voltages, possibility of application on flexible substrates.[55] In addition, color tunning can be achieved via structural modification in the polymer backbone [56] or side chain [57,58] or blending/dopping [59] with organic or inorganic molecules. Poly(p-phenylenevinylene) (PPV) [60] and polyfluorene (PF) [61,62] have emerged as suitable polymer light emitting (PLED) materials. High photo and thermal stability (even above their melting points), good solubility in organic solvents, high photoluminescence (PL) efficiency, good charge transport properties of polyfluorenes made them attractive class of light emitting polymers.

Fluorene bearing homopolymers usually have large band gap and their electroluminescent devices emit blue light.[62] Significant efforts and great success have been made to tune the light emitting color of polyfluorenes to a longer wavelength and decrease the band gap of the resultant polymers.[63] It is also crucial for organic photovoltaic device application to harvest more sunlight. With chemical modifications like copolymerization with other subunits it is possible to obtain different emission characteristics over the whole visible spectrum.

Copolymerization of fluorene monomer derivatives with different aromatic moieties allows for color tuning through modification of the band gap. Color tuning to the deep-red and NIR region in conjugated polymers can be achieved by incorporating narrow-band-gap comonomer into polyfluorene backbone. Emission color of polyfluorenes can be tuned in entire visible region by incorporating narrow band gap comonomer into polyfluorene backbone. Most widely used narrow band gap comonomers are a variety of aromatic heterocycles with S and N atoms.

Thieno[3,2-b]thiophene [64], Phenothiazine [65] , 4,7-di(2′- selenophenyl)-2,1,3-benzothiadiazole (SeBT) [66] and 4,7- di(2′-selenophenyl)-2,1,3-benzoselenadiazole (SeBSe) [63] naphthoselenadiazole [67] units were incorporated in polyfluorene backbone to obtain different electroluminescence properties. Shim et.al reported copolymers based on 2,5-bis(5’-bromothiophen-2-yl)-1cyanovinyl)-1-(2”-ethylhexyl)-4-methoxybenzene, obtained have luminescent properties having the full color range (blue to red) by controlling the feed ratios. [68] Figure 26 shows the structures of the copolymers based on flourene.

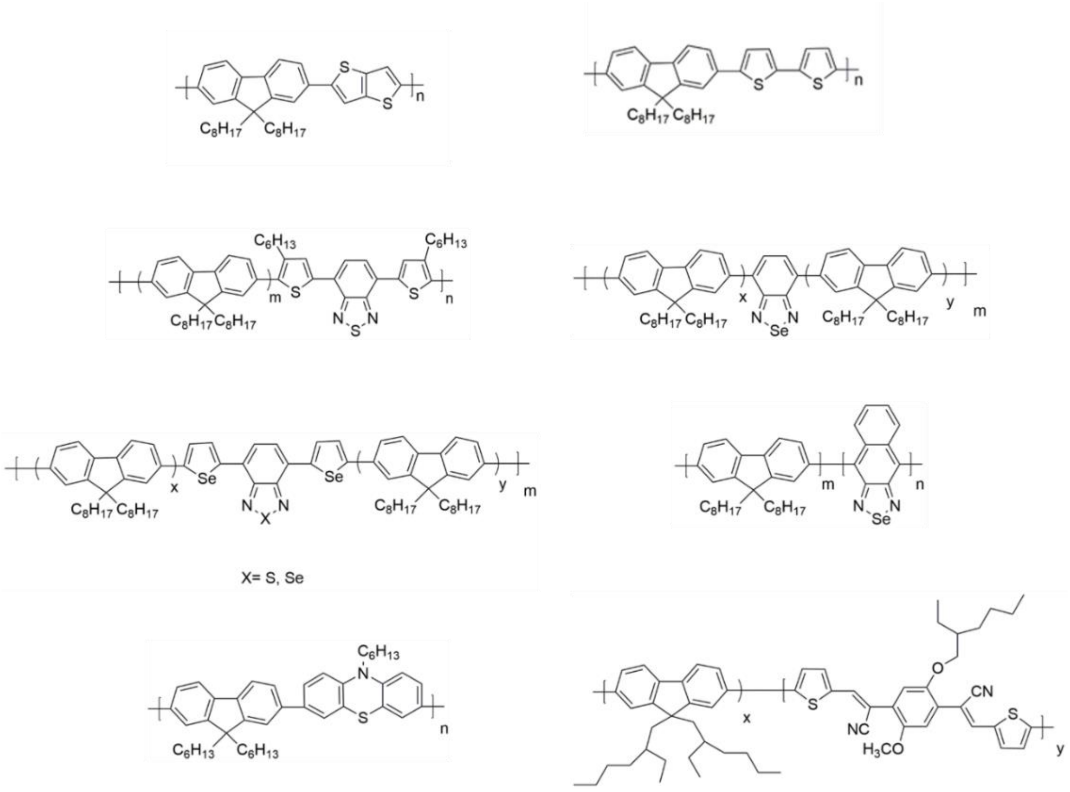

Figure 26 Structures of fluorene based copolymers

Although there are numerous studies about tuning the optical and electronic properties of polymers via structural modifications there are very few studies pointing out the importance of end capping. McCulloch and coworkers investigated the effect of bromine end groups in P3HT. It was concluded that lower Jsc and EQE values obtained in P3HT-Br based solar cell compared to P3HT-H solar cell were due to increased trapping of charges.[69]

Heeger group investigated the effect of bulky end cappers on electroluminescence properties. Polyhedral oligomeric silsesquioxanes (POSS) anchored poly(9,9-dihexylfluorenyl-2,7-diyl (PFO) and poly(2-methoxy-5-(2-ethylhexyloxy)-1.4-phenylenevinylene (MEH-PPV) were synthesized. Thermal stability of the polymers were improved with the POSS incorporation. POSS addition to MEH-PPV improved the brightness of the devices from 230cd/m^2 to 1320cd/m^2 with the same current passing and the same electroluminescence spectra. In the case of PFO, POSS addition as end capper, electroluminescence at 525nm which is arising from the formation fluorenone defects is significantly reduced. Devices based on PFO-POSS showed higher luminance values.[70]

Li et.al synthesized diphenylamino-end-capped oligofluorenylthiophene derivatives. Polythiophenes usually have low photoluminescence in solid state due to intersystem crossing caused by the heavy atom effect of sulfur and nonradiative decay via interchain interactions. With the structrural modifications resulting oligomers showed electroluminescence with luminance values up to 19800cd/m^2.[71] Structures of diphenylamino-end-capped oligofluorenylthiophene derivatives are depicted in Figure27.

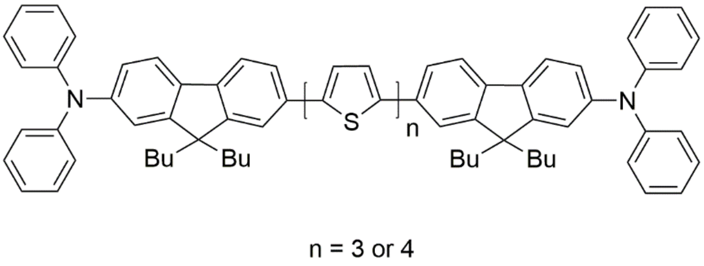

Figure 27 Structures of diphenylamino-end-capped oligofluorenylthiophene derivatives

Neher and coworkers improved the performance of polyfluorene (PF) based PLEDs via end capping. It was showed that non end capped PF are suffering from unwanted green light emission due to excimer formation which reduces the electroluminescence of the device, triphenylamine (TPA) end capping diminishes the green light emission. Authors proposed that in non capped PF, hole and electron recombinations happen in the excimer formation sites which lead to green light emission. However, in end capped PF recombinations may take place polymer main chain ends.[72] Structures of TPA end capped polyfluorenes are depicted in Figure 28.

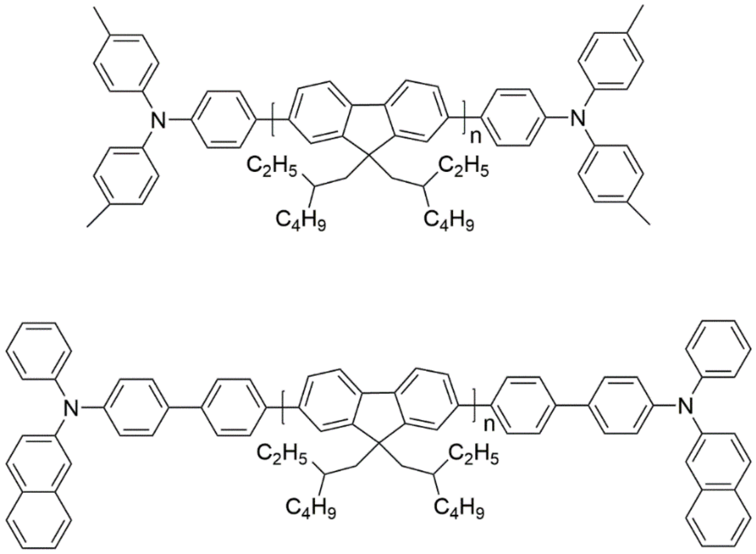

Figure 28 Structures of TPA end capped polyfluorenes

As can be evidenced from the literature examples, polyfluoerene comprising polymers showed electroluminescence. Band gaps and thus the emmissions of the resulting polymers can be manipulated via structural modifications. Electroluminescence of the devices based on polymers can be improved with end capping. For this purpose, in this study, fluorene, benzotrizaole and thiophene bearing polymers with different terminal ends were synthesized and their electroluminescent devices were constructed.

3.2 Experimental

In this study, fluorene, benzotrizaole and thiophene bearing polymers with different terminal ends were synthesized via Suzuki Coupling reaction. Molecular weights of the polymers were determined with Agilent Gel Permeation Chromotagraphy (GPC) using $CHCl_3$ as eluent and polystyrene as standart. For the GPC analysis, polymers were dissolved in $CHCl_3$ with 2mg/ml concentration and filtered throgh PTFE filter to remove undissolved particles. In electrochemistry experiments 3 electrode system was used. Silver (Ag) wire was used as reference electrode, Platinum (Pt) wire was used as the counter electrode and ITO was used as the working electrode.

ITO coated glass substrates (15ohm/square) were purchased from Visiontek. ITO sites are protected with tape and immersed into HCl and HNO_3 mixture at 100ºC for 3minutes. For neutralization, etched ITO substrates are immersed into K_2CO_3 solution and distilled water. Tape residues are removed with toluene. Substrates are cleaned using detergent (Hellmanex) - water, water and isopropyl alcohol sequentially in an ultrasonic bath for 15 minutes. Subsequently, oxygen plasma cleaning was performed in Harrick Plasma Cleaner to remove organic impurities. PEDOT:PSS (Heraeus V P Al 4083) is filtered through 0.45 µm pore sized PVDF filter. It is spin coated at 3500 rpm for 45 seconds resulting in 40 nm thick hole transport layer outside of the glove box. In order to remove residual water, substrates are dried on hot plate at 130ºC for 15 minutes. Polymer PCBM blends are prepared in different ratios. These blends are filtered through 0.22 µm pore sized PTFE filter. On top of PEDOT:PSS layer, active layer is spin coated in moisture and oxygen free MBraun glove box (H_2O< 0.1ppm, O_2 <0.1ppm) using spin coater. Ca and Al metals are evaporated with average deposition rate of 0.2 Å /s and 1 Å/s, respectively. Resulting device configuration is ITO/PEDOT:PSS/ polymer /Ca /Al. (Figure 29) Current density – voltage characteristics of the devices are tested under illumination of solar simulator (A.M. 1.5G) using Keithley 2400 and LabTracer program. For electroluminescence characterizations 100nm diameter sized fiber optic equipped Maya spectrophotometer was used.

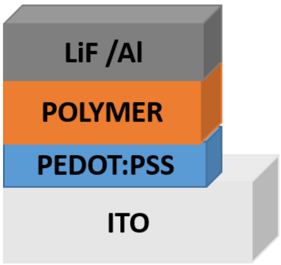

Figure 29 PLED stack

3.3 Results and Discussion

In this study, fluorene, benzotrizaole and thiophene bearing polymers with different terminal ends were synthesized. While P1 has triphenylamine terminal end, P2 has benzene end cap. Structures of the polymers with different end cappers are shown in Figure 30.

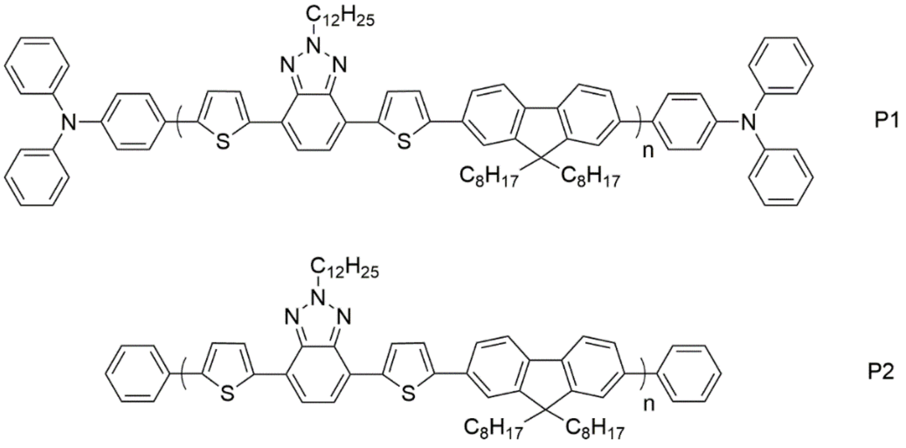

Figure 30 Structures of polymers P1 and P2

Scherf and Neher et.al demonstrated that by increasing the amount of end capper molecular weight of the resulting polymers are decreasing, drastically. [72] In this study, in order to obtain polymers with similar molecular weights, same amount of end capping reagents were used. Molecular weights of polymers were determined as (Mn-Mw) 9kDa- 14kDa and 22kDa-40kDa for P1 and P2, respectively.

Cyclic voltammetry was used to investigate the electrochemical behaviors of the polymers. Polymers were dissolved in $CHCl_3$ with a concentration of 2mg/ml and filtered through 0.45µm pore sized PTFE filter. Filtered polymer solutions were spray coated on ITO coated glass electrodes. Polymer films were subjected to cyclic voltammetry. Oxidation of polymer films were achieved at 1.30V and 1.28 with a reversible dedoping peaks at 0.81V and 0.66V for P1 and P2, respectively. (Figure 31) At negative potentials reversible doping and dedoping peaks were observed at -2.05V/ -1.63V and -1.88V/-1.45V for P1 and P2, respectively. Due to the ambipolar character of the polymers, Highest Occupied Molecular Orbital (HOMO) and Lowest Unoccupied Molecular Orbital (LUMO) energy levels and electronic band gap (Eg^{el})values can be estimated from oxidation and reduction onset values according to the following equations. (Equation 1 and 2). Oxidation and reduction onset values are calculated from the intersection of the tangent line to the increasing part of the current and the baseline. Electrochemical parameters are summarized in Table 1.

$$\text{HOMO} = -(-4.75 + E_{ox,onset}) \tag{8}$$

$$\text{LUMO} = -(-4.75 + E_{red,onset}) \tag{9}$$

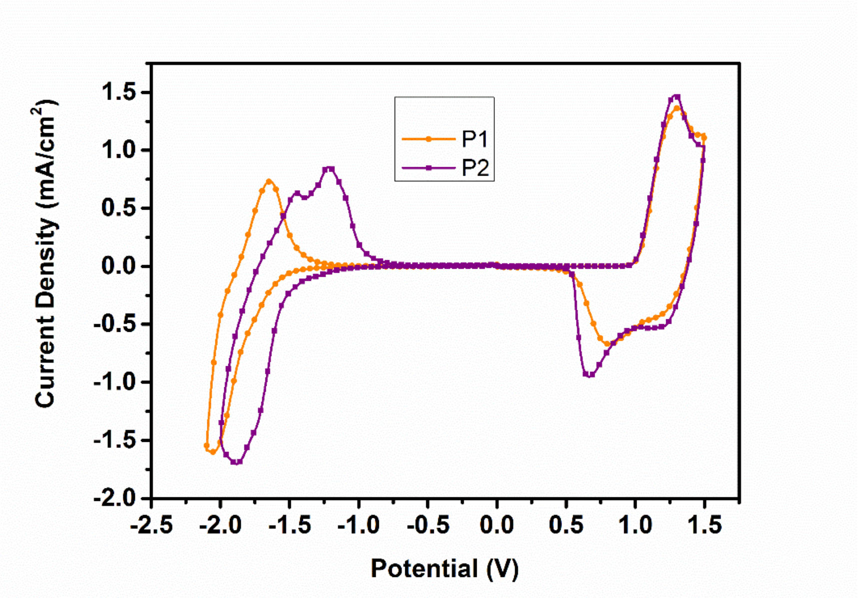

Figure 31 Cyclic Voltammetry of P1 and P2

Table 1 Summary of electrochemical parameters

Polymers	**$E_{ox,onset}$ (V)**	**$E_{red,onset}$ (V)**	**HOMO (EV)**	**LUMO (EV)**	**Eg^{el} (EV)**
P1	1.02	-1.71	-5.77	-3.04	2.73
P2	1.01	-1.51	-5.76	-3.34	2.42

Optical characterization of the polymers were carried out to determine the absorption and photoluminescence profiles of polymers. Absorption spectra of the polymers in thin film form are depicted in Figure 32. The absorption maximas are 488nm and 519nm with an intense shoulder at 489 corresponding to the π-π* transitions for the polymers P1 and P2, respectively.

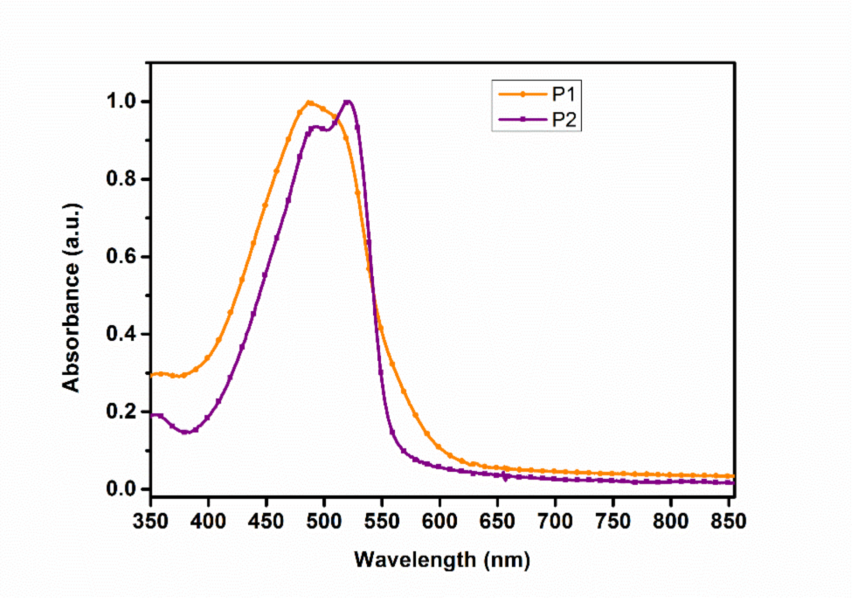

Figure 32 Absorption spectra of polymers P1 and P2 in thin film form

Photoluminescence properties of the polymers in solution and in thin film form were investigated. The luminescence maximas are 534 nm and 569 nm for P1 and P2, respectively. Very low broadening of the peaks takes place in the cases of thin film spectra compared to solution spectra, which shows the minority of aggregation in thin film form. Photoluminescence spectra of the polymers in $CHCl_3$ and in thin film form are depicted in Figure 33.

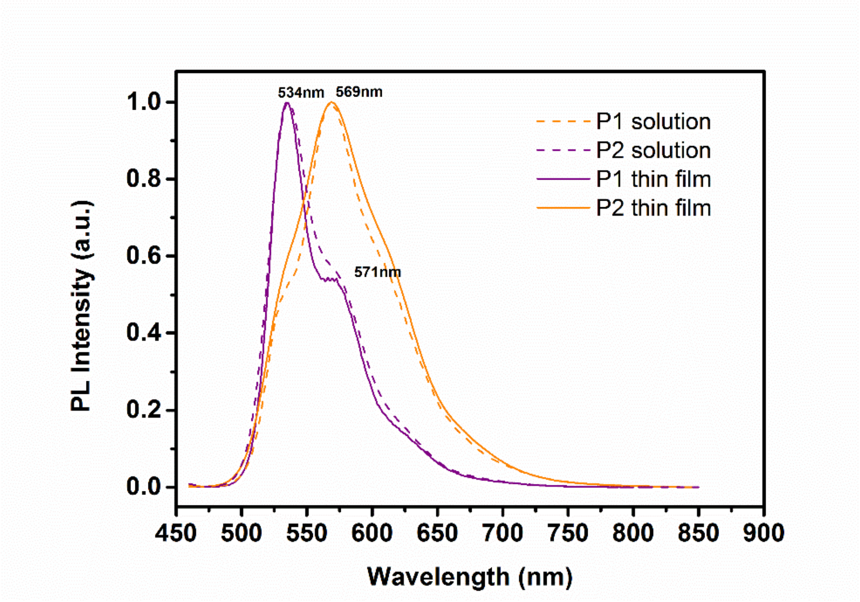

Figure 33 Photoluminescence spectra of polymers P1 and P2 both in solution and in thin film form

Electroluminescence (EL) properties of the polymers were investigated with the device structure of ITO/PEDOT:PSS/P1 or P2/Ca/Al. PLEDs were constructed following the procedure mentioned in the experimental part. Polymers were dissolved in $CHCl_3$ with 15mg/ml concentration and spin coated with 2000rpm resulting in 70-85nm thick polymer layer. Calcium (20nm) and aluminum (90nm) electrodes were evaporated. EL characteristics, luminance and current density versus applied voltage characteristics of the PLEDs were investigated. Figure 34 shows electroluminescence spectra of PLEDs in orange and yellow color of electromagnetic spectrum with EL peak centered at 589nm and 547 nm with a shoulder at 589nm, respectively. EL peaks are red-shifted by 41nm and 13nm with respect to PL peaks for P1 and P2.

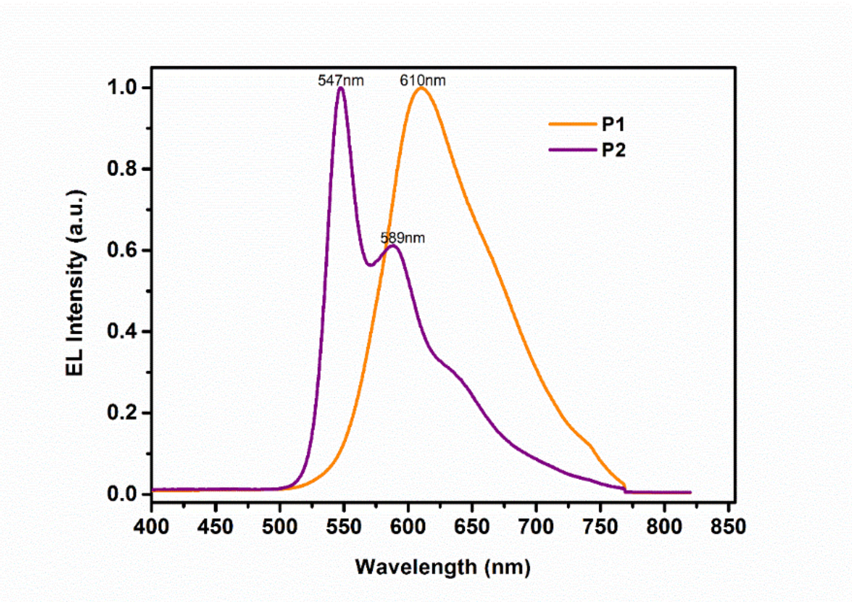

Figure 34 Electroluminescence spectra of the PLEDs based on P1 and P2.

Orange and yellow light emission were observed with Commission Internationale de l'Eclairage (CIE) coordinates measured at (0.5611, 0.4361) and (0.4527, 0.5389), for P1 and P2 incorporated PLEDs, respectively. Figure 35 shows the snapshot of the PLEDs.

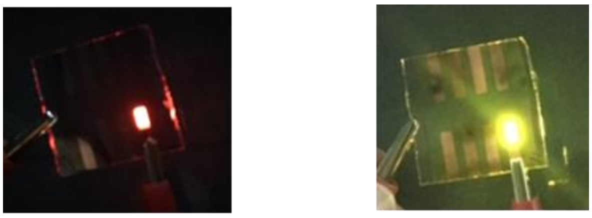

x: 0.5611 y: 0.4361	x: 0.4527 y: 0.5389

Figure 35 Snapshot of the PLEDs based on P1 (left) and P2 (right) with their CIE coordinates

In order to characterize the intensity of the emitted light luminance vs. voltage dependence of the PLEDs were determined. While voltage is swept luminance values and current values were recorded simultaneously. Luminance vs. voltage and current density vs. voltage dependence of the P1 and P2 based PLEDs are depicted in Figure 36. P1 based PLED shows luminance value of 10411cd/m^2 at 8.5V whereas P2 based PLED has the peak luminance value of 14583cd/m^2 at 8V. This lower performance of P1 is believed to originate from less efficient charge carrier recombination on aggregates which also leads to red shifted EL. [72]

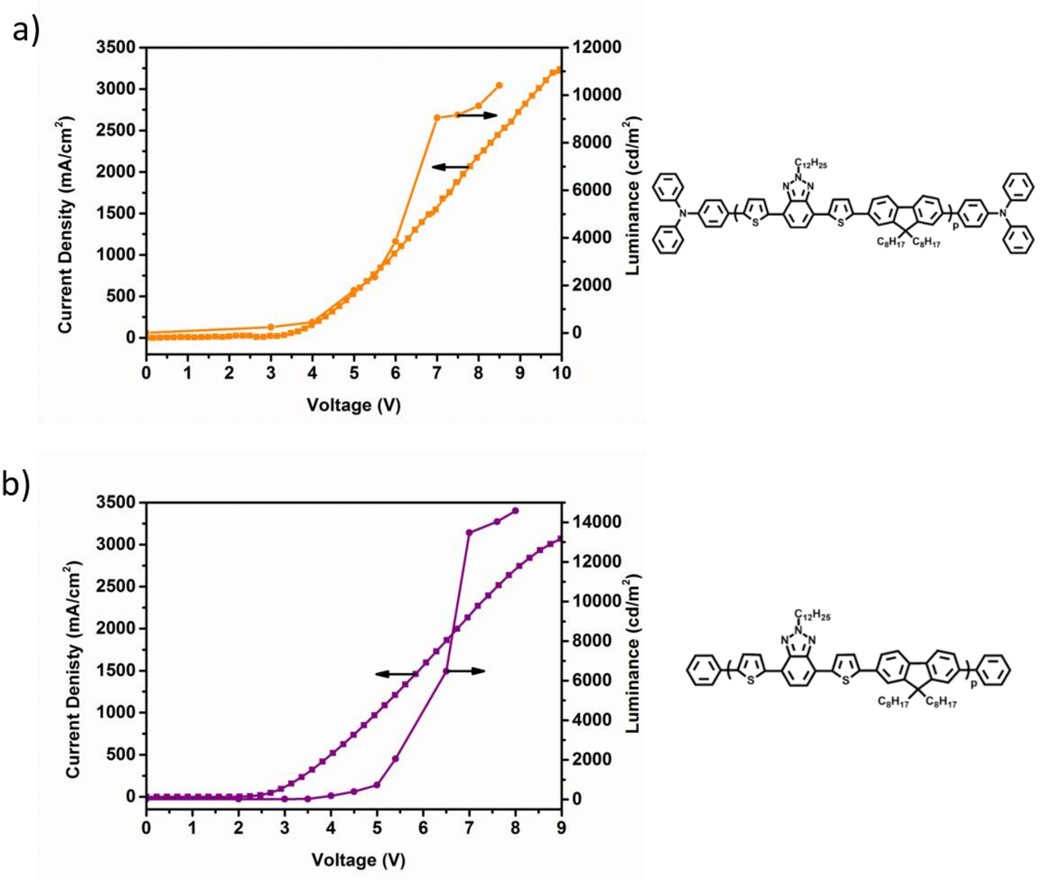

Figure 36 Luminance vs. voltage and current density vs. voltage dependence of the a) P1 and b) P2 based PLEDs.

Luminance efficacy values for P1 and P2 based PLEDs were calculated as 0.57cd/A at 7V luminance value of 9042cd/m^{2}and 0.632cd/A at 7V luminance value of 13474cd/m^2.

Chen and coworkers reported high brightness and stable yellow light emitting diodes using rubrene doped polyspirofluorenes and obtained 72000cd/m^2 luminance value with a luminance efficiency of 14cd/A. It is one of the highest brightness values in literature for yellow light emmiting diodes. [73]

Ma and coworkers constructed a multilayer yellow OLED device using phosphorescent Ir complex and polymer. Very high luminance efficiency value of 41.7cd/A was obtained with a lumiance value of around 2000cd/m^2. [74] To the best of knowledge it is the highest luminance efficiency value obtained for yellow light emitting diodes.

Although OLEDs based on doped polymers and host - guest systems show high luminance values, they are suffering from voltage dependent electroluminescence properties which leads to color change during operation. [75]

Bradley and coworkers reported PLEDs based on blend of poly(9,9-dioctylfluorene-co-benzothiadiazole) and poly(9,9-dioctylfluorene-co-N-(4-butylphenyl)diphenyl amine. With this device 5.9cd/A luminance efficiency value was attained at a luminance value of 100cd/m^2. [76]

Lee et. al reported yellow light emitting diodes based on super-yellow' poly-(p-phenylenevinylene) (SY-PPV) with the device structure of ITO/PEDOT:PSS/SY/LiF/Al. Maximum luminance value of 33800cd/m^2 was attained at 12.6V with 8.7cd/A luminous efficiency at 9.6V. [77]

Duan and coworkers constructed multistack OLEDs based on Ir complexes. They obtained high luminance efficiency of 26.2cd/Aand brightness of 58160cd/m^2.

However, these phosphorescent devices were prepared with vacuum deposition which brings high fabrication cost. [78]

Li et al reported one of the best performance orange red light emitting OLEDs for devices constructed with partially solution processable materials. 14.49cd/A luminance efficiency, 6613cd/m^2 brightness were obtained with phosphorescent materials. [79]

As seen in literature examples, phosphorescent small molecule based OLEDs have higher luminance values with luminance efficiencies compared to the those of polymer based OLEDs. Moreover, small molecules have advantages like easy purification and there are no batch to batch variations for molecular weight. However, these multistack devices are usually constructed by vacuum evaporation which brings high cost. In addition to this current values passing through the small molecule based OLEDs, operation voltages are high compared to the those of PLEDs. Polymer based OLEDs have advantages of solution processability and easy application on flexible substrates which is the main requirement for future OLEDs. For this purpose, P1 and P2 comprising PLEDs were constructed on ITO coated PEN substrates which gives flexibility to the device. Figure 37 shows the snapshot of the flexible PLEDs based on P1 and P2.

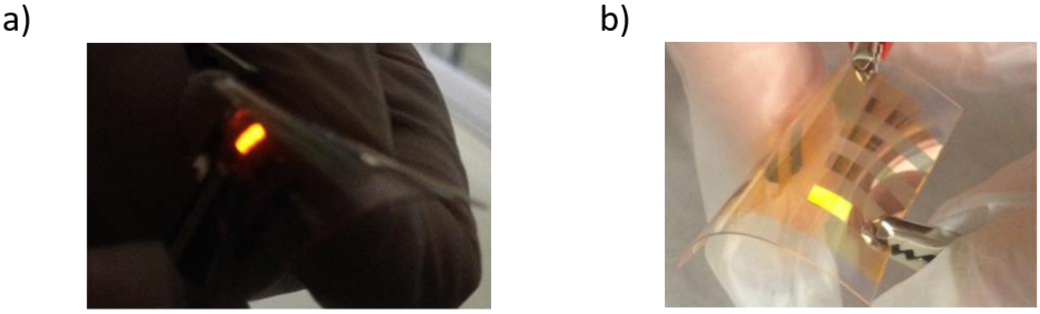

Figure 37 Snapshot of the PLEDs based on a) P1 and b) P2 constructed on ITO coated PET substrates

Electroluminescence behaviors of the P1 and P2 comprising flexible PLEDs were investigated. CIE coordinates of the PLEDs were determined as x =0.6163 y = 0.3790 and x =0.4527 y = 0.5389 for P1 and P2 based PLEDs. P1 based PLED exhibited highest luminance value of 8239cd/m^2 at 8V, whereas P2 based PLED exhibited highest luminance value of 9350cd/m^2 at 8V. Figure 38 demonstrates the electroluminescence spectra of the P1 and P2 compromised devices.

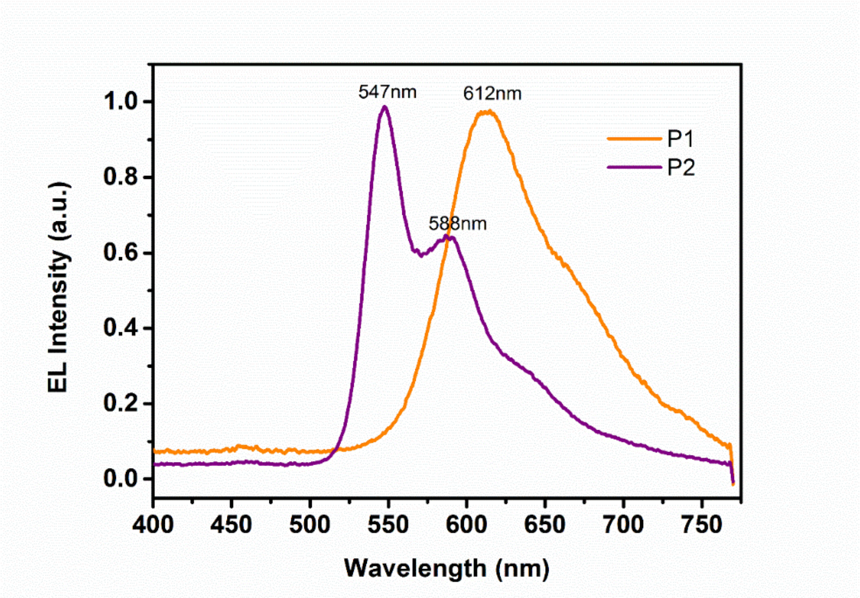

Figure 38 Electroluminescence spectra of the flexible PLEDs based on P1 and P2

Table 2 Summary of luminance values for P1 and P2 based PLEDs

polymer	**Luminance (cd/m^2)**
P1 on glass	10411 @8.5V
P2 on glass	14583 @8V
P1 on PET	8239 @8V
P2 on PET	9350 @8V

To conclude, for both devices on glass and flexible substrates, benzene end capped polymer exhibited superior electroluminescence performance. P1 compromised PLEDs had lower luminance values and red shifted electroluminescence compared to P2 compromised PLEDs. Lower luminance values may arise from less efficient charge carrier recombination on aggregates which also leads to red shifted EL.[72]

CHAPTER 4

EFFECTS OF TERMINAL STRUCTURE AND MOLECULAR WEIGHT ON PHOTOVOLTAIC PROPERTIES OF POLYMERS

4.1 Introduction and Aim of Work

Bulk heterojunction polymer solar cells (PSCs) are promising third generation photovoltaic technologies and a power conversion efficiency (PCEs) of 11.7 % has been achieved in single junction cells.[40] These progresses can be attributed to the advances in design of p and n type materials and device processing innovations.

Synthetic efforts have been made to improve the power conversion efficiency of the OPV device via enlarging the absorption spectra, controlling the energy levels of the donor and acceptor moieties. In addition to rational design of polymers, morphology optimizations and device processing innovations were also help to obtain high PCE values.

In addition to these, purity, molecular weight and end group of the polymers play important role on the performance of the PSCs.

Cao and coworkers synthesized poly[[4,8-bis[(2-ethylhexyl)oxy]benzo[1,2-b:4,5-b′]dithiophene-2,6-diyl][3-fluoro-2-[(2-ethylhexyl)carbonyl]thieno[3,4-b]thiophene diyl]] (PTB7) with different molecular weights (Mn=18, 40, 128kDa). In this study, effect of molecular weight on the photovoltaic performance was investigated. Polymers had similar electronic and optical properties. Power conversion efficiencies of the PSCs were found as 5.41%, 6.27% and 8.50% based on PTB7 with molecular weights of 18, 40, 128kDa, respectively. Structure of PTB7 is depicted in Figure 39. The hole mobilities of the polymers were enhanced from 2.85 $x10^{-4}$, 4.20 $x10^{-4}$, 6.30 $x10^{-4}$ cm/V.s with the increase in molecular weight. Authors attributed enhancement of PCE values to improvement of light absorption and mobility of charge carriers. Polymer with the highest molecular weight has the lowest PDI value which facilitates more ordered structure.The relation between the morphology of the active layer and the molecular weight proved with the TEM images which indicates the enhanced phase seperation with the increase of molecular weight.[34]

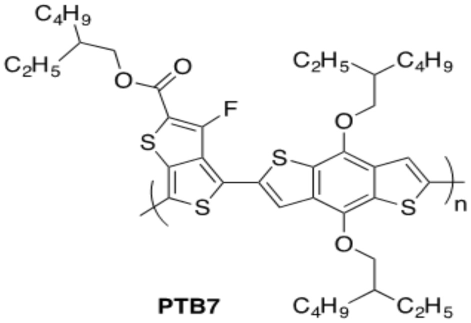

Figure 39 Structure of PTB7

Kim and coworkers also stressed the effect of molecular weight on performance of all polymer solar cells. In all polymer solar cells, mixing two polymers is a great challenge since entropy of mixing is reduced significantly. [80] In addition to this electron mobility of polymer acceptors are lower than the electron mobilities of the fullerene derivatives. Thus, having interconnected nanophase separated morphology becomes crucial for high performance all polymer solar cells. [81,82] It was stated that use of high Mn polymers enhances the mixing with n type polymer and prevent the formation of large domains. Power conversion efficiencies were enhanced from 1.54 to 2.39 and 3.59% along with the molecular weight of poly[(2,5-bis(2-hexyldecyloxy)phenylene)-alt-(5,6-difluoro-4,7-di(thiophen-2-yl)benzo[c][1,2,5] thiadiazole) (PPDT2FBT) increased from 12 to 24 and 40kDa.[83] Figure 40 shows the structure of PPDT2FBT.

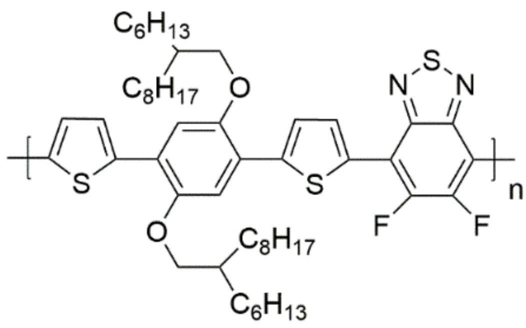

Figure 40 Structure of PPDT2FBT

There are also a few studies stressing the importance of terminal units. Heeger and Bazan investigated the effect of unreacted bromine and stanyl groups at the terminal ends of polymers. For this purpose poly[(4,4-didodecyldithieno[3,2- b :2',3'- d]silole)-2,6- diyl- alt -(2,1,3-benzothiadiazole)-4,7-diyl was synthesized with no terminal ends and also with thiophene end cappers. (Figure 41) Optical and morphological properties of the polymers were found very similar. However, unreacted bromine and stanyl ends were acting as charge carrier traps which led to lower fill factor values. Moreover unreacted end groups made the polymer more prone to thermal degradation.[84]

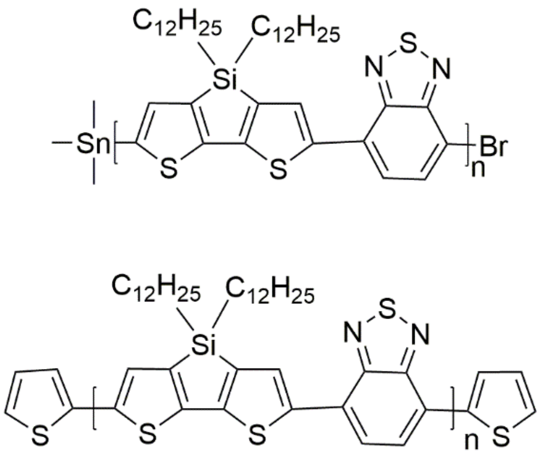

Figure 41 Structures of polymers with no terminal ends and with thiophene ends

Reynolds group also highlighted the effect of end caps on the mobility of the polymers and morphology. For this purpose, dithienogermole - 2,1,3-benzothiadiazole copolymers (DTG-BDT) were synthesized with H end caps and tolyl end caps.(Figure 42) One order of magnitude higher mobility values were obtained for the tolyl terminated polymer which may be due to enhanced π-π stacking resulting in ordered fibrous structure. [85]

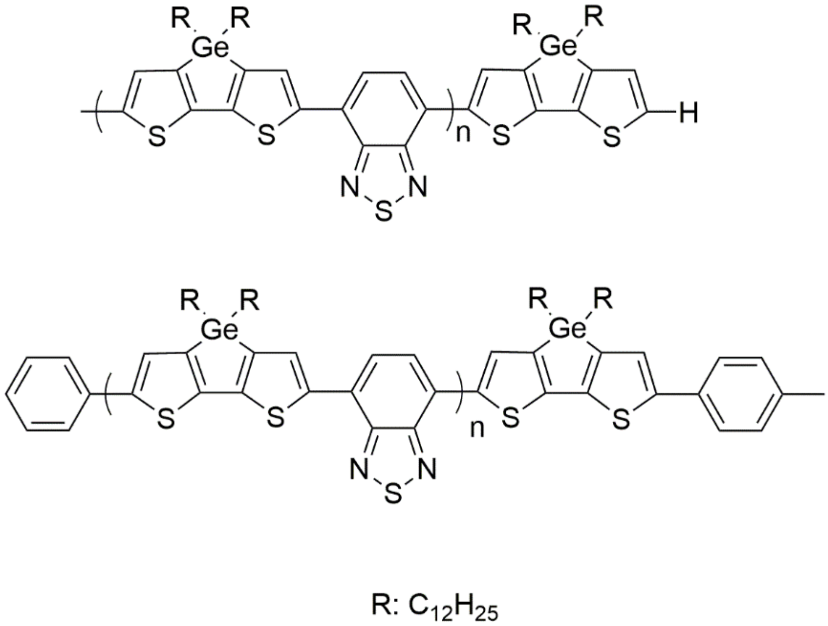

Figure 42 Structures of DTG-BDT copolymers with H and tolyl terminal ends

Kanbara and coworkers investigated the effect of terminal structure, purity and molecular weight of polymer. Experimental results showed that bromine terminal ends led to lower hole mobility and lower PCE values. Due to the amorphous nature of the polymer, effect of molecular weight had no influence on crystallinity, film morphology and the photovoltaic performance.[86] Structures of PEDOTF with bromine terminal end and H terminal end are depicted in Figure 43.

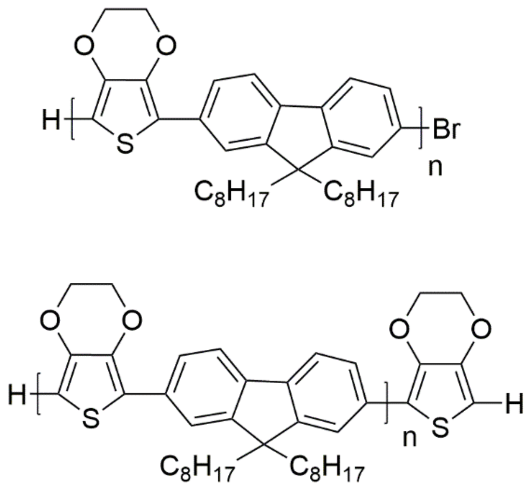

Figure 43 Structures of PEDOTF with bromine terminal end and H terminal end

In the light of these studies, it is concluded that both molecular weight and terminal structure have an impact on photovoltaic properties of polymers. These factors should be systematically investigated. However in literature effect of different terminal groups has not been examined. In this study, our aim is to figure out the effect of different terminal ends and molecular weight on the performance of PSCs.

4.2 Experimental

In this study, fluorene, benzotrizaole and thiophene bearing polymers with different terminal ends were synthesized via Suzuki Coupling reaction. Electrochemical and optical characterizations of the polymers were carried out. Details of these experiments were mentioned in Section 3.2.

4.3 Results and Discussion

In this study, fluorene, benzotrizaole and thiophene bearing polymers with different terminal ends and molecular weights were synthesized, structures of the polymers are depicted in Figure 44. Molecular weights (Mn - Mw) of polymers were determined as 9kDa -14kDa and 22kDa - 40kDa for P1 and P2, respectively.

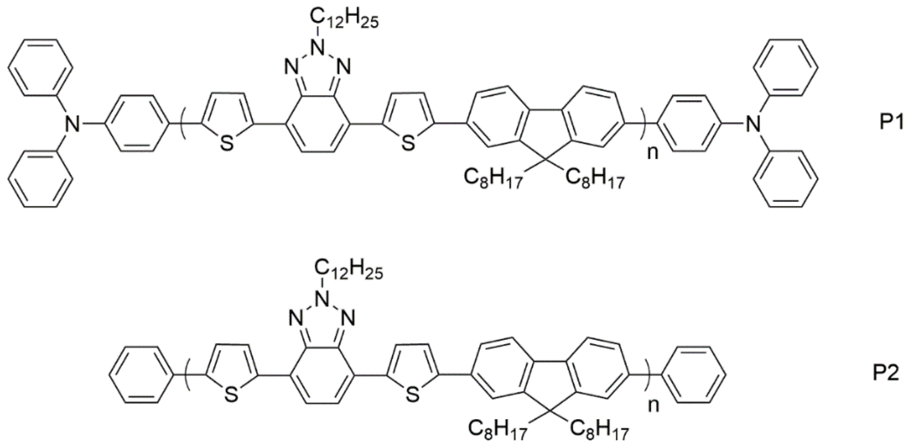

Figure 44 Structures of polymers P1 and P2.

Photovoltaic performance of the polymers were investigated with the device structure of ITO /PEDOT:PSS (V P Al 4083) / polymer:PC$_{71}$BM /LiF /Al. Polymer PCBM blends were prepared in different weight ratios. These blends were filtered through 0.22 µm pore sized PTFE filter. All polymer PCBM blends were dissolved in o-dcb. Polymer PCBM weight ratio was varied from 1:1 to 1:3. 1:2 P1:PCBM ratio showed PCE of 2.10% with a V$_{OC}$ value of 0.90 V, a J$_{SC}$ value of 5.98 mA/cm^2 and a FF of 0.39. Optimization studies are reported in Table 3 and corresponding J-V curve is shown in Figure 45 Neither thermal annealing, addition of additives nor MeOH treatment improve PCE of P1 based PSCs.

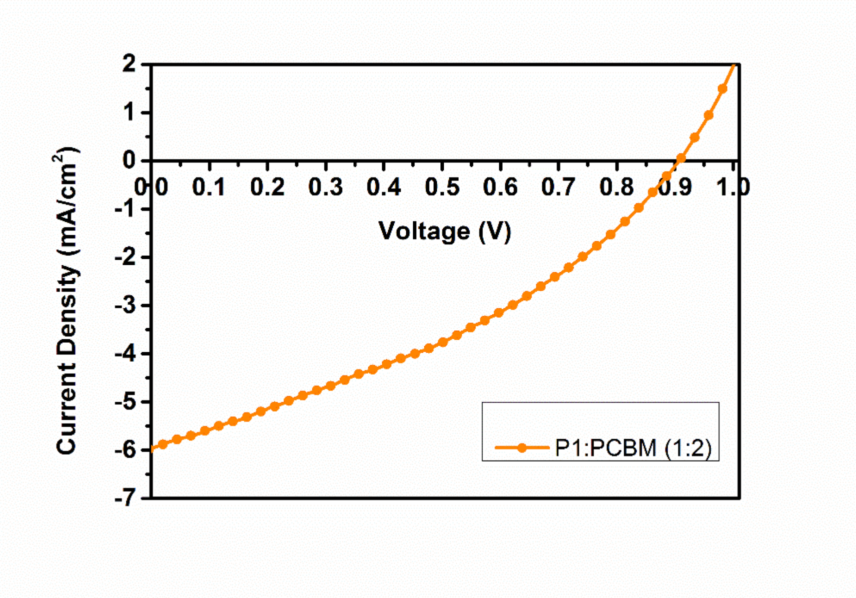

Figure 45 Current density (J) vs. voltage (V) characteristic for P1 based solar cells

Table 3 Summary of photovoltaic parameters for P1 based PSCs

Polymer:PC$_{71}$BM	**V$_{oc}$ (V)**	**J$_{sc}$ (mA/cm^2)**	**FF**	**PCE (%)**	**Thickness (nm)**
P1:PCBM (1:1)	0.90	5.67	0.36	1.84	100
P1:PCBM (1:2)	0.90	5.98	0.39	2.10	102
P1:PCBM (1:3)	0.90	5.83	0.38	1.99	134

For the optimization studies of P2, polymer PCBM weight ratio was varied from 1:1 to 1:3. 1:2 polymer PCBM blend achieved the highest power conversion efficiency of 2.59% with a V_{OC} value of 0.93V, J_{SC} of 5.07 mA/cm^2 and a FF of 0.55. Upon 1% DIO (1,8-diiodo octane) addition efficiency of the cell was improved to 3.55% through mainly a rise in FF values. DIO selectively dissolves PCBM and leads to intercalation of PCBM into polymer domains. Thus it reduces the domain size.[87] For efficient exciton dissociation, nanophase separated interconnected network morphology is required. MeOH treatment was also carried out to remove residual DIO and led to further improvement of PCE values. 4.11 % PCE value was achieved with a V_{OC} value of 0.99 V, a J_{SC} value of 6.59 mA/cm^2 and a FF of 0.63. J-V curves are depicted in Figure 46 and photovoltaic parameters are summarized in Table 4.

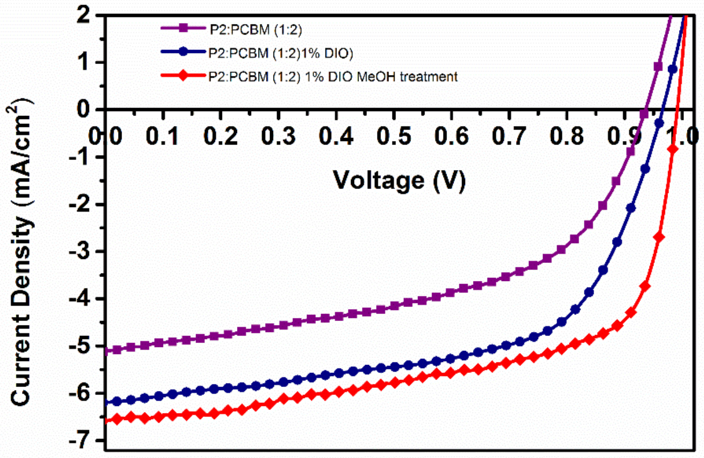

Figure 46 Current density (J) vs. voltage (V) characteristics for P2 based solar cells

Table 4 Summary of photovoltaic parameters for P2 based PSCs

Polymer:$PC_{71}BM$	V_{OC} (V)	J_{SC} (mA/cm^2)	FF	PCE (%)	Thickness (nm)
P2:PCBM (1:1)	0.93	4.60	0.50	2.14	108
P2:PCBM (1:2)	0.93	5.07	0.55	2.59	132
P2:PCBM (1:3)	0.93	3.99	0.55	2.04	117
P2:PCBM (1:2) DIO	0.97	6.19	0.59	3.55	148
P2:PCBM (1:2) DIO MeOH treatment	0.99	6.59	0.63	4.11	148

P2 based PSCs showed better performance than P1 based PSCs. Both effect of molecular weight and terminal units may lead this performance improvement. In order to figure out which factor was more dominating, benzene end capped polymer with lower molecular weight (Mn:8kDa Mw:13kDa) was synthesized. P3 comprising polymer solar cells showed PCE of 2.05% with a V_{OC} value of 0.81V, J_{SC} of 6.20 mA/cm^{-2} and a FF of 0.55. Table 5 summarizes the photovoltaic parameters of P1, P2 and P3 based polymer solar cells. Same polymer was previously synthesized in our group without end cappers with a Mn value of 7kDa and Mw of 17kDa. 0.56% PCE value was achieved with a V_{OC} of 0.60 V, FF of 0.28 and a J_{SC} value of 3.40 mA/cm^2.[88,89]

Table 5 Summary of photovoltaic parameters for P1, P2, P3, P4 based PSCs

Polymer	**Mwt**	**V_{OC} (V)**	**J_{SC} (mA/cm^2)**	**FF**	**PCE (%)**	**Thickness (nm)**
P1 (TPA)	9-14kDa	0.93	4.60	0.50	2.14	108
P2 (B)	22-40kDa	0.93	5.07	0.55	2.59	132
P3 (B)	8-13kDa	0.93	3.99	0.55	2.04	117
P4 (X)	7- 17kDa	0.60	3.40	0.28	0.56	----

EQE of the best performance PSCs based on P1, P2 and P3 were investigated. EQE measurements were performed to determine how efficiently a solar cell converts sunlight into electricity. Details of this experiment were mentioned in Section 2.4. EQE of the best performance PSCs based on P1, P2 and P3 were investigated and depicted in Figure 47. The EQE for P1 based PSC was determined as %52.29 at 470 nm. P2 incorporated PSC showed a maximum EQE at 470 nm with 46.43%. The maximum EQE in a cell composed of P3 was measured as 45.57 % at 480 nm.

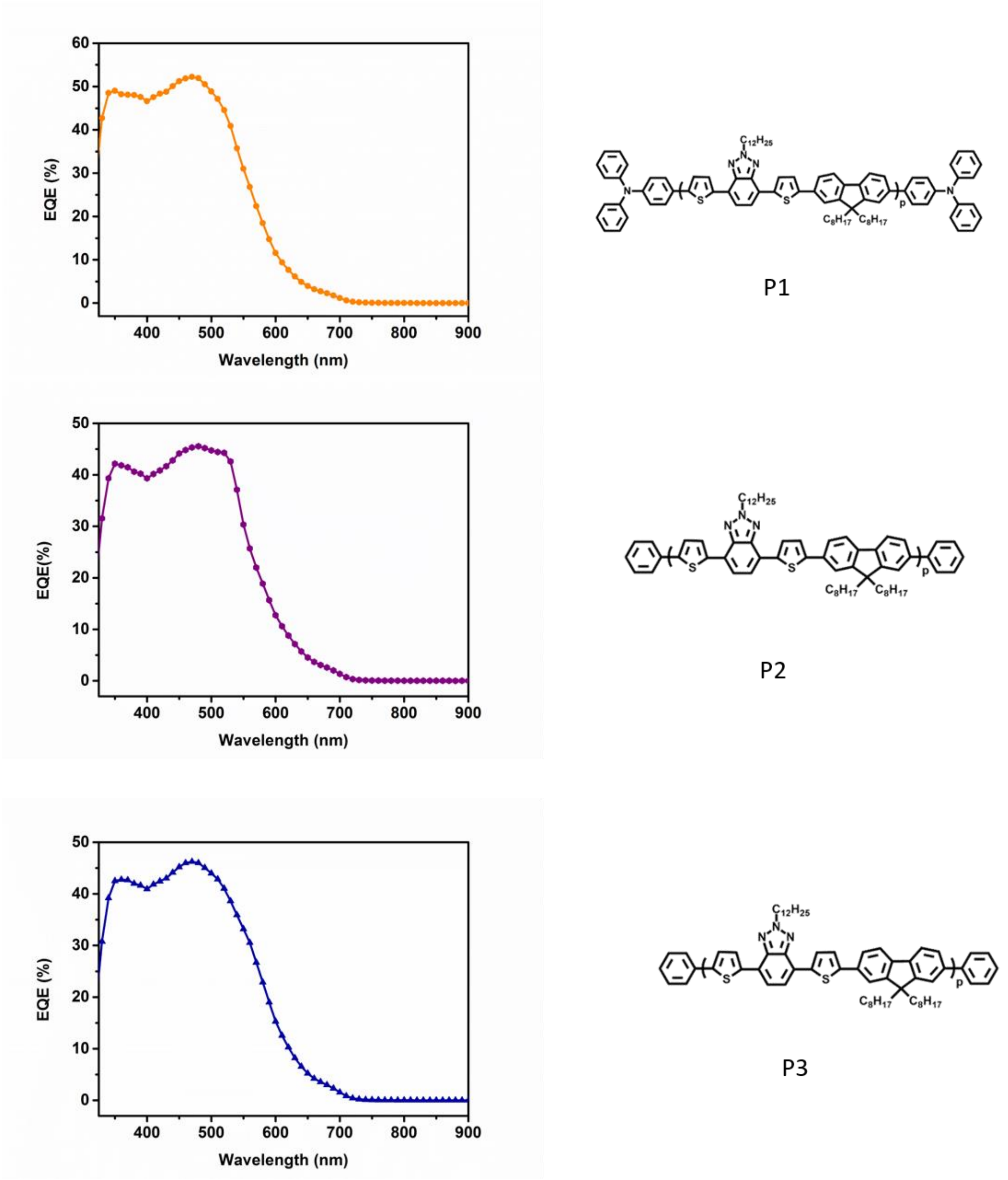

Figure 47 EQE of P1, P2 and P3 incorporated PSCs

The effect of molecular weight on the performance of PSC morphologies of the active layers were investigated with TEM and AFM analyses.

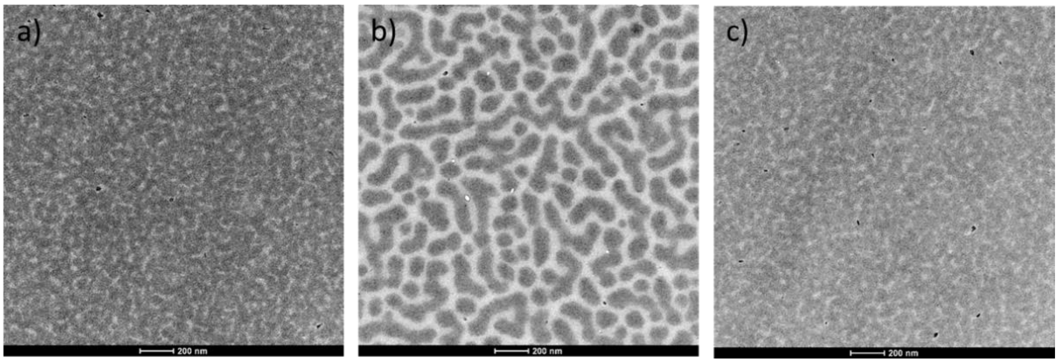

Figure 48 TEM analyses of a) P1:$PC_{71}BM$ blend b) P2:$PC_{71}BM$ blend c) P3:$PC_{71}BM$ blend with a scale bar of 200nm

As seen in Figure 48, for all the blends donor acceptor phase separation was observed. In Figure 48b which is the TEM image of P2:$PC_{71}BM$ blend, phase separation is more obvious and phases are bigger than the phases in 48a and 48c.

For a better understanding of the active layer morphologies, TEM images were also taken with different magnifications. Figure 49 demonstrates the TEM images with different magnifications.

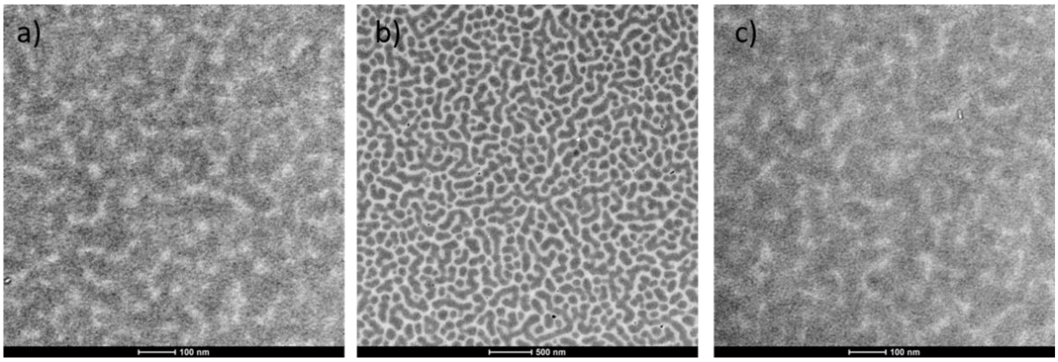

Figure 49 TEM analyses of a) P1:PC71BM blend with a scale bar of 100nm b) P2:PC71BM blend with a scale bar of 500nm c) P3:PC71BM blend with a scale bar of 100nm

In blends of P1:PC$_{71}$BM and P3:PC$_{71}$BM domain sizes are smaller than the domain sizes of P2:PC$_{71}$BM blend which is advantageous for charge separation. However more interconnected domains in Figure 49b leads to enhanced charge transport thus higher FF values.[90]

In order to investigate the surface topographical properties, AFM analyses were carried out. Figure 50 demonstrates the AFM analyses of a) P1:PC$_{71}$BM blend b) P2:PC$_{71}$BM blend c) P3:PC$_{71}$BM blend with a scale bar of 400nm

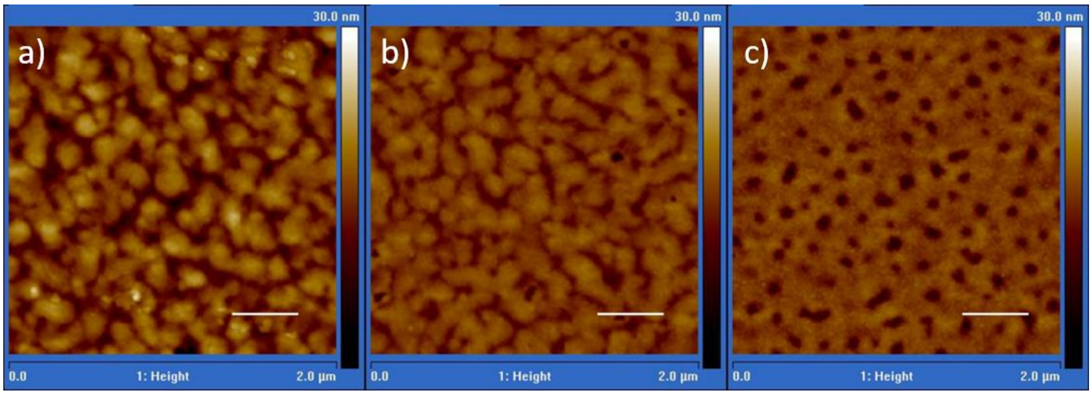

Figure 50 AFM analyses of a) P1:PC$_{71}$BM blend b) P2:PC$_{71}$BM blend c) P3:PC$_{71}$BM blend with a scale bar of 400nm

Surface roughness of P1:PC$_{71}$BM, P2:PC$_{71}$BM, P3:PC$_{71}$BM blends were determined as 2.94nm, 1.90nm, 2.54nm, respectively.

In the light of these studies, it is concluded that bromine terminal groups are detrimental for PSC performance. However, incorporation of different terminal units such as TPA or benzene has almost no effect on photovoltaic properties. On the other hand, higher molecular weight polymer showed superior photovoltaic performance mainly due to high fill factor values which depends on the donor acceptor morphology and mobilities of charge carriers

CHAPTER 5

SYNTHESIS, ELECTROCHEMICAL CHARACTERIZATIONS AND PHOTOVOLTAIC STUDIES OF ELECTROCHEMICALLY SYNTHESIZED POLYMERS

5.1 Introduction and Aim of Work

The name “polymer” is derived from Greek word “poly” which means many and “mer” which means part. The word polymer was first used by Berzelius in 1833.[91] Carothers classified polymers into two main groups according to repeating unit of the polymer whether it has the same atoms or not. Due to formation of by products, condensation polymers have fewer atoms, whereas addition polymers have the same atoms. The corresponding polymerizations are called step growth (condensation) and chain growth (addition) polymerizations which are the two main mechanisms involved in the polymer synthesis.[92]

Chain growth polymerization involves three main steps. Initiation starts with reaction between monomer and initiator which can lead to a radical, cation or anion. The activated monomer reacts with another monomer or polymer chain. The process of addition of monomers to the growing chain continues until monomer is depleted or termination reaction renders the chain end as inactive via combination or disproportionation. During the course of the chain polymerization molecular weight of the polymer is constant, as time passes, yield of the reaction increases.

Step growth polymerization involves stepwise reaction between the reactive groups of bifunctional monomers. In this polymerization, multifunctional monomers react to form dimers, trimers and higher oligomers. Polymerization rate decreases when the functional groups are depleting. In addition to this, increased viscosity of the reaction medium reduces the mobility of the reactive groups hence, decreases the rate of polymerization. In contrast to chain growth polymerization, high molecular weight polymers are formed at the high degree of polymerization.

Metal catalyzed cross coupling reactions that are used for synthesis of conducting polymers are following the step growth polymerization mechanism. Suzuki and Stille cross coupling reactions are the most commonly used polymerization reactions. Synthetic routes that are followed for the synthesis of conjugated polymers are mentioned in Table 6. Table 6 summarizes the reactants and catalysts of Stille, Suzuki, Negishi / Rieke, Kumada / McCullough, Direct Arylation, Heck, oxidative coupling, Knoevenagel and Wittig /Horner –Wadsworth –Emmons polymerization reactions.

Table 6 Synthetic routes for the synthesis of conducting polymers

REACTIONS	**REACTANTS**	**CATALYST**
STILLE	R_3Sn- Ar – SnR_3 Br- Ar’- Br	Pd complex
SUZUKI	$(RO)_2B$ – Ar – $B(OR)_2$ Br- Ar’- Br	Pd complex
NEGISHI / RIEKE	Br-Zn- Ar - Br	Ni complex
KUMADA / MCCULLOUGH	Br-Mg - Ar - Br	Ni Complex
DIRECT ARYLATION	Ar Br –Ar’ - Ar	Pd complex
HECK	CH_2 = CH – Ar – CH = CH_2 Br –Ar’ - Ar	Pd complex
OXIDATIVE COUPLING	Ar $FeCl_3$	-----
KNOEVENAGEL	CHO - Ar - CHO EWG - CH_2- Ar’ - CH2 - EWG	t- BuOK
WITTIG /HORNER – WADSWORTH - EMMONS	CHO - Ar - CHO $(RO)_2POCH_2$ - Ar – CH2PO$(OR)_2$	t- BuOK

One of the most important milestone in conducting polymer research was the discovery of conductivity of polythiophene [93] and development of its soluble, processable counterparts poly (3-alkylthiophenes).[94] For poly (3-alkylthiophenes) (P3AT) there are three possible connections between the alkylthiophene units. These are head-to-tail (H–T), head-to-head (H–H) or tail-to-tail (T–T) connections. Possible connections are shown in Figure 51.

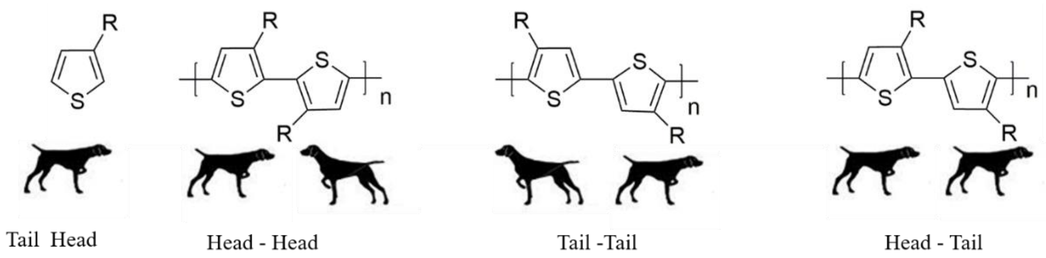

Figure 51 Overview of head to head (H-H), tail to tail (T-T) and head to tail (H-T), connections for P3AT

The polymers that followed the strict head to tail orientation are called regioregular (RR) polymers whereas regiorandom polymers comprise a mixture of head to tail, tail to tail and head to head orientations. Percentage of head to tail connections in the polymer backbone defines the regioregularity of the resulting polymer.

Studies proved that regioregular P3As showed superior crystallinity and electrical conductivity compared to regiorandom counterparts. For this purpose synthetic pathways yielding highly regioregular polymers were investigated by scientists.

McCullough and coworkers reported the synthesis of highly regioregular poly 3-alkylthiophenes using Grignard reagent and Ni catalyst for polymerization.[95,96] Figure 52 indicates the synthetic pathway for the synthesis of RR-P3AT.

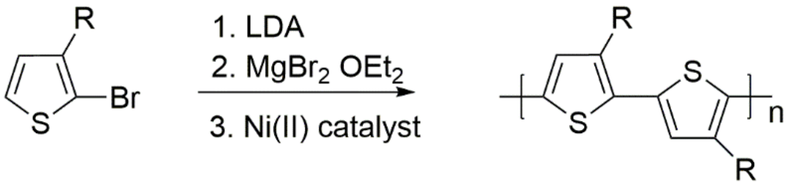

Figure 52 Synthetic pathway for the synthesis of RR-P3AT.

Rieke introduced a new synthetic method which uses activated Zinc (Rieke Zinc) to control regioregularity of the polymerization. 98.5% regioregularity was afforded with Rieke method.[97] Figure 53 indicates the synthetic pathway for the synthesis of RR-P3AT.

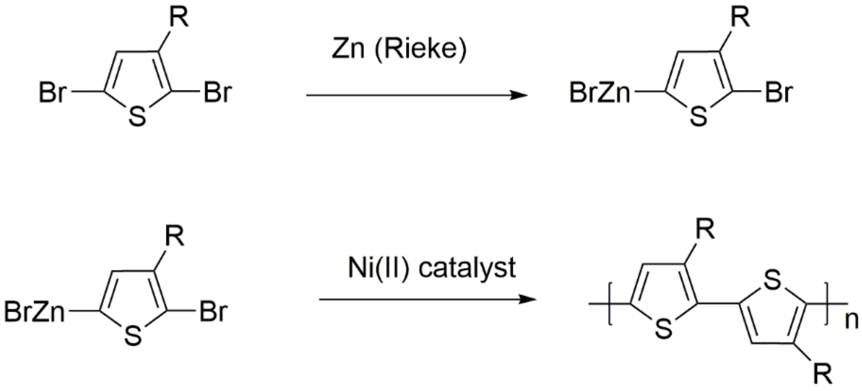

Figure 53 Synthetic pathway for the synthesis of RR-P3AT.

As mentioned in Table 5, Figure 52 and Figure 53 most of the routes that are followed in synthesis of conjugated polymers employ Pd or Ni catalysts and bromine functionalized starting materials. Usage of heavy metal catalysts and chlorinated solvents make these processes environmentally unfriendly and increase the cost of polymer production. Moreover, residues of these materials are detrimental for the operation of organic electronic devices based on conjugated polymers.

For commercialization of conjugated polymer based devices like PLEDs, PSCs and OFETs, efficiency, stability, scalability and cost issues should be solved. As mentioned in Section 1.5 versatility of organic chemistry has been used to improve efficiency and stability of the devices. However with the methods followed in synthesis of conjugated polymers it is very hard to obtain high amounts of polymers. At this point, we propose an environmentally friendly, cheap, easy way of producing substantial amount of polymers via electrochemical polymerization.

In literature there are enormous amount of works on the electrochemical synthesis of conducting polymers. However, polymers produced with electrochemical ways are usually insoluble in common organic solvents. There were very few studies reporting the synthesis of partially soluble polymers via electrochemistry.

Kaeriyama and co- workers electrochemically synthesized P3Alkyl thiophenes. In this study, poly(3-hexylthiophene) (PHT), poly(3-octylthiophene) (POT), poly(3-dodecylthiophene) (PDDT), poly(3-octadecylthiophene) (PODT) and poly(3-eicosylthiophene) (PEIT) were synthesized electrochemically. Structures of the corresponding polymers are depicted in Figure 54. Nitrobenzene was used as the solvent and tetraethylammonium hexafluorophosphate was used as the supporting electrolyte. The conductivities of PHT, POT, PDDT, PODT and PEIT were determined as 95, 78, 67, 17 and 11 S/cm in their oxidized form. The degrees of polymerization of PHT, POT and PDDT were calculated as $2.3x10^2$, $1.4x10^2$ and 9x10. Authors concluded that polymers with shorter pendant alkyl chains had higher degree of polymerization. Oxidized polymers were insoluble or had very limited solubility whereas neutral polymers were partially soluble in chloroform and benzene. PDDT had the highest solubility among the polymers due to its low molecular weight and long alkyl chains.[98]

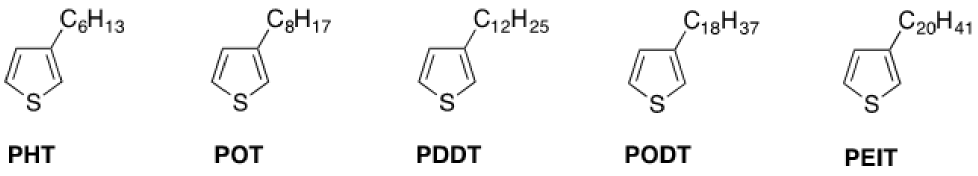

Figure 54 Structures of electrochemically synthesized polymers

Wei and coworkers also worked on electrochemical polymerization of thiophene and alkyl thiophenes. It was reported that with the addition of bithiophene and terthiophene to the polymerization medium, rate of polymerization increased and the necessary potential for polymerization decreased. Since the oxidation of monomer is the slowest and the rate determening step in polymerization, addition of dimers to the system bypasses this step and increases the rate of polymerization.[99]

Bedi and Zade reported the polymerization of thiophene and selenophene capped 7,8-didodecyloxybenzo[1,2-b:4,3-b′]dithiophene on Pt disks via electrochemical ways as depicted in Figure 55. Resulting polymers were soluble in THF. Effect of thiophene and selenophene incorparation on electronic and optical properties of benzodithiophene bearing polymers were investigated.[100]

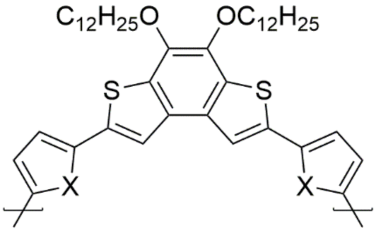

Figure 55 Electrochemically polymerized benzodithiophene derivatives where X is S or Se

These studies reported the production of partially soluble polymers via electrochemical means. However in none of these studies electrochemically produced polymers were used in photovoltaic applications. To the best of our knowledge this is the first study in the literature, where polymers that are produced by electrochemical means are used in photovoltaic studies. This study will open the way for synthesis of conjugated polymers with high purity and low cost.

5.2 Electrochemical Synthesis of Polymers

In this study P3ATs were synthesized via electrochemical ways. Structures of the polymers are depicted in Figure 56

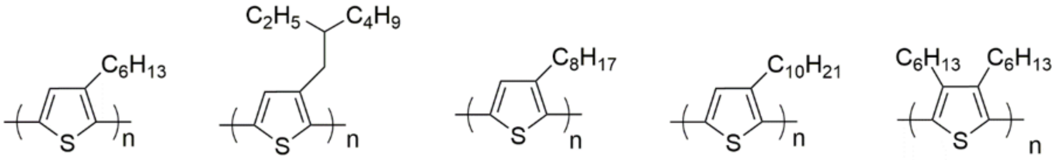

Figure 56 Structures of electrochemically synthesized polymers

For the synthesis of polymers platinum (Pt) electrodes were used as the working and counter electrodes and a silver (Ag) wire was used as the reference electrode. Tetrabutylammonuium hexafluorophosphate was used as the supporting electrolyte. As the solvent nitromethane was used. For electrochemical polymerization potentiostatic, galvanostatic, or cyclic potential sweep methods can be used. In this study, potential sweep technique was employed. Even though this method takes a longer time, it is more preferred due to easy control of electrochemical characteristics of the polymers.[99] During electrochemical polymerization some unwanted defects like cross linking and mislinkages may form as shown in Figure 57. With potential sweep technique formation of these defects are minimized.

Second precaution is the use of functionalized thiophenes at 3 - position to prevent crosslinking from this position.

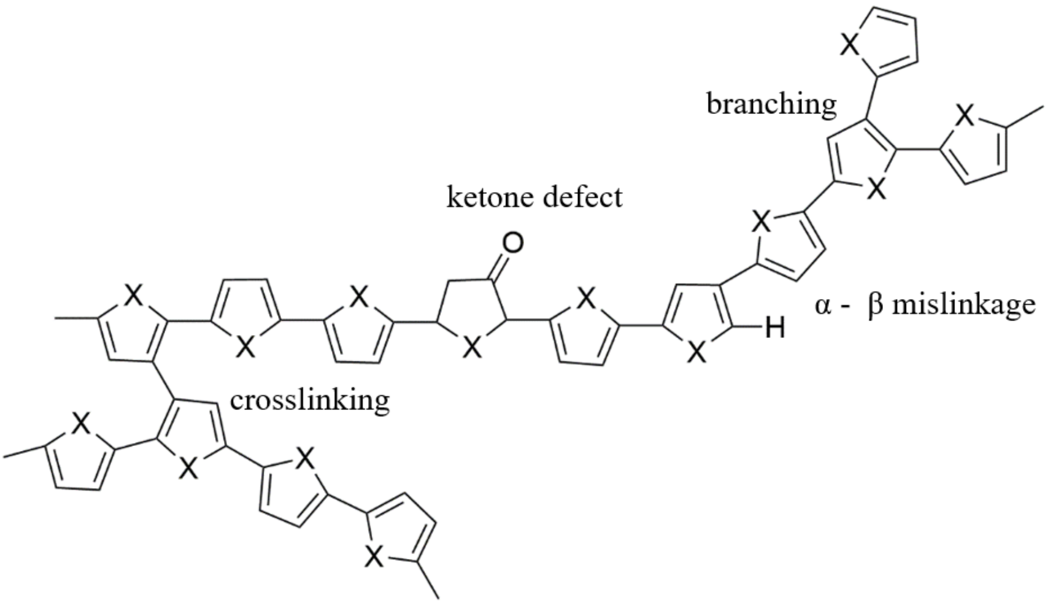

Figure 57 Possible defects that can be formed in the course of electrochemical polymerization

Before starting electrolysis N_2 gas purged in the cell, then potential was swept between 0.5V to 1.7V. As polymerization proceeded, polymer film was coated on Pt electrode. After polymerization was completed, polymer coated Pt electrode was immersed in hydrazine solution and polymer was peeled off. Since the polymer obtained with electrolysis was in oxidized form, hydrazine was used as the reducing agent and reduced the polymer into neutral form. In order to remove the excess supporting electrolyte, polymer was washed with methanol (MeOH). Since Pd catalysts, stanylated, brominated compounds are not used, there is no need for Soxhlet extraction. After washing with MeOH, polymer was kept in vacuum oven at 40˚C for 2 days. Experimental set up for the electrochemical synthesis of polymers is depicted in Figure 58

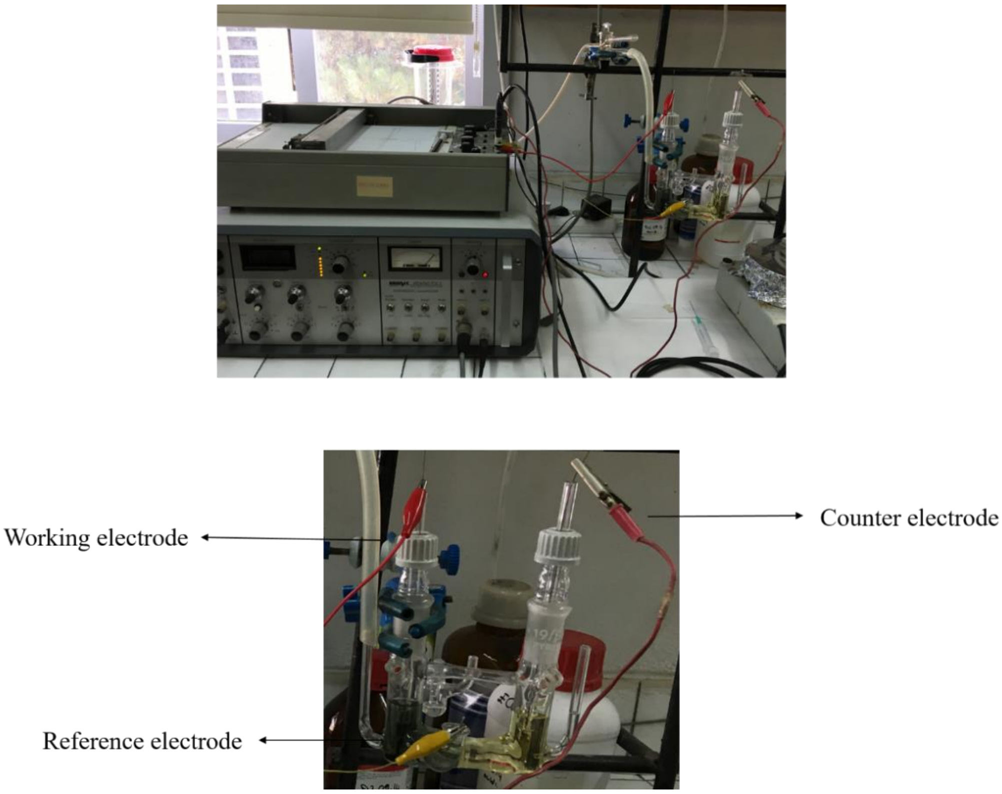

Figure 58 Experimental set up for the electrochemical synthesis of polymers

5.3 Results and Discussion

3-Hexylthiophene, 3-ethylhexylthiophene, 3-octylthiophene, 3-decylthiophene and 3, 4-dihexylthiophene were polymerized using electrolysis. Electrochemical polymerization follows E (electrochemical) – C (chemical) – E mechanism. This mechanism is stated in Figure 59.

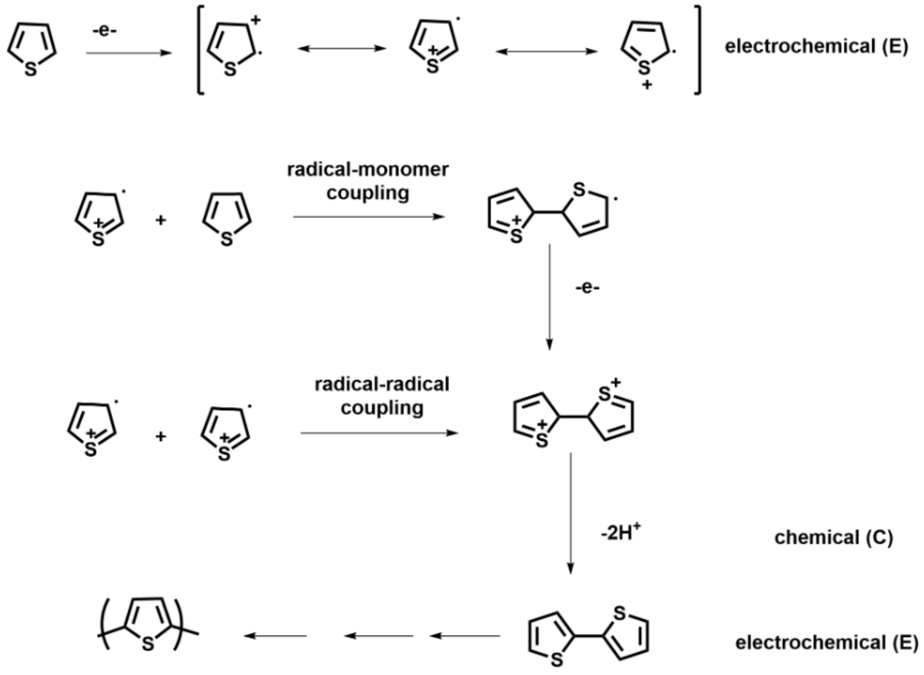

Figure 59 E-C-E mechanism of electrochemical polymerization

Electrochemical polymerization is initiated with an applied potential which leads to the oxidation of monomer via release of an electron. Radical cation formed at this step is resonance stabilized. (E) Second step is a chemical reaction between either two radical cations formed at the first step or between a radical cation and monomer. Formed dications lose two protons and neutral dimers are formed. At further steps, formed dimer is preferentially oxidized due to is lower oxidation potential compared to monomer oxidation potential. For the electrochemical polymerization of P3AT derivatives, potential was swept between 0.5V and 1.7V. Electropolymerization via cyclic voltammetry is depicted in Figure 60. As the electrochemical polymerization continues, in the successive cycles current value increases which proves the polymer film growth on the working electrode. In addition to current raise, potential values are also shifted. Potential shift can be attributed to heterogeneous electron-transfer kinetics, reduced mobility of counter ions and conductivity of the film. For the P3HT, P3OT and P3DecT, doping dedoping peaks are broad which can be attributed to the slow diffusion of dopants in and out of the polymer film.

Monomer oxidation peaks were not observed in the electrochemical polymerization cyclic voltammetries as depicted in Figure 60. The resaon behind the formation of monomer oxidation peak is the depletion of the electroactive monomer in the diffusion layer thus the current decreases and peak formation is observed. If formed dimers, trimers have high electroactivity, concentration of electroactive species will not deplete in diffusion layer thus current will not drop and peak is not observed.

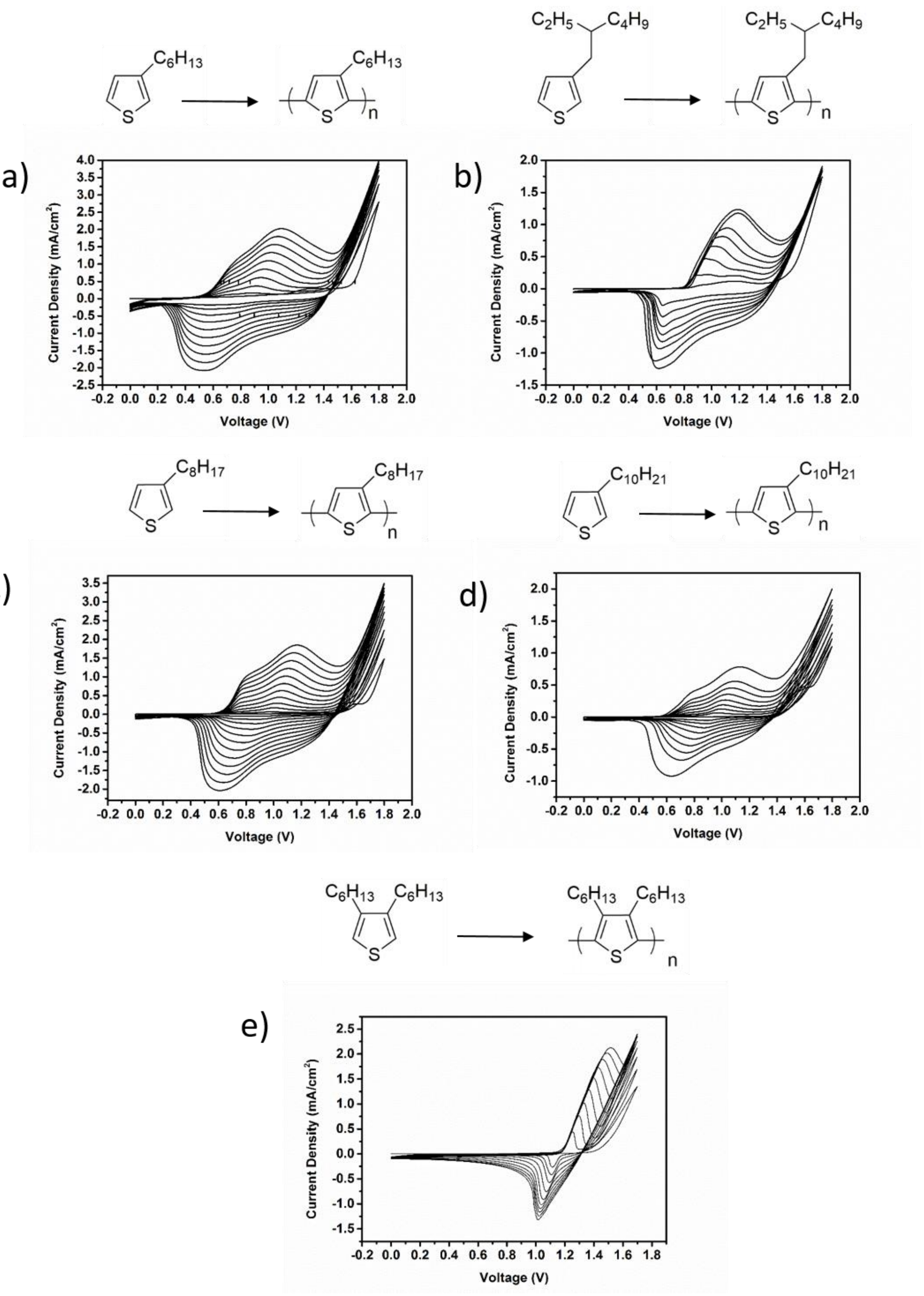

Figure 60 Repeated potential scan electropolymerizations of a) 3-Hexylthiophene b) 3-Ethylhexylthiophene c) 3-Octylthiophene d) 3-Decylthiophene e) 3, 4-Dihexylthiophene at 250mV/s in 0.1 M $TBAPF_6$ on platinum electrode.

Molecular weights (Mn, Mw) of polymers were determined as 43-125kDa, 6-16kDa, 17-20kDa, 33-104kDa and 32-98kDa for P3HT, P3EHT, P3OT, P3DecT and PDHT, respectively. In order to investigate the electronic properties of the polymers cyclic voltammetry studies were carried out in a monomer free environment. (Figure 61) Acetonitrile was used as the solvent, $TBAPF_6$ was used as the supporting electrolyte. Potential was swept between 1.7V and -2.3V (-2.65 V for P3DecT) versus Ag wire reference electrode. The first run of P3HT resulted in a reversible redox couple at positive potentials peaked at 1.05 V and 0.74 V which is 1.04 - 0.72V, 1.54 - 0.69, 1.11 - 0.68V, 1.45 -1.01 for P3EHT, P3OT, P3DecT and PDHT, respectively. All polymers showed ambipolar character except P3EHT and PDHT. Steric hindrance arising from branched alkyl chain of the P3EHT and excess alkyl chains of the PDHT may impede n doping property. Reduction of the P3HT was realized at -2.22 V with a reversible dedoping peak at -1.91 V. Whereas n doping of P3OT was observed at -2.45V with a dedoping at -1.56V. Since P3DecT possesses the longest alkyl chains, redox for P3DecT were observed at relatively higher potentials (-2.08 V/-1.57 V) compared to those of other P3AT analogs.

Oxidation and reduction onset values were used to calculate the HOMO–LUMO energy levels of the polymers from the cyclic voltammetry experiment. Reduction and oxidation onset values were estimated by taking the intersection between the base line and the tangent drawn to the increasing part of the current (Explained in section 2.3 in detail.) HOMO – LUMO energy levels were calculated relative to the vacuum level, considering that the value of NHE is - 4.75 eV vs. vacuum.[101]

Electronic band gap values were calculated for the polymers showing ambipolar property. It is basically the energy gap between the HOMO and LUMO levels.

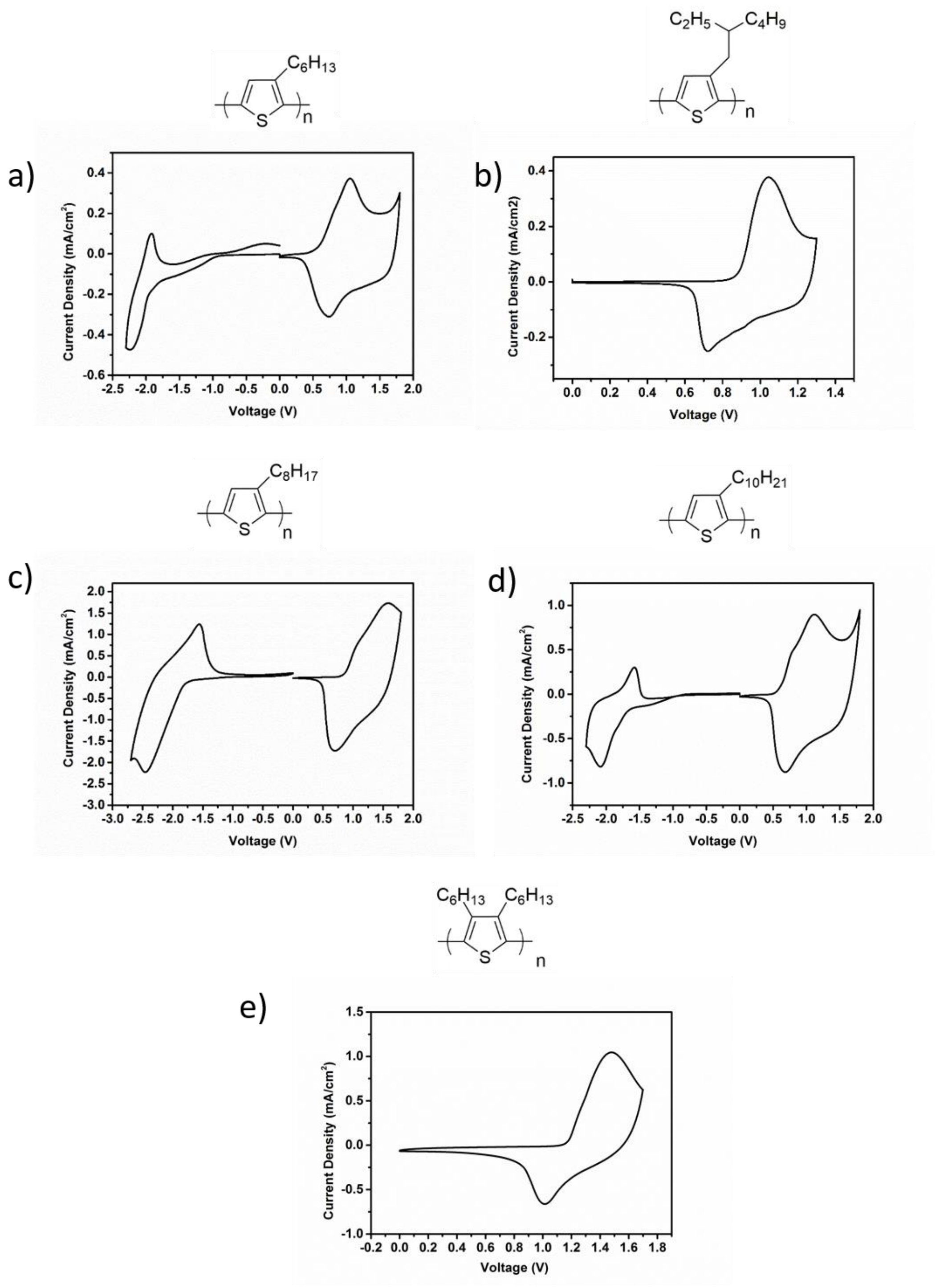

Figure 61 Cyclic voltammetry of a) P3HT b) P3EHT c)P3OT d) P3DecT e) PDHT in the presence of 0.1 M $TBAPF_6$.

UV-Vis absorbance spectra of the polymers both in solution and thin film forms are shown in Figure 62. π- π* transitions of the polymers in solution are at 446, 437, 447, 443, 320nm for P3HT, P3EHT, P3OT, P3DecT and PDHT, respectively. For the thin films lowest energy electronic transitions are positioned at 495, 443, 502, 476, 325 nm for P3HT, P3EHT, P3OT, P3DecT and PDHT respectively. Table 7 summarizes the optical properties of the polymers. For all polymers, red shift in thin film absorbance spectra compared to solution spectra was observed. This is expected and due to reduced conformational freedom, diminished polymer solvent interactions and tendency to aggregation in thin film form.[102] In the case of P3EHT 5nm shift was observed which shows the minority of aggregation in thin film form. Branched alkyl chains attached to the polymer backbone in P3EHT may prevent aggregation in thin film form. Optical band gap values were calculated from the absorption onset values using Equation 8 as mentioned in Section 2.4.3.

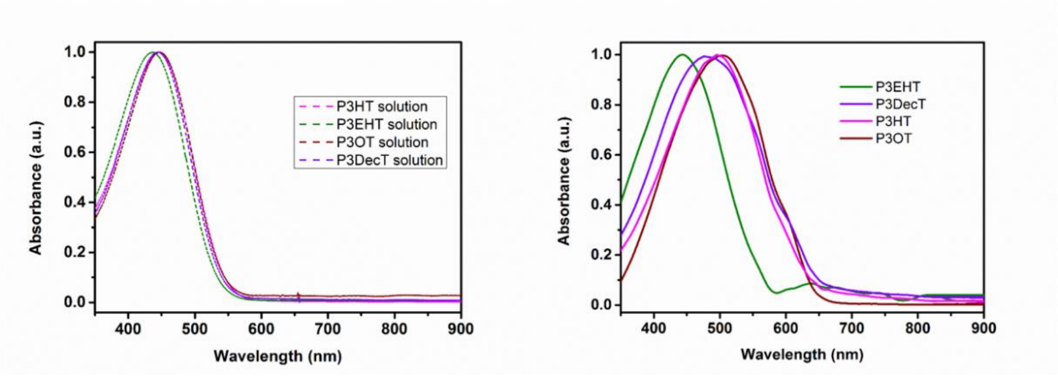

Figure 62 Absorption spectra of polymers in solution and in thin film form

Table 7 Summary of the optical properties of the polymers

Polymer	**λ_{max} solution**	**λ_{max} thin film**	**onset**
P3HT	446	495	634
P3EHT	437	443	587
P3OT	447	502	646
P3DecT	443	476	648
PDHT	320	325	430

Table 8 reviews oxidation and reduction potentials, onset values, HOMO and LUMO energy levels and band gaps of the polymers. As depicted in table, PDHT has the deepest lying HOMO energy level which is ascribed to the bulkiness of the alkyl chains. [103] As seen in Table 8, electronic band gap values are higher than the optical band gap values due to creation of free ions in the electrochemical synthesis of polymers.

Table 8 Summary of the electronic properties of the polymers

Polymers	**p doped**	**n doped**	**$E_{ox,onset}$ (V)**	**$E_{red,onset}$ (V)**	**HOMO (eV)**	**LUMO (eV)**	**Eg^{el} (eV)**	**Eg^{op} (eV)**
P3HT	1.05	-2.22	0.53	-1.77	-5.28	-2.98	2.30	1.96
	0.74	-1.91						
P3EHT	1.04		0.85		-5.60	-3.49		2.11
	0.72							
P3OT	1.54	-2.45	0.74	-1.76	-5.49	2.99	2.50	1.92
	0.69	-1.56						
P3DecT	1.11	-2.08	0.56	-1.63	5.31	3.12	2.15	1.92
	0.68	-1.57						
PDHT	1.45		1.14		-5.89	3.01		2.88
	1.01							

5.3.2 Photovoltaic studies

To the best of our knowledge this is the first study in literature where electrochemically synthesized polymers are utilized in photovoltaic devices. ITO /PEDOT:PSS / polymer:PCBM / LiF /Al device architecture was used to investigate the photovoltaic parameters. ITO was chosen as the transparent conducting oxide due to its excellent transparency and conductivity. PEDOT:PSS was used as the hole transport layer. It increases the work function of ITO and it also smoothes ITO layer. Polymer PCBM was blended at several weight ratios and spin coated to obtain interconnected nanophase separated D-A domains. Insertion of thin LiF layer leads to lowering the work function of Al metal, protection of active layer from hot Al in the course of evaporation and formation of a dipole moment across the active layer Al interface due to either chemical reactions resulting in charge transfer across the interface or orientation of the LiF.[104]

P3HT incorporated solar cells were processed from chlorobenzene (cb) and 1,2-dicholorobenzene (o-dcb). P3HT:PCBM (1:1) blend dissolved in chlorobenzene revealed V_{OC} of 0.51 V, J_{SC} of 4.03 mA/cm^2, FF of 0.30, and PCE of 0.62 % without any treatment. Whereas P3HT:PCBM (1:1) based device processed from o-dcb showed V_{OC} of 0.60 V, J_{SC} of 7.32 mA/cm^2, FF of 0.33, and PCE of 1.46 %. As seen, PCE values were enhanced from 0.62% to 1.46% through mainly a rise in current values which depends on absorption of light. Limited solubility of the polymer in chlorobenzene may lead to lower photocurrent values. As reported in Table 5.4, 0.51V V_{OC} value was obtained with chlorobenzene processed PSCs whereas 0.6V V_{OC} was obtained with dichlorobenzene processed PSCs. Either formation of different charge transfer states [105] and / or the dissolution of higher molecular weight polymer chains in dichlorobenzene may lead to improvement of V_{OC}. After solvent optimizations, polymer PCBM ratio optimizations were carried out. Polymer PCBM ratio was varied from 1:0.8 to 1:3 and 1:1 polymer PCBM ratio gave the best results for P3HT incorporated PSC. Optimization studies are reported in Table 9 and corresponding J-V curves are shown in Figure 63.

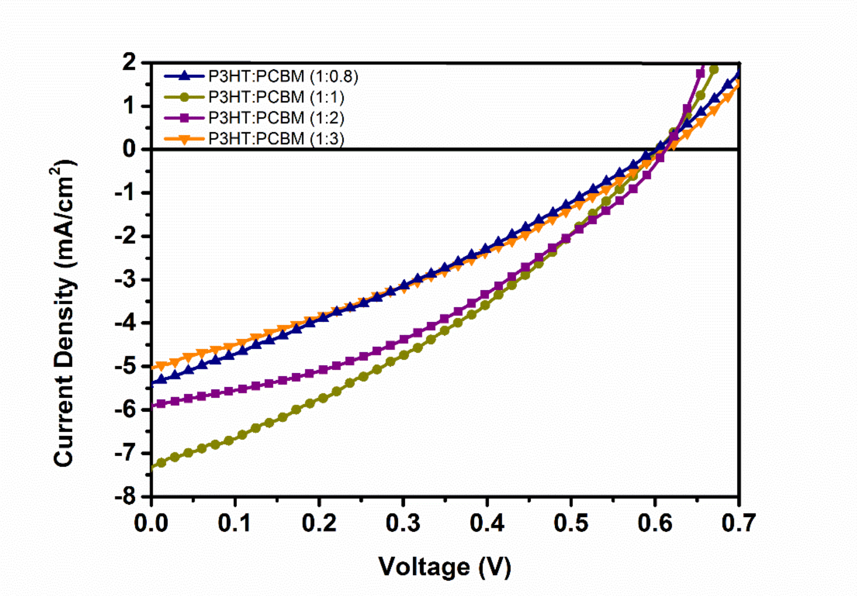

Figure 63 Current density (J) vs. voltage (V) characteristic for P3HT based solar cells

Table 9 Summary of photovoltaic parameters of PSC based on P3HT

P3HT:$PC_{71}BM$	solvent	V_{oc} (V)	J_{sc} (mA/cm^2)	FF	PCE (%)
(1:0.8)	dcb	0.60	5.38	0.30	0.97
(1:1)	dcb	0.60	7.32	0.33	1.46
(1:1)	cb	0.51	4.03	0.30	0.62
(1:2)	dcb	0.61	5.90	0.38	1.36
(1:3)	dcb	0.61	5.04	0.32	0.98

Photovoltaic performance of P3EHT was examined with the device structure of ITO /PEDOT:PSS / polymer:PCBM / LiF /Al. Primary to weight ratio optimization studies solvent optimization studies were carried out. P3EHT:PCBM blend processed from dichlorobenzene showed the best performance.

Polymer PCBM weight ratio was varied from 1:2 to 1:4. J-V curves are depicted in Figure 64 and photovoltaic parameters are summarized in Table 10. 1:3 polymer PCBM ratio showed PCE of 2.03% with a V_{OC} value of 0.83V, a J_{SC} value of 5.10mA/cm^2 and a FF of 0.48.

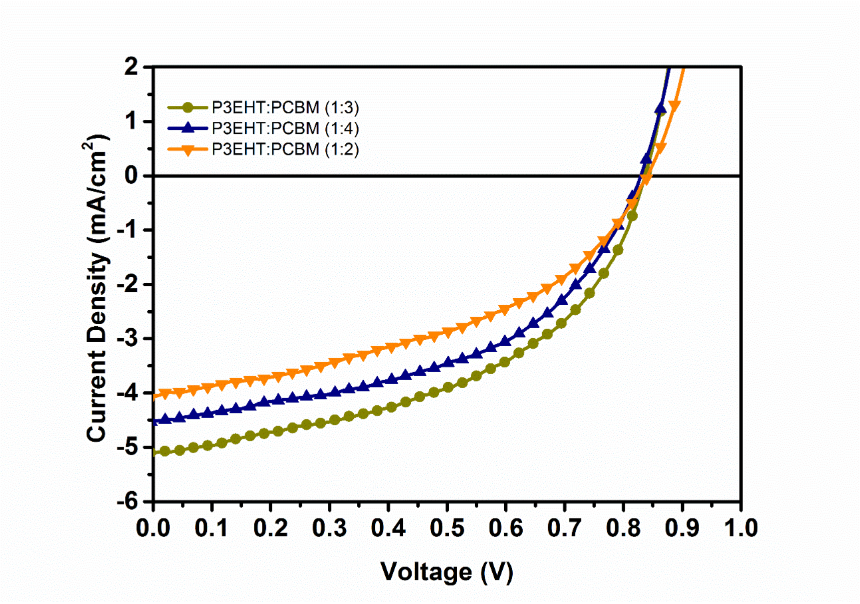

Figure 64 Current density (J) vs. voltage (V) characteristic for P3EHT based solar cells

Table 10 Summary of photovoltaic parameters of PSC based on P3EHT

P3EHT:PC$_{71}$BM	**solvent**	**V_{oc} (V)**	**J_{sc} (mA/cm^2)**	**FF**	**PCE (%)**
(1:2)	dcb	0.83	4.05	0.44	1.47
(1:3)	dcb	0.83	5.10	0.48	2.03
(1:3)	cb	0.61	2.02	0.30	0.37
(1:3)	tcb	0.60	1.75	0.41	0.43
(1:4)	dcb	0.83	4.51	0.49	1.81

Photovoltaic performance of P3OT was examined with the device structure of ITO /PEDOT:PSS / polymer:PCBM / LiF /Al. Due to limited solubility of the P3OT in dicholorobenzene, with blend of polymer PCBM (1:1) photovoltaic results cannot be obtained. Tricholorobenzene processed PSCs showed higher performance through mainly a rise in fill factor values which is an indication of better morphology obtained with tricholorobenzene. Polymer PCBM ratio was varied from 1:1 to 1:3 and 1:2 polymer PCBM ratio gave the best results for P3OT incorporated PSCs. 1.71 % PCE was achieved with V_{OC} value of 0.76V, J_{SC} of 5.11 mA/cm^2 and FF of 0.44. Photovoltaic results of PSC based on P3OT are reviewed on Table 11, corresponding J-V curves are depicted in Figure 65.

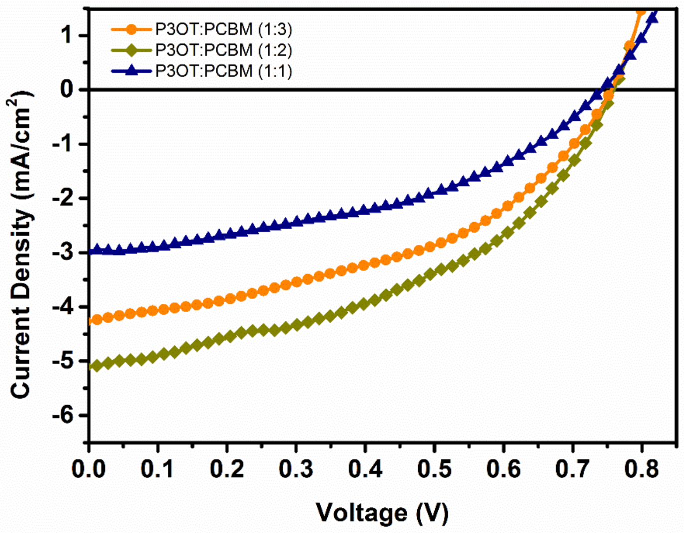

Figure 65 Current density (J) vs. voltage (V) characteristic for P3OT based solar cells

Table 11 Summary of photovoltaic parameters of PSC based on P3OT

P3OT:PC$_{71}$BM	**solvent**	**V$_{oc}$ (V)**	**J$_{sc}$ (mA/cm^2)**	**FF**	**PCE (%)**
(1:1)	odcb				-----
(1:2)	odcb	0.62	4.92	0.34	1.04
(1:3)	odcb	0.62	6.23	0.32	1.16
(1:1)	tcb	0.74	2.98	0.44	0.97
(1:2)	tcb	0.76	5.11	0.44	1.71
(1:3)	tcb	0.76	4.26	0.45	1.45

Preliminary photovoltaic studies of P3DecT was performed. Dicholorobenzene was used as the solvent. Polymer PCBM ratio was varied from 1:1 to 1:3. With 1:2 polymer PCBM ratio 0.95% PCE was obtained with a V_{OC} value of 0.65V, J_{SC} of 3.40 mA/cm^2 and FF of 0.43. Photovoltaic results of PSC based on P3DecT are reviewed on Table 12, corresponding J-V curves are depicted in Figure 66.

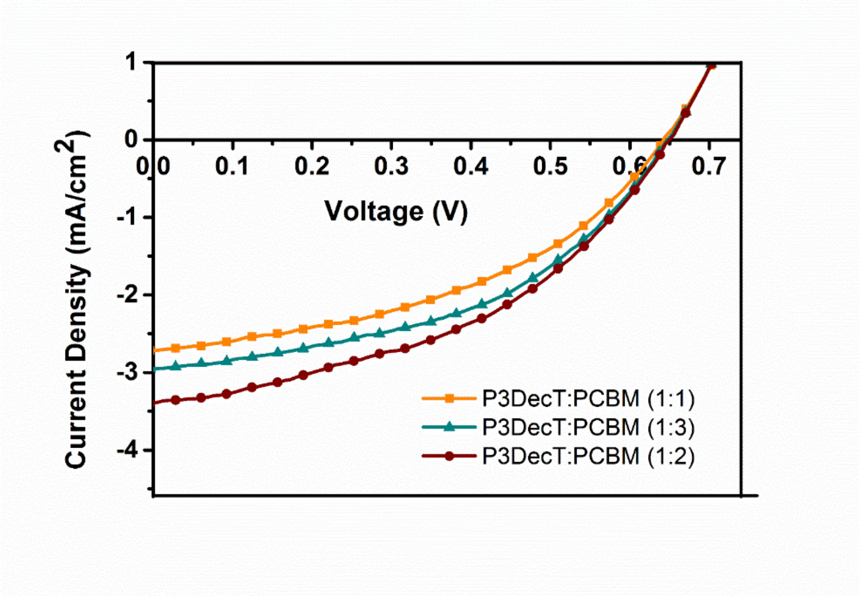

Figure 66 Current density (J) vs. voltage (V) characteristic for P3DecT based solar cells

Table 12 Summary of photovoltaic parameters of PSC based on P3DecT

P3DecT:PC$_{71}$BM	**V$_{oc}$ (V)**	**J$_{sc}$ (mA/cm^2)**	**FF**	**PCE (%)**
(1:1)	0.64	2.71	0.44	0.76
(1:2)	0.65	3.40	0.43	0.95
(1:3)	0.65	2.96	0.46	0.88

P3HT:PCBM based OPV are called “best seller in photovoltaic research” due to tremendous amount of papers mentioning P3HT based solar cells. Just in the year 2010, 1953 papers were published. Regioregular P3HT based devices showed the average power conversion efficiency of 3%.[20] Record efficiency of P3HT incorporated solar cells belongs to P3HT: ICBA (indene-C60-bisadduct) solar cells.

Without any additive, PCE of 4.12% was obtained with a V_{OC} of 0.87V, J_{SC} of 7.76mA/cm^2 and a FF of 0.61. With the addition of 1-chloronaphtalene (CN) solvent additive 7.4% PCE value was achieved with a V_{OC} value of 0.87V, J_{SC} value of 11.35mA/cm^2 and FF value of 0.75.[21] With non- fullerene acceptors P3HT based solar cells had the record PCE value of 6.4% [22]

As a result of this study, among P3alkylthiophenes, P3EHT revealed the highest photovoltaic performance. Photovoltaic parameters of best performance PSCs based on P3HT, P3EHT, P3OT and P3DecT P3EHT are summarized in Table 13. P3EHT incorporated PSCs had the highest V_{OC} values which is ascribed to low lying HOMO level of the P3EHT. Due to less electron donating nature of branched alkyl chains, P3EHT has lower HOMO energy level than P3HT. Moreover, branched alkyl chains lower the conjugation length of the polymers. Deep lying HOMO levels are favorable to obtain high VOC values, since it is proportional to the difference between the LUMO level of the acceptor and the HOMO level of the donor moiety.[106]

Highest JSC values were obtained in the P3HT incorporated PSCs. For P3HT, P3EHT, P3OT and P3DecT based best performance PSCs, J_{SC} values were 7.32 mA/cm^2, 5.10 mA/cm^2, 5.11 mA/cm^2 and 3.40 mA/cm^2, respectively. As the length of the alkyl chain attached to the 3 – position of thiophene ring increased, J_{SC} values were decreased. Due to enhanced d – space between the polymer chains as the length of the alkyl chain increases, hole mobilities of the resulting polymers decrease. [107,108] Decreased hole mobility of the polymers having long alkyl chains may be the reason for lower current values. However long alkyl chains improve the solubility of the polymers in organic solvents.

Table 13 Summary of photovoltaic parameters of best performance PSC based on P3HT, P3EHT, P3OT and P3DecT

P3AT:PC$_{71}$BM	**solvent**	**V_{oc} (V)**	**J_{sc} (mA/cm^2)**	**FF**	**PCE (%)**
P3HT(1:0.8)	dcb	0.60	7.32	0.33	1.46
P3EHT(1:3)	dcb	0.83	5.10	0.48	2.03
P3OT(1:2)	tcb	0.76	5.11	0.44	1.71
P3DecT(1:2)	dcb	0.65	3.40	0.43	0.95

IPCE measurements were performed to determine how efficiently a solar cell converts sunlight into electricity. Details of this experiment were mentioned in 2.4. After Si photodiode calibration, cell was illuminated by monochromatic light and photocurrent response of the cell was measured. The IPCE for P3HT based PSC was as %35.98 at 470 nm. P3EHT incorporated PSC showed a maximum IPCE at 470 nm with 37.24%. The maximum EQE in a cell composed of P3OT was measured as 39.05 % at 480 nm. The lowest maximum IPCE value among the four polymers was acquired for P3DecT as 20.71% at 470 nm which is consistent with the lowest photocurrent value. IPCE curves of P3HT, P3EHT, P3OT, and P3DecT based PSCs are depicted in Figure 67.

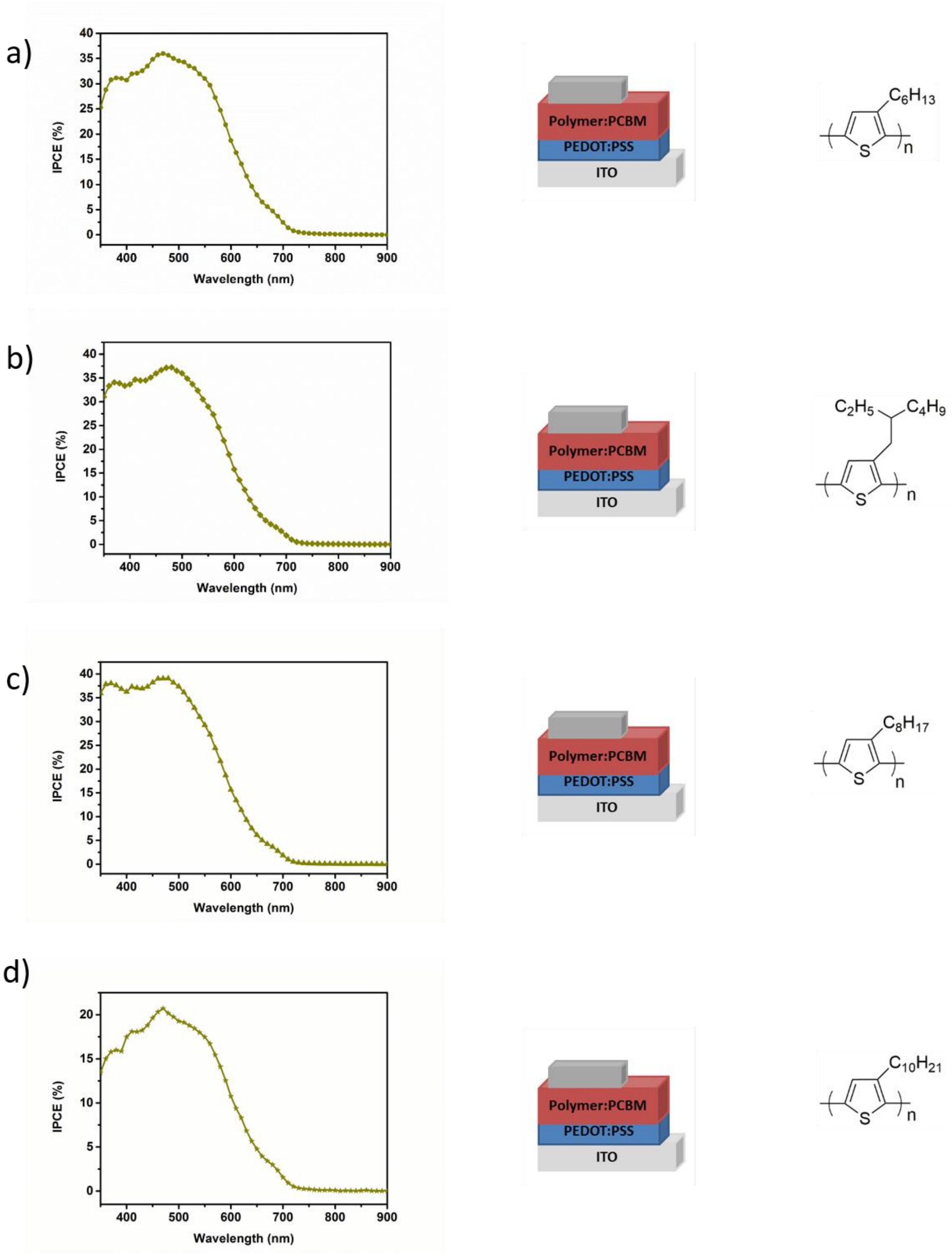

Figure 67 IPCE curves of P3HT, P3EHT, P3OT, and P3DecT based PSCs

5.4. Ternary Solar Cells

In the last part of this chapter ternary solar cells comprising P3EHT, PTB7 and $PC_{71}BM$ solar cells were fabricated. Structures of polymers are shown in Figure 68.

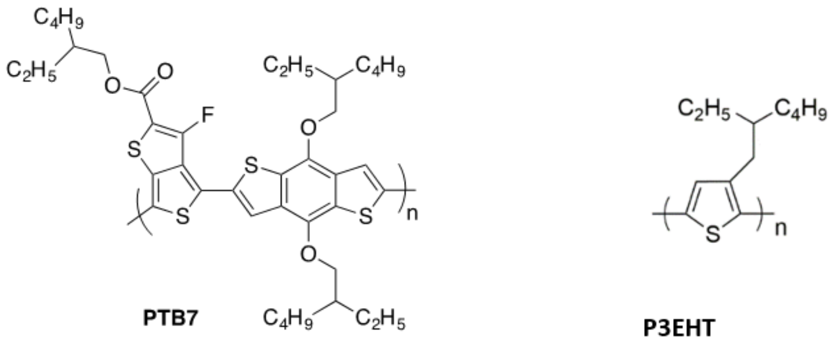

PTB7

P3EHT

Figure 68 Structures of PTB7 and P3EHT

In ternary solar cells two polymers having complemantary absorption profiles were used in the active layer. P3EHT has a strong absorption in the visible region from 360 to 515 nm however lower energy region of electromagnetic spectrum is wasted. PTB7 has selected as the second donor moiety due to its high photovoltaic performance mentioned in Section 1.1.8. In addition to this PTB7 absorbs photons in the longer wavelength part of spectrum. Thus, P3EHT, PTB7 comprising ternary solar cells have complementary absorption profiles. Absorption spectrum of a) P3EHT and PTB7 in thin film form b) ternary blend in thin film form are depicted in Figure 69.

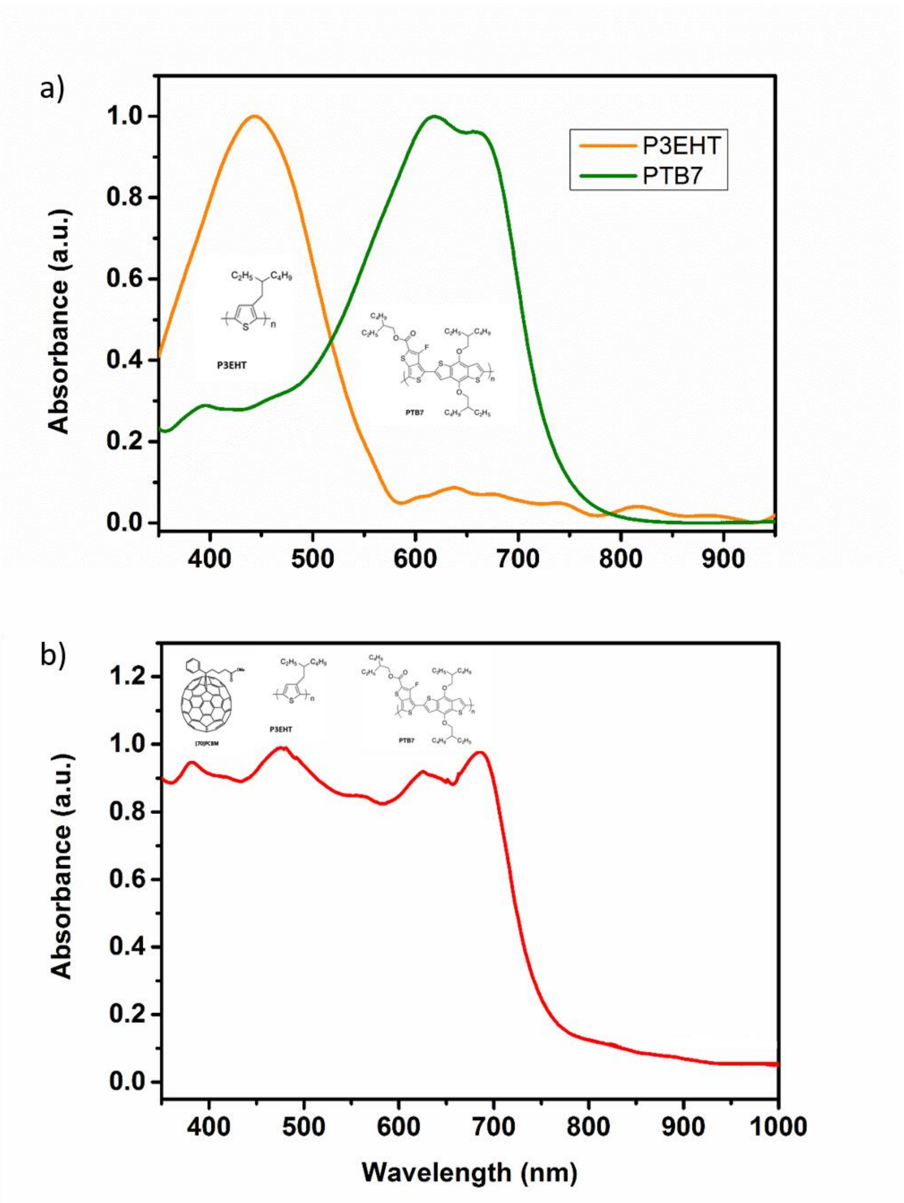

Figure 69 Absorption spectrum of a) P3EHT and PTB7 in thin film form b) ternary blend in thin film form

Three possible working mechasims are proposed for ternary solar cells, namely chrage transfer, energy transfer and parallel linkage mechanisms.[109] In the charge transfer mechanism, both of the donors absorb light and excitons are formed. They both have interfaces with acceptor moiety. Electrons are transported through the acceptor while holes first transported to one of the donor moeity and then collected at the anode.

In the energy transfer mechanism, all the holes are formed at one of the donor moieties this donor is called light absorber and it transfers energy via Förster or Dexter transfer mechanisms.

In the parallel linkage mechanism, charge charge carriers are genereated in both of the donors. They are dissociated at their respective donor - acceptor interfaces and transported to the anode and cathode.[109]

In order to compare the performance of ternary solar cells with PTB7 based PSCs, PTB7:PC71BM (1:1.5) incorporated solar cells were constructed. Best performance device exhibited PCE value of 6.26% with a V_{OC} of 0.72V, J_{SC} of $13.59 mA.cm^{-2}$ and a FF of 0.64. P3EHT based solar cells had shown PCE value of 2.03% with a V_{OC} of 0.83V, J_{SC} of $5.10 mA/cm^2$ and a FF of 0.48 as mentioned in section 5.3. Although P3EHT based devices had high VOC values, limited PCE value was obtained due to its limited absorption of light. To annihilate this problem, ternary solar cells comprising PTB7:P3EHT:PC_{71}BM were fabricated. Due to limited solubility of the P3EHT in chlorobenzene, ternary blends were dissolved in diclorobenzene. PTB7:P3EHT:PC_{71}BM ratio of 1:0.2:1.5 showed the best performance. PCE value of 6.50 % were achieved with a V_{OC} of 0.71V, J_{SC} of $14.50 mA/cm^2$ and a FF of 0.62. J-V relation of the corresponding device is shown in Figure 70, photovoltaic parameters were summarized in Table 14.

Further optimization studies will be conducted to improve the power conversion efficiencies of ternary devices.

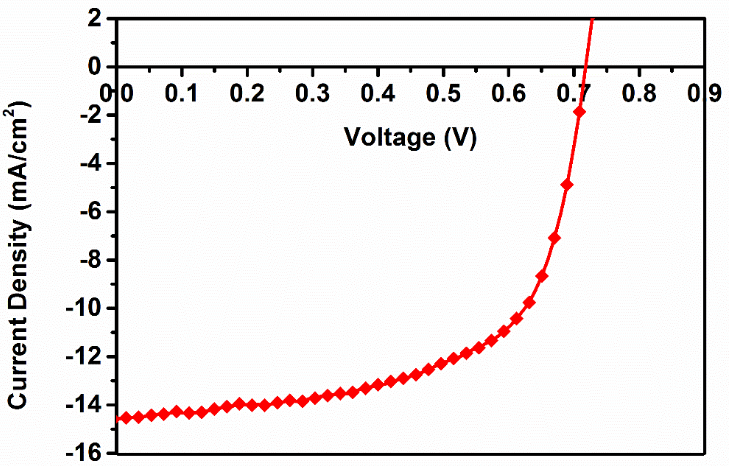

Figure 70 J-V curve for a PTB7:P3EHT:PC$_{71}$BM comprising ternary device

Table 14 Summary of photovoltaic parameters for PTB7: PCBM, P3EHT:PC71BM, PTB7:P3EHT:PC71BM comprising devices

PTB7 :P3EHT:PC71BM	**V_{oc} (V)**	**J_{sc} (mA/cm^2)**	**FF**	**PCE (%)**
1:0:2	0.72	13.59	0.64	6.26
0:1:3	0.83	5.10	48	2.03
1:0.2:1.5	0.72	14.60	62	6.50

CHAPTER 6

ITO FREE ORGANIC PHOTOVOLTAICS AND OLEDS

6.1 Introduction and aim of work

Liquid crystal displays (LCDs), touch panels, photovoltaics, and organic light-emitting diodes are costructed on transparent conducting films (TCFs). The LCD industry is the leader in TCF consumption with 1.5 billion dolars in 2014.[110] The transparent conducting film market that are used in touch panels was USD 1 billion in 2012, and it is expected to reach USD 4.8 billion by 2019. [111]

Due to its excellent conductivity and transparency, indium tin oxide coated substrates are the most commonly used anode materials. However, ITO has some drawbacks. ITO coated substrates are usually produced by sputtering techniques which brings high production cost. Scarcity of indium, crack tendency of ITO and diffusion of indium into the active layer are the other problems. [111]

Main requirements of electrodes for PSC and PLED applications are high transparency conductivity and flexibility. However there is a comprimise between transparency and conductivity. ITO has sheet resistance (Rsq) value of $\sim 10\ \Omega^{-2}$ at 90% transparency.[112]

As an alternative to ITO layer, in literature single-wall carbon nanotubes (SWNTs) [113], graphene [114], conducting polymers [115] and copper nanowires [116] and silver nanowires [117–120] were used as transparent conductive materials.

In this study, Ag nanowires were used as bottom and top electrodes. Polymer solar cells comprising P3HT and P1 were constructed on silver nanowire transparent electrodes. In addition to this Ag nanowires were also used as anode materials in

PLEDs. At the last part, Ag nanowires were used as top electrodes in the semitransparent OPV devices.

6.2 Experimental

Silver nanowires were synthesized with polyol method according to a previous literature report. [121] Ag nanowire dispersion in ethanol were spray coated on glass slides. For reproducibility of the experiments, distance between the spray gun and the samples and the pressure of the gun set to 10 cm and 2 atm, respectively. [119]

On top of Ag nanowire electrodes PEDOT:PSS was spin coated. For full surface coverage PEDOT:PSS was diluted with isoproylalcohol (IPA). PEDOT:PSS IPA ratio was varied from 1:2 to 4:1. Spin coating speeds were also optimized. 4:1 PEDOT:PSS IPA ratio and 1500 rpm spin coating speed formed the best quality PEDOT:PSS films. Throughout the study same procedure was applied. On top of PEDOT:PSS layer, for PSC applications polymer $PC_{71}BM$ blends were spin coated and metal electrodes were evaporated. For PLED applications light emitting polymer was spin coated and metal electrodes were evaporated on top of polymer layer. Details of PSC, PLED fabrication were mentioned in Section 2.2 and 2.3, respectively.

6.3 Results and Discussion

6.3.1 Ag Nanowires as Anode Materials in PSCs

6.3.1.1 Ag Nanowires as Anode Materials in P3HT:PC$_{71}$BM Comprising Solar Cells

In the first part of this chapter, P3HT comprising solar cells on Ag nanowire transparent electrodes were constructed. Glass/ Ag nanowire/PEDOT:PSS/ P3HT:PC$_{71}$BM / LiF/Al device structure was utilized as shown in Figure 71.

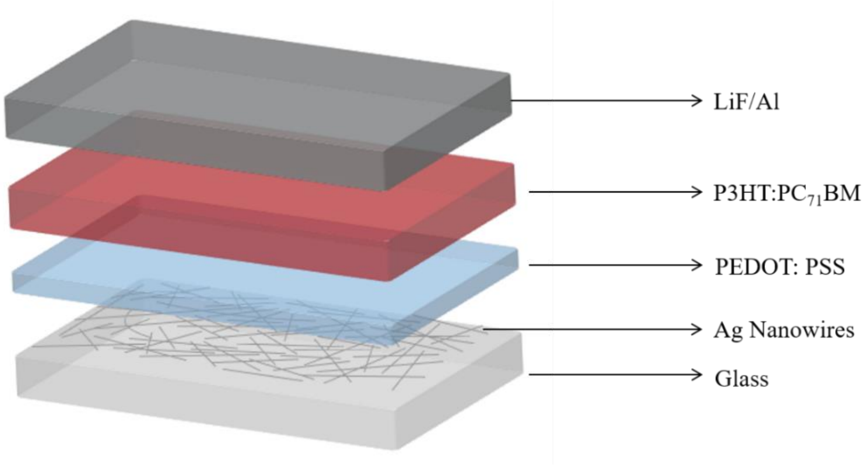

Figure 71 Schematic representation for Glass/ Ag nanowire/PEDOT:PSS/ P3HT:PC$_{71}$BM / LiF/Al device

In the construction of the PSCs, two different kinds of PEDOT:PSS were used. In the regular manner of PSC construction before PEDOT:PSS (Clevios 4083) coating, oxygen plasma cleaning was performed to remove organic residues and increase hydrophilicity of the surface thus, wettability properties of the surface is improved. However oxygen plasma cleaning results in oxidation of silver nanowires. Therefore in this study, PEDOT:PSS layers were coated without oxygen plasma cleaning. Without oxygen plasma cleaning, quality of the PEDOT:PSS (Clevios 4083) film was very poor. The PSC fabricated on this film showed PCE of 0.56% with a V_{OC} value of 0.54V, a J_{SC} value of 3.15mA/cm^2 and a FF of 0.33. Low J_{SC} and FF values may arise from the pinholes. To annihilate poor film quality of PEDOT:PSS, different PEDOT:PSS (Clevios HTL) was coated. PEDOT:PSS HTL can be coated to surfaces that are difficult to wet with an aqueous solution. It is usually used for inverted polymer solar cells and coated on top of active layer. With Glass/ Ag nanowire/ PEDOT:PSS(HTL) / P3HT:$PC_{71}BM$ / LiF/Al device architecture 1.13% PCE value was achieved with a V_{OC} value of 0.53V, a J_{SC} value of 4.99mA/cm^2 and a FF of 0.43. Corresponding J-V curve is shown in Figure 61. Photovoltaic parameters are summarized in Table 15.

Table 15 Summary of photovoltaic parameters Glass/ Ag nanowire/ PEDOT:PSS(HTL) / P3HT:$PC_{71}BM$ / LiF/Al device

P3HT:$PC_{71}BM$	**V_{oc} (V)**	**J_{sc} (mA/cm^2)**	**FF**	**PCE (%)**	**PEDOT:PSS**
(1:0.8)	0.54	3.15	0.33	0.56	Clevios 4083
(1:0.8)	0.53	4.99	0.43	1.13	Clevios HTL

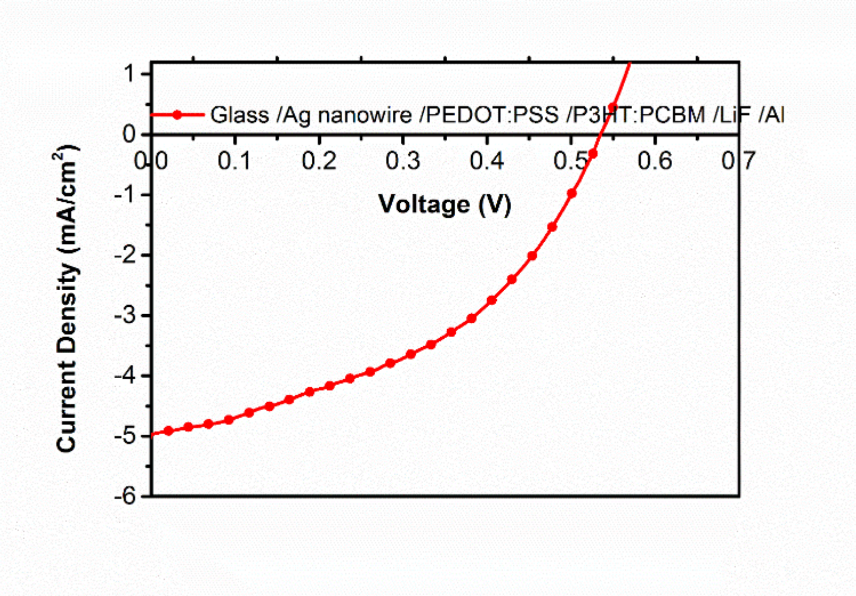

Figure 72 J-V curve for P3HT comprising solar cell on Ag nanowire transparent electrode

6.3.1.2. Ag nanowires as anode materials in P1:PC71BM comprising solar cells

In the second part of this chapter, P1:PC$_{71}$BM comprising solar cells constructed on Ag nanowire transparent conducting anode as described. Photovoltaic parameters were investigated with the device structure of glass/ Ag nanowire/ PEDOT:PSS(HTL) / P1:PC$_{71}$BM / LiF/Al. (Figure 73)

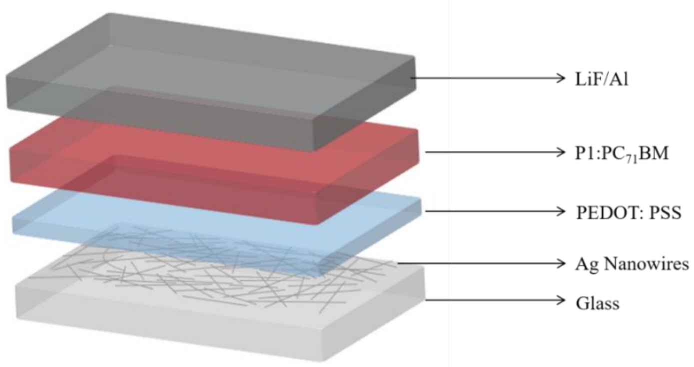

Figure 73 Schematic representation for Glass/ Ag nanowire/PEDOT:PSS/ P3HT:$PC_{71}BM$ / LiF/Al device

As mentioned in Section 4.3, P1 incorporated PSC showed PCE value of 2.10 % with a V_{OC} value of 0.90 V, a J_{SC} value of 5.98 mA/cm^2 and a FF of 0.39. The PSC based on Ag nanowires as the anode material exhibited PCE value of 0.50 % with a V_{OC} value of 0.34 V, a J_{SC} value of 4.64 mA/cm^2 and a FF of 0.32. Corresponding J-V relation is shown in Figure 74 and photovoltaic parameters are summarized in Table 16.

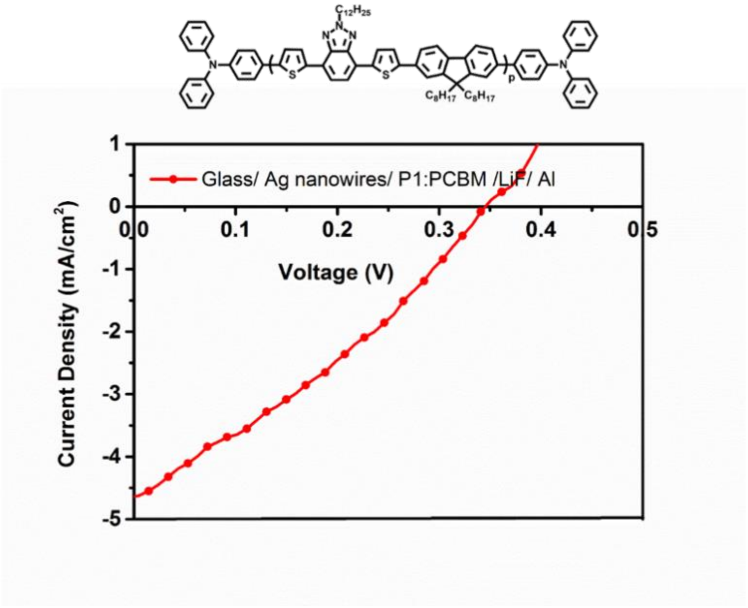

Figure 74 J-V curve for P1 comprising solar cell on Ag nanowire transparent electrode

Table 16 Summary of photovoltaic parameters for glass/ Ag nanowire/ PEDOT:PSS(HTL) / P1:PC71BM / LiF/Al

P1:PC$_{71}$BM	**V$_{oc}$ (V)**	**J$_{sc}$ (mA/cm^2)**	**FF**	**PCE (%)**
(1:2)	0.342	4.64	0.32	0.50

6.3.2 Ag Nanowires as Anode Materials in PLEDs

In the third part of this chapter P2 comprising PLEDs on Ag nanowire transparent electrodes were constructed. Glass/ Ag nanowire/PEDOT:PSS/ P2/ Ca/Al device structure was utilized as shown in Figure 75. PLEDs were constructed following the procedure mentioned in the Section 2.3.

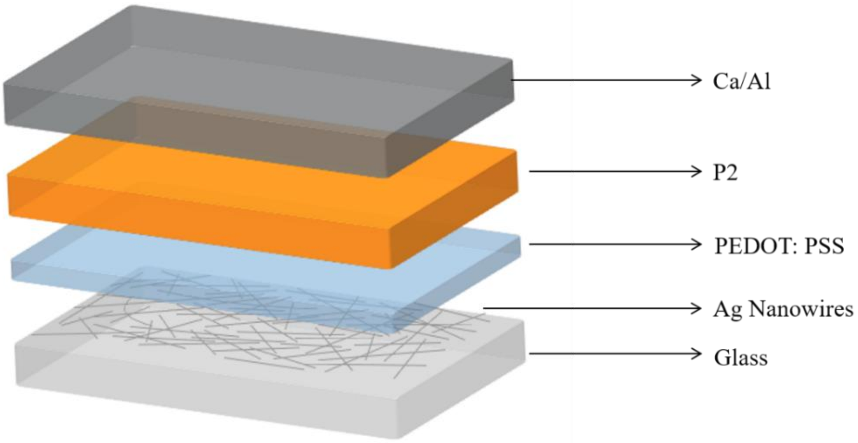

Figure 75 Schematic representation for glass/ Ag nanowire/PEDOT:PSS/ P2 / Ca /Al device

PLEDs characterizations were performed following the procedure described in Section 2.4.6. Electroluminescence characteristics, luminance and current density versus applied voltage characteristics of the PLEDs were investigated. Figure 76 shows electroluminescence spectra of PLEDs in yellow color of electromagnetic spectrum with EL peaks centered at 554 nm and 591nm. EL peak is red-shifted by 20nm and with respect to PL peak for P2. EL peaks are red shifted by 2nm and intensity of the peak at around 550nm increased with respect to the EL peak of ITO based PLED.

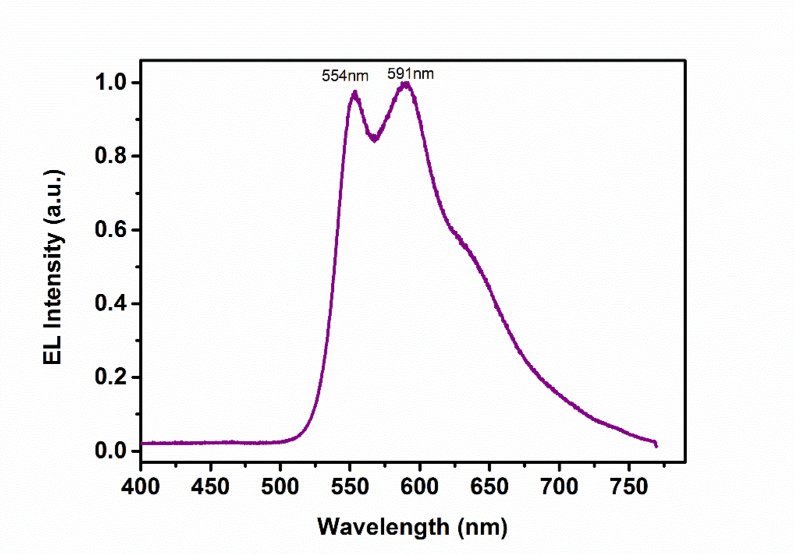

Figure 76 Electroluminescence spectrum for Ag nanowire based PLED

J-V relation for the glass/ Ag nanowire/PEDOT:PSS/ P2 / Ca /Al device was investigated. Upon applied potential current values were recorded and the relation is shown in Figure 65.

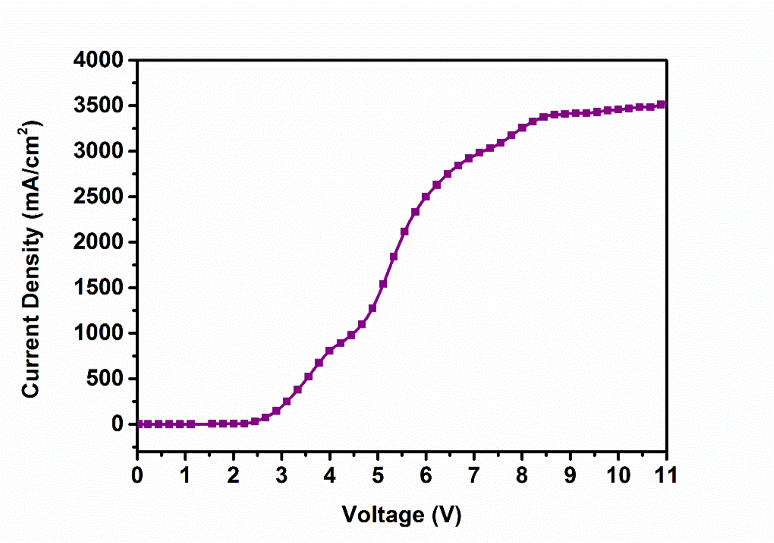

Figure 77 J-V relation for a glass/ Ag nanowire/PEDOT:PSS/ P2 / Ca /Al device

Turn on voltage of the Ag nanowire based PLED was determined as 2.8V which was 3.0V for ITO based PLED. During storage and handling, a thin layer of oxide was formed and the work function of the oxide layer (Ag_2O) is around -5.1eV[122] which is 0.4eV lower than the work function of ITO (- 4.7eV). Since the energy barrier between the anode and the polymer decreases, charge injection process become easier, thus turn on voltage of the PLED decreases.[119]

Maximum luminance value was determined as 2625cd/m^2 at 8V for PLED devices fabricated using Ag nanowire networks as the anode. Luminance and turn on voltage values are summarized in Table 17.

Table 17 Summary of PLED performances fabricated using Ag nanowires and ITO as anode materials

Anode	**Luminance (cd/m^2)**	**Turn on voltage (V)**
ITO based device	14583@8 V	3
Ag nanowire based device	2625 @8V	2.8

Yellow light emission was observed with Commission Internationale de l'Eclairage (CIE) coordinates measured at x: 0.4527 and y: 0.5389, for P2 incorporated PLEDs. Figure 78 shows the snapshot of the PLED.

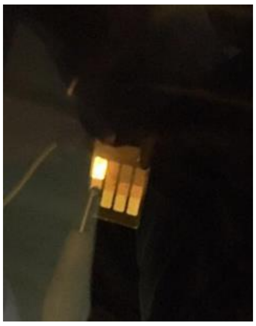

Figure 78 Snapshot of the glass/ Ag nanowire/PEDOT:PSS/ P2 / Ca /Al device

Lower luminance values of Ag nanowire based PLEDs and lower performance of PSCs are believed to originate from high roughness of Ag nanowires and non-continuous films of Ag nanowires which were proven by SEM images. SEM images of Ag nanowire thin films are depicted in Figure 79a. As seen in the figure full surface coverage cannot be established leading to performance loss of PSC and PLED devices. Cross sectional SEM image of P1:PC$_{71}$BM incorporated PSC is seen in Figure 79 b. Cathode metals can migrate through the pinholes (marked) and may lead to shorts or lower performance.

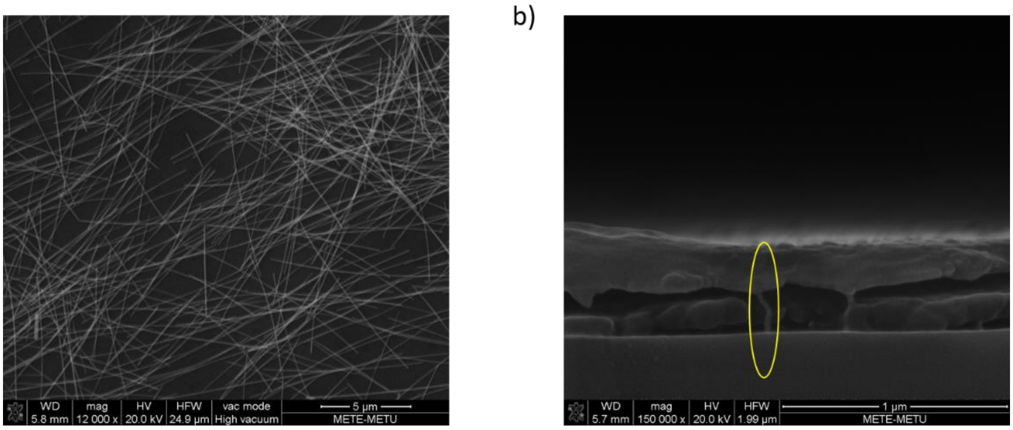

Figure 79 a) SEM image of Ag nanowire thin films b) Cross sectional SEM image of the device

6.3.3 Ag Nanowires as Top Electrode in PSCs

In the fourth part of this study, Ag nanowires were used as the top electrode material in polymer solar cells in order to fabricate semitransparent organic photovoltaic devices (SOPVs). In the regular and the inverted device architecture usually aluminum and silver or gold metals are used as the top electrode material, respectively. However these metals are forming opaque films and it is not feasible to coat the windows of buildings. To annihilate this problem semitransparent top electrode materials are utilized in PSCs.

For this purpose, devices with the structure of ITO/ZnO /P3HT:PC$_{71}$BM / PEDOT:PSS /Ag nanowire were fabricated. For device fabrication experimental procedure mentioned in Section 2.2 were followed. As the top electrode material, Ag nanowires were spray coated through a shadow mask in order to define device area. Resulting semitransparent devices were shown in Figure 80.

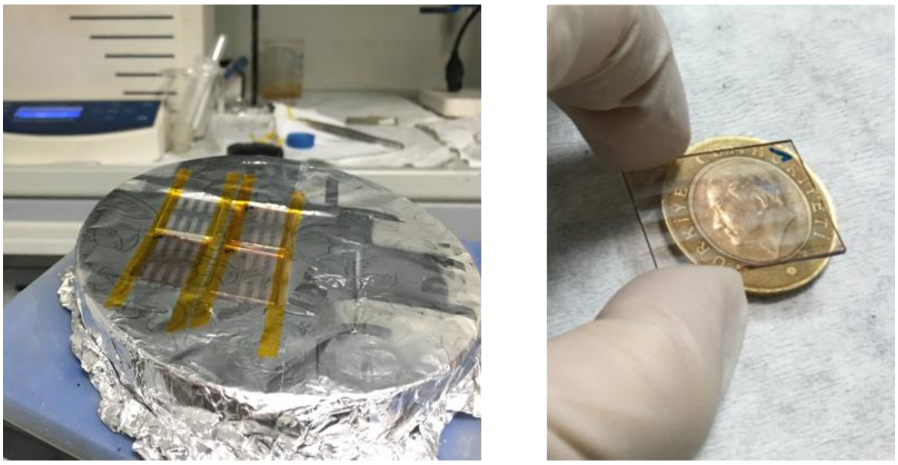

Figure 80 Snapshot of the semitransparent polymer solar cells

Photovoltaic performances of the devices were investigated under illumination of AM1.5G. Semitransparent P3HT:$PC_{71}BM$ devices exhibited PCE value of 0.20% with a V_{OC} value of 0.29 V, a J_{SC} value of 2.34 mA/cm^2 and a FF of 0.29. Corresponding J-V curve is shown in Figure 81, photovoltaic parameters were summarized in Table 18. These are the preliminary results, studies on semitransparent photovoltaic devices will continue.

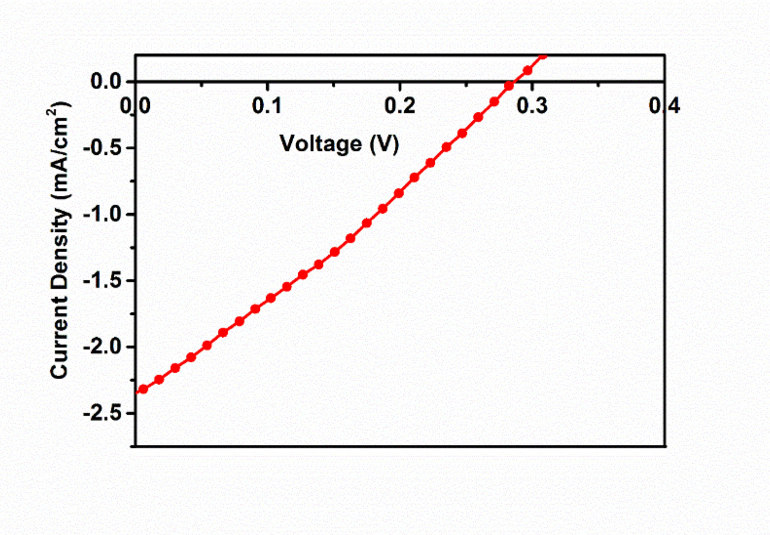

Figure 81 J-V curve for P3HT:$PC_{71}BM$ comprising semitransparent solar cells

Table 18 Summary of photovoltaic parameters for P3HT:$PC_{71}BM$ comprising semitransparent solar cells

P3HT:$PC_{71}BM$	**V_{oc} (V)**	**J_{sc} (mA/cm^2)**	**FF**	**PCE (%)**
(1:1)	0.29	2.34	0.29	0.20

CHAPTER 7

CONCLUSIONS AND OUTLOOK

7.1 Conclusions

In the first chapter of this thesis dissertation, introductory information, historical development and current status of polymer solar cells and polymer based OLEDs were mentioned.

In the second part, experimental procedures followed and the main principles of the instruments used were mentioned.

In the third and fourth chapters effect of terminal structure and molecular weight on electroluminescence and photovoltaic properties were covered. Benzene and triphenylamine end capped fluorene, benzotriazole and thiophene bearing polymers were synthesized. Electroluminescence spectra of PLEDs were in orange and yellow colors of the electromagnetic spectrum with EL peak centered at 610nm and 547 nm with a shoulder at 589nm, respectively. P1 based PLED shows luminance value of 10411cd/m^2 at 8.5V whereas P2 based PLED has the peak luminance value of 14583cd/m^2 at 8V. This lower performance of P1 may originate from less efficient charge carrier recombination on aggregates which also leads to red shifted EL.

In order to determine whether effect of end capper or the effect of molecular weight is dominant on power conversion efficiency, P3, lower molecular weight version of P2 was synthesized. P2 showed the highest performance whereas P1 and P3 had similar photovoltaic performances. The best performance device based on P2 exhibits a power conversion efficiency (PCE) of 4.11 % with a current density (J_{sc}) of 6.59 mA/cm^2, an open-circuit voltage (V_{oc}) of 0.99 V, and a fill factor (FF) of

0.63 under illumination of AM 1.5 G. It was concluded that rather than the effect of different end cappers, effect of molecular weight was a more dominating factor on the power conversion efficiency of PSCs.

In the fifth chapter, advantages of electrochemical polymerization and photovoltaic studies of the electrochemically synthesized polymers were mentioned. To the best of our knowledge, **this is the first study in literature** that electrochemically synthesized polymers were used in organic photovoltaic applications. P3HT, P3EHT, P3OT, P3DecT and P3DHT were synthesized via electrochemical means. P3EHT based solar cells showed the highest performance. PCE of 2.03% was obtained with a J_{sc} value of 5.10mA/cm^2, V_{oc} value of 0.83V, FF value of 48 %. Ternary solar cells comprising P3EHT, PTB7 and $PC_{71}BM$ was fabricated. PCE value of 6.50 % were achieved with a V_{OC} of 0.71V, J_{SC} of 14.60 mA.cm^{-2} and a FF of 0.62.

In the sixth part, ITO free polymer solar cell and PLED characterizations was covered. Instead of ITO, Ag and Cu nanowires were used as the anode materials in polymer solar cell and polymer light emitting diode applications. 1.13% PCE value was achieved with a VOC of 0.53V, JSC of 4.99mA/cm^2 and FF of 0.43 with the device structure of glass /Ag nanowire / P3HT:PC71BM/ LiF /Al. 2625cd/m^2 luminance value was obtained with P2 incorporated electroluminescent device with a lower turn on voltage than ITO based device.

Preliminary studies on semitransparent organic photovoltaic devices were carried out. Aluminum and silver metals are usually used as top contacts in OPV devices. However they are suffering not being transparent and this inhibits their application on windows. For this purpose, transparent Ag nanowires were used as top contacts and semitransparent P3HT:$PC_{71}BM$ devices exhibited PCE value of 0.20% with a V_{OC} value of 0.29 V, a J_{SC} value of 2.34 mA/cm^2 and a FF of 0.29.

7.2 Outlook

For commercialization of conjugated polymer based devices like PLEDs, PSCs and OFETs, efficiency, stability, scalability and cost issues should be solved. As mentioned in Section 1.5 versatility of organic chemistry has been used to improve efficiency and stability of the devices. However with the methods followed in synthesis of conjugated polymers it is very hard to obtain high amounts of polymers. At this point, we propose an environmentally friendly, cheap, easy way of producing substantial amount of polymers via electrochemical polymerization.

In this study, fullerene derivatives were used as the acceptor materials in P3AT based PSCs. Higher V_{OC} values may be obtained with ICBA and non-fullerene acceptors with higher lying LUMO energy levels. Thus, higher power conversion efficiencies may be achieved. In addition to this, copolymers with different feed ratios will be produced electrochemically.

To the best of our knowledge this is the first study in the literature, where polymers produced by electrochemical means were used in photovoltaic studies. In this context we believe that a problem was solved and a unique solution was proposed in this PhD thesis. This study will open the way for synthesis of conjugated polymers with high purity and low cost.

REFERENCES

1. Becquerel, E. Recherches sur les effets de la radiation chimique de la lumiere solaire au moyen des courants electriques. *Comptes Rendus L'Academie des Sci.* **9,** 145–149 (1839).
2. Chapin, D.M., Fuller, C.S., & Pearson, G.L. A new silicon p-n junction photocell for converting solar radiation into electrical power. *J. Appl. Phys.* **25,** 676–677 (1954).
3. Krebs, F. *Polymeric Solar Cells: Materials, Design, Manufacture*. (DEStech Publications, 2010).
4. NREL. Best Research Cell Efficiencies. Available at: https://www.nrel.gov/pv/assets/images/efficiency-chart.png. (Accessed: 29th August 2017)
5. Chiang, C.K., Fincher, C.R., Park, Y.W., Heeger, A.J., Shirakawa, H., Louis, E.J., Gau, S.C., & MacDiarmid, A.G. Electrical conductivity in doped polyacetylene. *Phys. Rev. Lett.* **39,** 1098–1101 (1977).
6. Hoppe, H., Sariciftci, N.S., & Meissner, D. Optical Constants of Conjugated Polymer / Fullerene Based Bulk-Heterojunction Organic Solar Cells. *Sol. Cells* **385,** 233–240 (2002).
7. Tang, C.W. Two-layer organic photovoltaic cell. *Appl. Phys. Lett.* **48,** 183–185 (1986).
8. Hiramoto, M., Fujiwara, H., & Yokoyama, M. P-I-N Like Behavior in Three-Layered Organic Solar Cells Having a Co-Deposited Interlayer of Pigments. *J. Appl. Phys.* **72,** 3781–3787 (1992).
9. Yu, G., Gao, J., Hummelen, J.C., Wudl, F., & Heeger, A.J. Polymer Photovoltaic Cells: Enhanced Efficiencies via a Network of Internal Donor-Acceptor Heterojunctions. *Science (80-.).* **270,** 1789–1791 (1995).

10. Halls, J.J.M., Walsh, C.A., Greenham, N.C., Marseglia, E.A., Friend, R.H., Moratti, S.C., & Holmes, A.B. Efficient photodiodes from interpenetrating polymer networks. *Nature* **376,** 498–500 (1995).

11. Nunzi, J.-M. Organic photovoltaic materials and devices. *Comptes Rendus Phys.* **3,** 523–542 (2002).

12. Singh, T.B., Marjanović, N., Matt, G.J., Günes, S., Sariciftci, N.S., Montaigne Ramil, A., Andreev, A., Sitter, H., Schwödiauer, R., & Bauer, S. High-mobility n-channel organic field-effect transistors based on epitaxially grown C60 films. *Org. Electron.* **6,** 105–110 (2005).

13. Günes, S., Neugebauer, H., & Sariciftci, N.S. Conjugated polymer-based organic solar cells. *Chem. Rev.* **107,** 1324–1338 (2007).

14. Kaminski, A., Marchand, J., & Laugier, A. Non ideal dark I–V curves behavior of silicon solar cells. *Sol. Energy Mater. Sol. Cells* **51,** 221–231 (1998).

15. Lindmayer, J. & Allison, J.F. The violet cell: An improved silicon solar cell. *Sol. Cells* **29,** 151–166 (1990).

16. Peumans, P. & Forrest, S.R. Very-high-efficiency double-heterostructure copper phthalocyanine/ C60 photovoltaic cells. **126,** 126–129 (2013).

17. Wudl, F. & Srdanov, G. Conducting polymer formed of poly(2 - methoxy - 5-(2’-ethylhexyloxy) - p - phenylene vinylene). *US Patent* **189,** 136 (1993).

18. Knight, B., Hummelen, J., F, L., & Wudl, F. Preparation and Characterization of Fulleroid and Methanofullerene Derivatives. *J. Org. Chem* **60,** 532–538 (1995).

19. Wienk, M.M., Kroon, J.M., Verhees, W.J.H., Knol, J., Hummelen, J.C., van Hal, P.A., & Janssen, R.A.J. Efficient Methano[70]fullerene/MDMO-PPV Bulk Heterojunction Photovoltaic Cells. *Angew. Chemie Int. Ed.* **42,** 3371–3375 (2003).

20. Dang, M.T., Hirsch, L., & Wantz, G. P3HT:PCBM, best seller in polymer photovoltaic research. *Adv. Mater.* **23,** 3597–3602 (2011).

21. Guo, X., Cui, C., Zhang, M., Huo, L., Huang, Y., Hou, J., & Li, Y. High efficiency polymer solar cells based on poly(3-hexylthiophene)/indene-C70 bisadduct with solvent additive. *Energy Environ. Sci.* **5,** 7943 (2012).

22. Holliday, S., Ashraf, R.S., Wadsworth, A., Baran, D., Yousaf, S.A., Nielsen, C.B., Tan, C.-H., Dimitrov, S.D., Shang, Z., Gasparini, N., Alamoudi, M., Laquai, F., Brabec, C.J., Salleo, A., Durrant, J.R., & McCulloch, I. High-efficiency and air-stable P3HT-based polymer solar cells with a new non-fullerene acceptor. *Nat. Commun.* **7,** 11585 (2016).

23. Mühlbacher, D., Scharber, M., Morana, M., Zhu, Z., Waller, D., Gaudiana, R., & Brabec, C. High photovoltaic performance of a low-bandgap polymer. *Adv. Mater.* **18,** 2884–2889 (2006).

24. Peet, J., Soci, C., Coffin, R.C., Nguyen, T.Q., Mikhailovsky, A., Moses, D., & Bazan, G.C. Method for increasing the photoconductive response in conjugated polymer/fullerene composites. *Appl. Phys. Lett.* **89,** 7–9 (2006).

25. Peet, J., Kim, J.Y., Coates, N.E., Ma, W.L., Moses, D., Heeger, A.J., & Bazan, G.C. Efficiency enhancement in low-bandgap polymer solar cells by processing with alkane dithiols. *Nat. Mater.* **6,** 497–500 (2007).

26. Cho, S., Coates, N., Moon, J.S., Park, S.H., Roy, A., Beaupre, S., Moses, D., Leclerc, M., Lee, K., & Heeger, A.J. Bulk heterojunction solar cells with internal quantum efficiency approaching 100. *Nat. Photonics* **3,** 297–302 (2009).

27. Liang, Y., Wu, Y., Feng, D., Tsai, S.-T., Son, H.-J., Li, G., & Yu, L. Development of New Semiconducting Polymers for High Performance Solar Cells. *J. Am. Chem. Soc.* **131,** 56–57 (2008).

28. Chen, H.-Y., Hou, J., Zhang, S., Liang, Y., Yang, G., Yang, Y., Yu, L., Wu, Y., & Li, G. Polymer Solar Cells with Enhanced Open-Circuit Voltage and Efficiency. *Nat. Photonics* **3,** 649–653 (2009).

29. Zou, Y., Najari, A., Berrouard, P., Beaupre, S., Aïch, B.R., Tao, Y., & Leclerc, M. A Thieno[3, 4-c]pyrrole-4, 6-dione-Based Copolymer for Efficient Solar Cells. *J. Am. Chem. Soc.* **132,** 5330–5331 (2010).

30. Piliego, C., Holcombe, T.W., Douglas, J.D., Woo, C.H., Beaujuge, P.M., & Fre, J.M.J. Synthetic Control of Structural Order in N -Alkylthieno [3 , 4- c] pyrrole-4 , 6-dione-Based Polymers for Efficient Solar Cells. *J. Am. Chem. Soc.* **132,** 7595–7597 (2010).

31. Zhang, G., Fu, Y., Zhang, Q., & Xie, Z. Benzo[1,2-b:4,5-b']dithiophene-dioxopyrrolothiophene copolymers for high performance solar cells. *Chem. Commun.* **46,** 4997–4999 (2010).

32. Zhang, Y., Hau, S.K., Yip, H.L., Sun, Y., Acton, O., & Jen, A.K.Y. Efficient polymer solar cells based on the copolymers of benzodithiophene and thienopyrroledione. *Chem. Mater.* **22,** 2696–2698 (2010).

33. Liang, Y., Xu, Z., Xia, J., Tsai, S.T., Wu, Y., Li, G., Ray, C., & Yu, L. For the bright future-bulk heterojunction polymer solar cells with power conversion efficiency of 7.4%. *Adv. Mater.* **22,** 135–138 (2010).

34. Liu, C., Wang, K., Hu, X., Yang, Y., Hsu, C.-H., Zhang, W., Xiao, S., Gong, X., & Cao, Y. Molecular Weight Effect on the Efficiency of Polymer Solar Cells. *ACS Appl. Mater. Interfaces* **5,** 12163–12167 (2013).

35. He, Z., Zhong, C., Su, S., Xu, M., Wu, H., & Cao, Y. Enhanced Power-Conversion Efficiency in Polymer Solar Cells Using an Inverted Device Structure Enhanced power-conversion efficiency in polymer solar cells using an inverted device structure. *Nat. Photonics* **6,** 591–595 (2012).

36. Blom, P.W.M., Mihailetchi, V.D., Koster, L.J.A., & Markov, D.E. Device physics of polymer:Fullerene bulk heterojunction solar cells. *Adv. Mater.* **19,** 1551–1566 (2007).

37. Ye, L., Zhang, S., Zhao, W., Yao, H., & Hou, J. Highly efficient 2D-conjugated benzodithiophene-based photovoltaic polymer with linear alkylthio side chain. *Chem. Mater.* **26,** 3603–3605 (2014).

38. He, Z., Xiao, B., Liu, F., Wu, H., Yang, Y., Xiao, S., Wang, C., Russell, T.P., & Cao, Y. Single-junction polymer solar cells with high efficiency and photovoltage. *Nat. Photonics* **9,** 174–179 (2015).

39. Li, Z., Jiang, K., Yang, G., Lai, J.Y.L., Ma, T., Zhao, J., Ma, W., & Yan, H. Donor polymer design enables efficient non-fullerene organic solar cells. *Nat. Commun.* **7,** 13094 (2016).

40. Zhao, J., Li, Y., Yang, G., Jiang, K., Lin, H., Ade, H., Ma, W., & Yan, H. Efficient organic solar cells processed from hydrocarbon solvents. *Nat. Energy* **1,** 15027 (2016).

41. Pope, M., Kallmann, H.P., & Magnante, P. Electroluminescence in Organic Crystals. *J. Chem. Phys.* **38,** 2042–2043 (1963).

42. Tang, C.W. & Vanslyke, S.A. Organic electroluminescent diodes. *Appl. Phys. Lett.* **51,** 913–915 (1987).

43. Burroughes, J.H., Bradley, D.D.C., Brown, A.R., Marks, R.N., Mackay, K., Friend, R.H., Burns, P.L., & Holmes, A.B. Light-emitting diodes based on conjugated polymers. *Nature* **347,** 539–541 (1990).

44. Shinar, J. *Organic light-emitting devices : a survey*. (Springer, 2004).

45. Yang, Y., Westerweele, E., Zhang, C., Smith, P., & Heeger, A.J. Enhanced performance of polymer light-emitting diodes using high-surface area polyaniline network electrodes. *J. Appl. Phys.* **77,** 694–698 (1995).

46. Simonato, D.L., Giusti, G., Mayousse, C., Celle, C., Bellet, D., & Jean-Pierre. Flexible transparent conductive materials based on silver nanowire networks: a review. *Nanotechnology* **24,** 452001 (2013).

47. Wu, J., Agrawal, M., Becerril, H.A., Bao, Z., Liu, Z., Chen, Y., & Peumans, P. Organic light-emitting diodes on solution-processed graphene transparent electrodes. *ACS Nano* **4,** 43–48 (2010).

48. Malliaras, G.G., Shen, Y., & Scott, J.C. *Organic Light Emitting Materials and Devices 4*. (SPIE 4105, 2000).

49. Xu, J., Wang, Y., Chen, Q., Lin, Y., Shan, H., Roy, V.A.L., & Xu, Z. Enhanced lifetime of organic light-emitting diodes using soluble tetraalkyl-substituted copper phthalocyanines as anode buffer layers. *J. Mater. Chem. C* **4,** 7377–7382 (2016).

50. Maglione, M.G., Minarini, C., Miscioscia, R., Nenna, G., Romanelli, E., & Tassini, P. Efficiency and Aging Comparison Between N,N'-Bis (3-methylphenyl)-N,N'-diphenylbenzidine (TPD) and N,N'-Di-[(1-naphthalenyl)-N,N'-diphenyl]-1,1'- biphenyl-4,4'-diamine (NPD) Based OLED Devices. *Macromol. Symp.* **247,** 311–317 (2007).

51. Kim, H., Ou, K.-L., Wu, X., Ndione, P.F., Berry, J., Lambert, Y., Mélin, T., Armstrong, N.R., & Graham, S. Investigation of ultra-thin titania films as hole-blocking contacts for organic photovoltaics. *J. Mater. Chem. A* **3,** 17332–17343 (2015).

52. Ma, Z., Zhao, J., Wang, X., & Yu, J. Effect of bulk and planar heterojunctions based charge generation layers on the performance of tandem organic light-emitting diodes. *Org. Electron. physics, Mater. Appl.* **30,** 136–142 (2016).

53. Fleetham, T., Ecton, J., Wang, Z., Bakken, N., & Li, J. Single-doped white organic light-emitting device with an external quantum efficiency over 20%. *Adv. Mater.* **25,** 2573–2576 (2013).

54. Defining standard spectra for solar panels. Available at: http://www.greenrhinoenergy.com/solar/radiation/spectra.php. (Accessed: 3rd September 2017)

55. Rees, I.D., Robinson, K.L., Holmes, A.B., Towns, C.R., & O'Dell, R. *MRS Bulletin*. (2002).

56. Burn, P.L., Holmes, A.B., Kraft, A., Bradley, D.D.C., Brown, A.R., Friend, R.H., & Gymer, R.W. Chemical tuning of electroluminescent copolymers to improve emission efficiencies and allow patterning. *Nature* **356,** 47 (1992).

57. Chen, X., Liao, J.L., Liang, Y., Ahmed, M.O., Tseng, H.E., & Chen, S.A. High-efficiency red-light emission from polyfluorenes grafted with cyclometalated iridium complexes and charge transport moiety. *J. Am. Chem. Soc.* **125,** 636–637 (2003).

58. Gupta, A., Watkins, S.E., Scully, A.D., Singh, T.B., Wilson, G.J., Rozanski, L.J., & Evans, R.A. Band-gap tuning of pendant polymers for organic light-emitting devices and photovoltaic applications. *Synth. Met.* **161,** 856–863 (2011).

59. Gong, X., Ma, W., Ostrowski, J.C., Bazan, G.C., Moses, D., & Heeger, a. J. White Electrophosphorescence from Semiconducting Polymer Blends. *Adv. Mater.* **16,** 615–619 (2004).

60. Jin, S.H., Park, H.J., Kim, J.Y., Lee, K., Lee, S.P., Moon, D.K., Lee, H.J., & Gal, Y.S. Poly(fluorenevinylene) derivative by Gilch polymerization for light-emitting diode applications. *Macromolecules* **35,** 7532–7534 (2002).

61. Chen, P., Yuan, D., Niu, L., Gao, C., & Xiong, Z. Triplet harvesting in polyfluorene copolymer-based organic light emitting diodes through thermally activated reverse intersystem crossing. *Org. Electron. physics, Mater. Appl.* **41,** 100–106 (2017).

62. Vasilopoulou, M., Palilis, L.C., Botsialas, A., Georgiadou, D.G., Bayiati, P., Vourdas, N., Petrou, P.S., Pistolis, G., Stathopoulos, N.A., & Argitis, P. Flexible organic light emitting diodes (OLEDs) based on a blue emitting polyfluorene. *Phys. Status Solidi Curr. Top. Solid State Phys.* **5,** 3658–3662 (2008).

63. Yang, R., Tian, R., Yan, J., Zhang, Y., Yang, J., Hou, Q., Yang, W., Zhang, C., & Cao, Y. Deep-red electroluminescent polymers: Synthesis and characterization of new low-band-gap conjugated copolymers for light-emitting diodes and photovoltaic devices. *Macromolecules* **38,** 244–253 (2005).

64. Lim, E., Jung, B.J., & Shim, H.K. Synthesis and characterization of a new light-emitting fluorene-thieno 3,2-b thiophene-based conjugated copolymer. *Macromolecules* **36,** 4288–4293 (2003).

65. Kong, X., Kulkarni, A.P., & Jenekhe, S.A. Phenothiazine-Based Conjugated Polymers: Synthesis, Electrochemistry, and Light-Emitting Properties. *Macromolecules* **36,** 8992–8999 (2003).

66. Hou, Q., Zhou, Q., Zhang, Y., Yang, W., Yang, R., & Cao, Y. Synthesis and electroluminescent properties of high-efficiency saturated red emitter based on copolymers from fluorene and 4,7-Di(4-hexylthien-2-yl)-2,1, 3-benzothiadiazole. *Macromolecules* **37,** 6299–6305 (2004).

67. Yang, J., Jiang, C., Zhang, Y., Yang, R., Yang, W., Hou, Q., & Cao, Y. High-Efficiency Saturated Red Emitting Polymers Derived from Fluorene and Naphthoselenadiazole. *Macromolecules* **37,** 1211–1218 (2004).

68. Cho, N.S., Hwang, D.H., Lee, J.I., Jung, B.J., & Shim, H.K. Synthesis and color tuning of new fluorene-based copolymers. *Macromolecules* **35,** 1224–1228 (2002).

69. Kim, Y., Cook, S., Kirkpatrick, J., Nelson, J., Durrant, J.R., Bradley, D.D.C., Giles, M., Heeney, M., Hamilton, R., & McCulloch, I. Effect of the end group of regioregular poly(3-hexylthiophene) polymers on the performance of polymer/fullerene solar cells. *J. Phys. Chem. C* **111,** 8137–8141 (2007).

70. Xiao, B.S., Nguyen, M., Gong, X., Cao, Y., Wu, H., Moses, D., & Heeger, A.J. Stabilization of Semiconducting Polymers with Silsesquioxane **. **13,** 25–29 (2003).

71. Li, Z.H., Wong, M.S., Tao, Y., & Fukutani, H. Ambipolar diphenylamino end-capped oligofluorenylthiophenes as excellent electron-transporting emitters. *Org. Lett.* **9,** 3659–3662 (2007).

72. Miteva, T., Meisel, A., Knoll, W., Nothofer, H.G., Scherf, U., Müller, D.C., Meerholz, K., Yasuda, A., & Neher, D. Improving the performance of polyfluorene-based organic light-emitting diodes via end-capping. *Adv. Mater.* **13,** 565–570 (2001).

73. Peng, K.Y., Huang, C.W., Liu, C.Y., & Chen, S.A. High brightness stable white and yellow light-emitting diodes from ambipolar polyspirofluorenes with high charge carrier mobility. *Appl. Phys. Lett.* **91,** 17–20 (2007).

74. Ye, T., Shao, S., Chen, J., Wang, L., & Ma, D. Efficient phosphorescent polymer yellow-light-emitting diodes based on solution-processed small molecular electron transporting layer. *ACS Appl. Mater. Interfaces* **3,** 410–416 (2011).

75. Fan, S., Sun, M., Wang, J., Yang, W., & Cao, Y. Efficient white-light-emitting diodes based on polyfluorene doped with fluorescent chromophores. *Appl. Phys. Lett.* **91,** 2005–2008 (2007).

76. Huang, J., Wang, X., deMello, a. J., deMello, J.C., & Bradley, D.D.C. Efficient flexible polymer light emitting diodes with conducting polymer anodes. *J. Mater. Chem.* **17,** 3551 (2007).

77. Lee, B.R., Kim, J.J.Y., Kang, D., Lee, D.W., Ko, S.-J., Lee, H.J., Lee, C.-L., Shin, H.S., & Song, M.H. Highly efficient polymer light-emitting diodes using graphene oxide as a hole transport layer. *ACS Nano* **6,** 2984–91 (2012).

78. Duan, J.P., Sun, P.P., & Cheng, C.H. New Iridium Complexes as Highly Efficient Orange–Red Emitters in Organic Light-Emitting Diodes. *Adv. Mater.* **15,** 224–228 (2003).

79. Wang, R., Liu, D., Zhang, R., Deng, L., & Li, J. Solution-processable iridium complexes for efficient orange-red and white organic light-emitting diodes. *J. Mater. Chem.* **22,** 1411 (2012).

80. Veenstra, S.C., Loos, J., & Kroon, J.M. Nanoscale structure of solar cells based on pure conjugated polymer blends. *Prog. Photovoltaics Res. Appl.* **15,** 727–740 (2007).

81. Hwang, Y.-J., Earmme, T., Subramaniyan, S., & Jenekhe, S.A. Side chain engineering of n-type conjugated polymer enhances photocurrent and efficiency of all-polymer solar cells. *Chem. Commun.* **50,** 10801–10804 (2014).

82. Kang, H., Kim, K.-H., Choi, J., Lee, C., & Kim, B.J. High-Performance All-Polymer Solar Cells Based on Face-On Stacked Polymer Blends with Low Interfacial Tension. *ACS Macro Lett.* **3,** 1009–1014 (2014).

83. Kang, H., Uddin, M.A., Lee, C., Kim, K.H., Nguyen, T.L., Lee, W., Li, Y., Wang, C., Woo, H.Y., & Kim, B.J. Determining the role of polymer molecular weight for high-performance all-polymer solar cells: Its effect on polymer aggregation and phase separation. *J. Am. Chem. Soc.* **137,** 2359–2365 (2015).

84. Park, J.K., Jo, J., Seo, J.H., Moon, J.S., Park, Y.D., Lee, K., Heeger, A.J., & Bazan, G.C. End-capping effect of a narrow bandgap conjugated polymer on bulk heterojunction solar cells. *Adv. Mater.* **23,** 2430–2435 (2011).

85. Koldemir, U., Puniredd, S.R., Wagner, M., Tongay, S., McCarley, T.D., Kamenov, G.D., Müllen, K., Pisula, W., & Reynolds, J.R. End Capping Does Matter: Enhanced Order and Charge Transport in Conjugated Donor-Acceptor Polymers. *Macromolecules* **48,** 6369–6377 (2015).

86. Kuwabara, J., Yasuda, T., Takase, N., & Kanbara, T. Effects of the Terminal Structure, Purity, and Molecular Weight of an Amorphous Conjugated Polymer on Its Photovoltaic Characteristics. *ACS Appl. Mater. Interfaces* **8,** 1752–1758 (2016).

87. Lou, S.J., Szarko, J.M., Xu, T., Yu, L., Marks, T.J., & Chen, L.X. Effects of additives on the morphology of solution phase aggregates formed by active layer components of high-efficiency organic solar cells. *J. Am. Chem. Soc.* **133,** 20661–20663 (2011).

88. Kaya, E., Balan, A., Baran, D., Cirpan, A., & Toppare, L. Electrochromic and optical studies of solution processable benzotriazole and fluorene containing copolymers. *Org. Electron. physics, Mater. Appl.* **12,** 202–209 (2011).

89. Kaya, E., Apaydn, D.H., Yldz, D.E., Toppare, L., & Cirpan, A. Solution processable benzotriazole and fluorene containing copolymers for photovoltaic applications. *Sol. Energy Mater. Sol. Cells* **99,** 321–326 (2012).

90. Zusan, A., Gieseking, B., Zerson, M., Dyakonov, V., Magerle, R., & Deibel, C. The effect of diiodooctane on the charge carrier generation in organic solar cells based on the copolymer PBDTTT-C. *Sci. Rep.* **5,** 8286 (2015).

91. Berzelius, J.J. *Jahresberichte*. **12,** (1833).

92. Carothers, W.H. An Introduction to the General Theory of Condensation Polymers. *Am. Chem. Soc.* **51,** 2548–2559 (1929).

93. Yamamoto, T., Sanechika, K., & Yamamoto, A. Preparation of Thermostable and Electric-Conducting Poly(2,5-Thienylene). *J. Polym. Sci. Polym. Lett. Ed.* **18,** 9–12 (1980).

94. Jen, K., Miller, G.G., & Elsenbaumer, R.L. Highly Conducting, Soluble, and Environmentally-stable Poly(3-alkylthiophenes). *J. Chem. Soc, Chem. Commun.* **5,** 1346–1347 (1986).

95. Mccullough, R.D., Lowe, R.D., Jayaraman, M., & Anderson, D.L. Design, Synthesis, and Control. *J. Org. Chem.* **58,** 904–912 (1993).

96. McCullough, R.D., Tristram-Nagle, S., Williams, S.P., Lowe, R.D., & Jayaraman, M. Self-orienting head-to-tail poly(3-alkylthiophenes): new insights on structure-property relationships in conducting polymers. *J. Am. Chem. Soc.* **115,** 4910–4911 (1993).

97. Chen, T.-A., Wu, X., & Rieke, R.D. Regiocontrolled Synthesis of Poly(3-alkylthiophenes) Mediated by Rieke Zinc: Their Characterization and Solid-state Properties. **117,** 233–244 (1995).

98. Sato, M., Tanaka, S., & Kaeriyama, K. Soluble Conducting Polymers By Electrochemical Polymerization of Thiophenes Having Long Alkyl Substituents. **18,** 229–232 (1987).

99. Wei, Y., Chan, C.C., Tian, J., Jang, G.W., & Hsueh, K.F. Electrochemical polymerization of thiophenes in the presence of bithiophene or terthiophene: kinetics and mechanism of the polymerization. *Chem. Mater.* **3,** 888–897 (1991).

100. Bedi, A. & Zade, S.S. Electrochemical Route to Solution-Processable Polymers of Thiophene/Selenophene Capped Didodecyloxybenzo[1,2 - b :4,3 - b ′]dithiophene and Their Optoelectronic Properties. 2–10 (2013).

101. Kötz, E.R., Neff, H., & Müller, K. A UPS, XPS and work function study of emersed silver, platinum and gold electrodes. *J. Electroanal. Chem.* **215,** 331–344 (1986).

102. Nguyen, T.-Q., Martini, I.B., Liu, J., & Schwartz, B.J. Controlling Interchain Interactions in Conjugated Polymers: The Effects of Chain Morphology on Exciton−Exciton Annihilation and Aggregation in MEH−PPV Films. *J. Phys. Chem. B* **104,** 237–255 (2000).

103. Klimovich, I. V., Susarova, D.K., Inasaridze, L.N., Akkuratov, A. V., Chernyak, A. V., & Troshin, P.A. Effect of Alkyl Side Chains on the Photovoltaic Performance of 2,1,3-Benzoxadiazole-Based (-X-DADAD-) $_n$ -Type Copolymers. *Macromol. Chem. Phys.* **201700055,** 1700055 (2017).

104. Brabec, C.J., Shaheen, S.E., Winder, C., Sariciftci, N.S., & Denk, P. Effect of LiF/metal electrodes on the performance of plastic solar cells. *Appl. Phys. Lett.* **80,** 1288–1290 (2002).

105. Zou, Y. & Holmes, R.J. Correlation between the Open-Circuit Voltage and Charge Transfer State Energy in Organic Photovoltaic Cells. *ACS Appl. Mater. Interfaces* **7,** 18306–18311 (2015).

106. Scharber, M.C., Mühlbacher, D., Koppe, M., Denk, P., Waldauf, C., Heeger, A.J., & Brabec, C.J. Design rules for donors in bulk-heterojunction solar cells - Towards 10 % energy-conversion efficiency. *Adv. Mater.* **18,** 789–794 (2006).

107. Yamamoto, T. π-conjugated polymers with electronic and optical functionalities: Preparation by organometallic polycondensation, properties, and applications. *Macromol. Rapid Commun.* **23,** 583–606 (2002).

108. Kim, Y., Cook, S., Tuladhar, S.M., Choulis, S.A., Nelson, J., Durrant, J.R., Bradley, D.D.C., Giles, M., McCulloch, I., Ha, C.-S., & Ree, M. A strong regioregularity effect in self-organizing conjugated polymer films and high-efficiency polythiophene:fullerene solar cells. *Nat. Mater.* **5,** 197–203 (2006).

109. Yang, L., Yan, L., & You, W. Organic solar cells beyond one pair of donor-acceptor: Ternary blends and more. *J. Phys. Chem. Lett.* **4,** 1802–1810 (2013).

110. Chang, D.S. & Lai, S. Te. Implementation of cross-generation automation transportation system in the TFT-LCD industry. *Int. J. Adv. Manuf. Technol.* **78,** 753–763 (2015).

111. Du, J., Pei, S., Ma, L., & Cheng, H.M. 25th anniversary article: Carbon nanotube- and graphene-based transparent conductive films for optoelectronic devices. *Adv. Mater.* **26,** 1958–1991 (2014).

112. Tahar, R.B.H., Ban, T., Ohya, Y., & Takahashi, Y. Tin doped indium oxide thin films: Electrical properties. *J. Appl. Phys.* **83,** 2631–2645 (1998).

113. Chandra, B., Afzali, A., Khare, N., El-Ashry, M.M., & Tulevski, G.S. Stable charge-transfer doping of transparent single-walled carbon nanotube films. *Chem. Mater.* **22,** 5179–5183 (2010).

114. Becerril, H.A. Evaluation of Solution-Processed Reduced Graphene Oxide Films as Transparent Conductors. *ACS Nano* **2,** 463–470 (2008).

115. Alemu, D., Wei, H.-Y., Ho, K.-C., & Chu, C.-W. Highly conductive PEDOT:PSS electrode by simple film treatment with methanol for ITO-free polymer solar cells. *Energy Environ. Sci.* **5,** 9662 (2012).

116. Zhang, D., Wang, R., Wen, M., Weng, D., Cui, X., Sun, J., Li, H., & Lu, Y. Synthesis of ultralong copper nanowires for high-performance transparent electrodes. *J. Am. Chem. Soc.* **134,** 14283–14286 (2012).

117. Hu, L., Kim, H.S., Lee, J., Peumans, P., & Cui, Y. Scalable Coating and Properties of transparent Ag nanowire. *ACS Nano* **4,** 2955–2963 (2010).

118. Yim, J.H., Joe, S.Y., Pang, C., Lee, K.M., Jeong, H., Park, J.Y., Ahn, Y.H.,

De Mello, J.C., & Lee, S. Fully solution-processed semitransparent organic solar cells with a silver nanowire cathode and a conducting polymer anode. *ACS Nano* **8,** 2857–2863 (2014).

119. Coskun, S., Selen Ates, E., & Unalan, H.E. Optimization of silver nanowire networks for polymer light emitting diode electrodes. *Nanotechnology* **24,** 125202 (2013).

120. Guo, F., Zhu, X., Forberich, K., Krantz, J., Stubhan, T., Salinas, M., Halik, M., Spallek, S., Butz, B., Spiecker, E., Ameri, T., Li, N., Kubis, P., Guldi, D.M., Matt, G.J., & Brabec, C.J. ITO-free and fully solution-processed semitransparent organic solar cells with high fill factors. *Adv. Energy Mater.* **3,** 1062–1067 (2013).

121. Coskun, S., Aksoy, B., & Unalan, H.E. Polyol synthesis of silver nanowires: An extensive parametric study. *Cryst. Growth Des.* **11,** 4963–4969 (2011).

122. Barik, U.K., Srinivasan, S., Nagendra, C.L., & Subrahmanyam, A. Electrical and optical properties of reactive DC magnetron sputtered silver oxide thin films: Role of oxygen. *Thin Solid Films* **429,** 129–134 (2003).

APPENDIX A : THERMAL ANALYSES

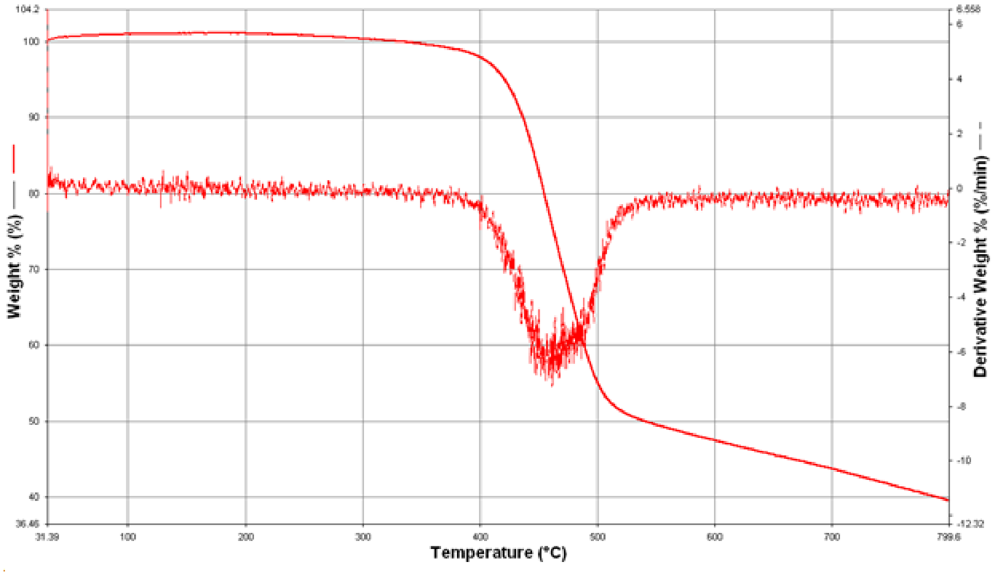

Figure 82 TGA analysis of P1

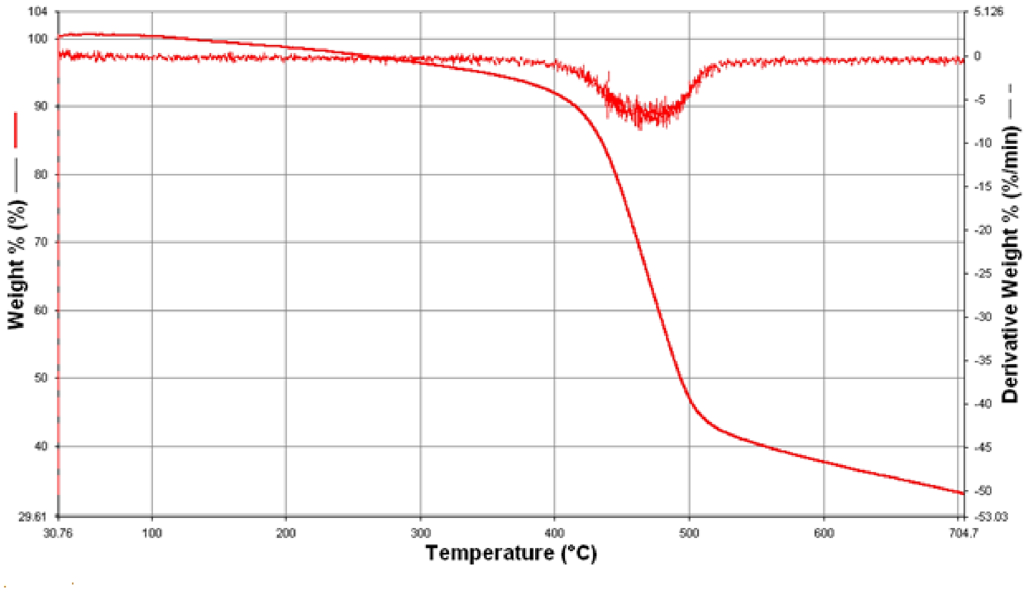

Figure 83 TGA analysis of P2

APPENDIX B: SPECTROELECTROCHEMISTRY

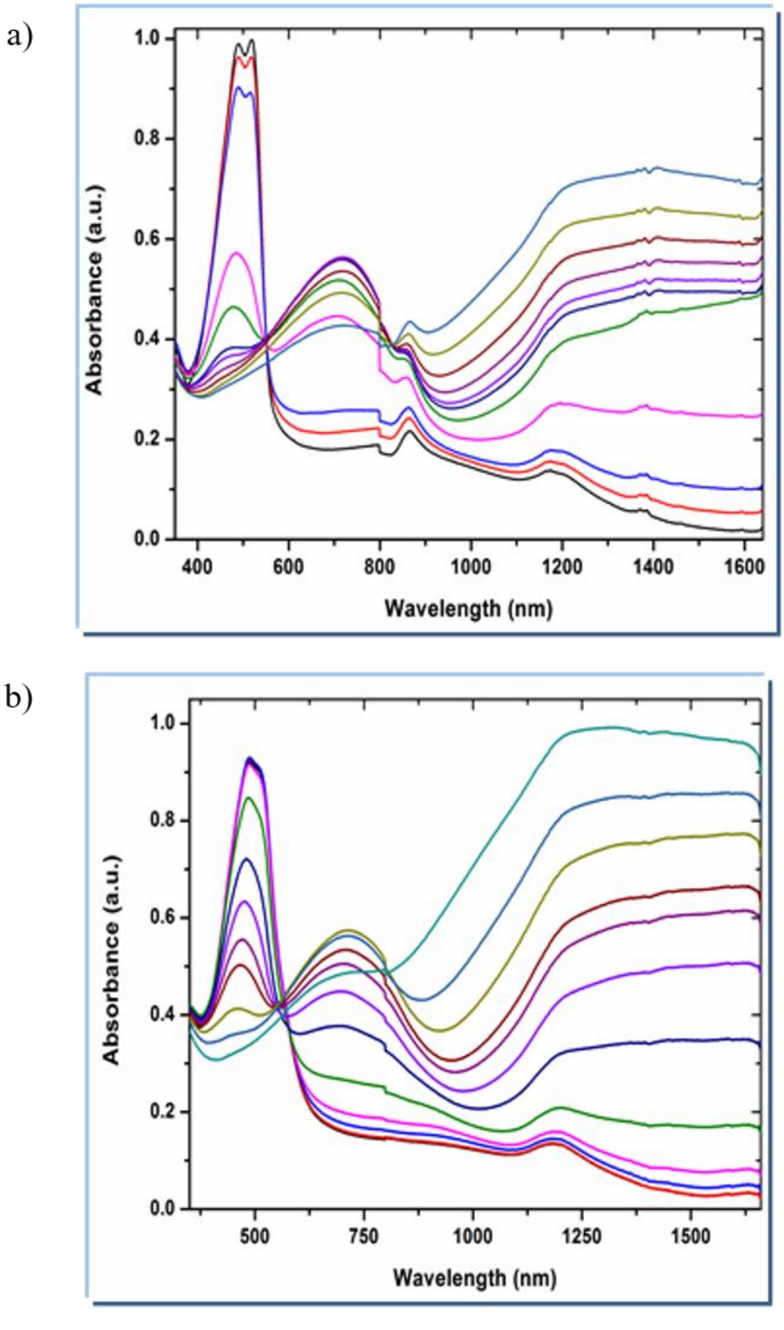

Figure 84 Spectroelectrochemistry of P1 and P2

APPENDIX C: PLED CHARACTERIZATION

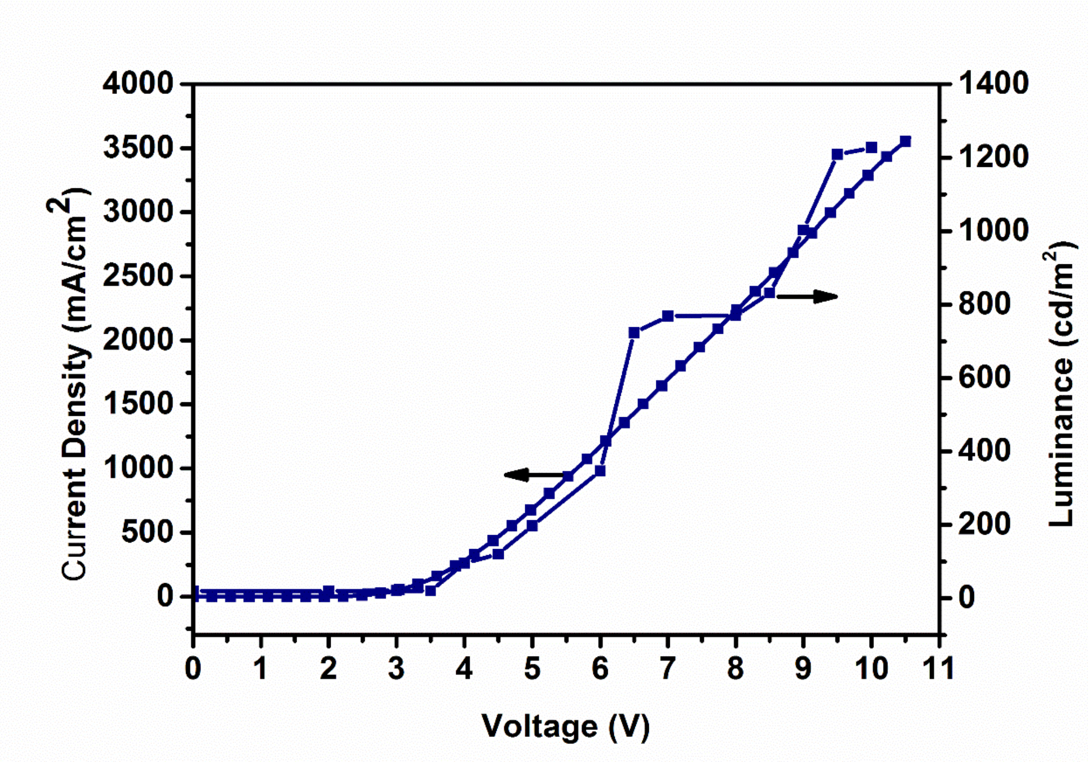

Figure 85 Current density vs voltage and luminance vs voltage characteristics of P3 based PLED

CURRICULUM VITAE

Gönül Hızalan Özsoy
03.07.1986
hizalangonul@gmail.com
Ankara/Turkey

EDUCATION

2011- 2017	PhD: Middle East Technical University /Ankara Chemistry 3.64/4.00
2010 Summer	Summer School: Utrecht University/Utrecht-HOLLAND Nanomaterials: Science and Applications
2010 - 2011	MSc: Middle East Technical University /Ankara – Chemistry GPA:3.64/4.00
2008 - 2010	Bs-Minor: Middle East Technical University /Ankara – Food Engineering GPA:3.02/4.00 Graduated as honor student
2004 – 2010	Bs-Major: Middle East Technical University /Ankara – Chemistry Education GPA: 3.39 / 4.00
1997 - 2004	High School Mehmet Akif Ersoy Anadolu Lisesi / Çorlu GPA:5.00/5.00

PROFESSIONAL EXPERIENCE

2014- 2016	ECOPIX European Union Project FPE-7-SME-2013 Eco-friendly digital advertising display based on novel printable electrochromic polymers
2012 - 2015	SSM (Savunma Sanayii Müsteşarlığı) Project Elmas Project- ODTÜ- ASELSAN
2012 - 2015	Santez Project- ODTÜ- ASELSAN 01294.STZ.2012-1 Development of flexible displays with conjugated polymers
2010 – 2017	Research and Teaching Assistant Department of Chemistry/METU General Chemistry Laboratory, Physical Chemistry Laboratory I, Physical ChemistryLaboratory II
2011 Summer	Visiting Researcher in Delft University of Technology, HOLLAND under the supervision of Assoc. Prof. Dr. Ferdinand Grozema

PUBLICATIONS

1. Gonul Hizalan, Abidin Balan, Derya Baran, Levent Toppare, Spray Processable Ambipolar Benzotriazole Bearing Electrochromic Polymers with Multi-Colored and Transmissive States, Journal of Materials Chemistry, 2010, 21, 1804.

2. Melis Kesik, Fulya Ekiz Kanik, Gonul Hizalan, Duygu Kozanoglu, Emren Nalbant Esenturk, Suna Timur, Levent Toppare, A Functional İmmobilization Matrix Based on A Conducting Polymer and Functionalized Gold Nanoparticles: Synthesis and Its Application as an Amperometric Glucose Biosensor, Polymer, 2013, 54, 4463.

3. Seza Goker, Gonul Hizalan, Yasemin Arslan Udum, Levent Toppare, Electrochemical and Optical Properties of 5,6-Bis(Octyloxy)-2,1,3 Benzooxadiazole Containing Low Band Gap Polymers, Synthetic Metals, 2014, 191, 19.

4. Fulya Ekiz Kanik, Didem Ag, Muharrem Seleci, Firat Baris Barlas, Melis Kesik, Gonul Hizalan, Hava Akpinar, Suna Timur, Levent Toppare, A Novel DAD Type and Folic Acid Conjugated Fluorescent Monomer as a Targeting Probe for Imaging of Folate Receptor Overexpressed Cells, Biotechnology Progress, 2014, 30, 952.

5. Melis Kesik, Huseyin Akbulut, Saniye Soylemez, Sevki Can Cevher, Gonul Hizalan, Yasemin Arslan Udum, Takeshi Endo, Shuhei Yamada, Ali Cirpan, Yusuf Yagci, Levent Toppare, Synthesis and Characterization of Conducting Polymers Containing Polypeptide and Ferrocene Side Chains as Ethanol Biosensors, Polymer Chemistry, 2014, **5**, 6295.

6. Hande Unay, Naime A. Unlu, Gonul Hizalan, Serife O. Hacioglu, Dilber Esra Yildiz, Levent Toppare, Ali Cirpan, Benzotriazole and Benzodithiophene Containing Medium Band-Gap Polymer for Bulk Heterojunction Polymer Solar Cells Applications, Journal Polymer Science Part:A Polymer Chemistry, 2015, 53, 528.

7. Seza Göker, Gonul Hizalan, Merve Ileri, Serife O. Hacioglu, Levent Toppare, The Effect Of The Different Donor Units on Fluorescent Conjugated Polymers Containing 2,1,3-Benzooxadiazole as the Acceptor Unit, Journal of Electroanalytical Chemistry, 2015, 751, 80.

8. Hande Unay, Naime A. Unlu, Gonul Hizalan, Serife O. Hacioglu, Levent Toppare, Ali Cirpan, Selenophene as π-Bridge in Molecular Architecture of Benzotriazole Containing Conjugated Polymers to Gain Insight its Effect on

Optical and Electrochemical Properties of Polymers Phosphorus, Sulfur and Silicon and the Related Elements, 2015, 190, 1294.

9. Ozan Erlik, Naime A. Unlu, Gonul Hizalan, Serife O. Hacioglu, Seda Comez, Esra D. Yildiz, Levent Toppare, Ali Cirpan, Silafluorene based Polymers for Electrochromic and Polymer Solar Cell Applications, Journal of Polymer Science Part:A Polymer Chemistry, 2015, 53, 1541.

10. Cagla Istanbulluoglu, Seza Göker, Gonul Hizalan, Serife O. Hacioglu, Yasemin Arslan Udum, Esra D. Yildiz, Ali Cirpan, Levent Toppare, Synthesis of a Benzotriazole Bearing Alternating Copolymer For an Organic Photovoltaic Application, New Journal of Chemistry, 2015, 39, 6623.

11. Seza Goker, Gonul Hizalan, Seda Kutkan, Yasemin Udum, Ali Cirpan, L. Toppare, Incorporation of Different Conjugated Linkers into Low Band Gap Polymers based on 5,6-bis(octyloxy)-2,1,3 benzooxadiazole for Tuning Optoelectronic Properties Journal of Polymer Science, Part A: Polymer Chemistry, 2016, 54, 2459.

12. Sevki Can Cevher, Gonul Hizalan, Cansel Temiz, Yasemin Udum, Levent Toppare, Ali Cirpan Effect of Substituent Groups on Quinoxaline-Based Random Copolymers on The Optoelectronic and Photovoltaic Properties, Polymer, 2016, 101, 208.

13. Seza Goker, Gonul Hizalan, Ece Aktas, Seda Kutkan, Ali Cirpan, Levent Toppare "2,1,3-Benzooxadiazole, Thiophene and Benzodithiophene Based Random Copolymers for Organic Photovoltaics: Thiophene versus Thieno[3,2-B]Thiophene as π-Conjugated Linkers, New Journal of Chemistry, 2016, 40, 10455.

14. Ebru Isık, Seza Goker, Gonul Hizalan, Serife Hacioglu, Levent Toppare, Random Copolymers of 1,2,3-Benzotriazole and Alkoxy-Modified Naptho[2,3-

B:3,4-B′]Dithiophene: Syntheses, Characterization and Optoelectronic Properties, Journal of Electroanalytical Chemistry, 2017, 786, 50.

15. Seza Goker, Serife Hacioglu, Gonul Hizalan, Ece Aktas, Ali Cirpan, Levent Toppare, Triphenylamine Based Random Copolymers: The Effect of Molecular Weight on Performance of Solar Cell and Optoelectronic Properties, Macromolecular Chemistry and Physics, 2017, *1600544.*

16. Ipek Onk, Gonul Hizalan, Sevki Can Cevher, Serife O. Hacioglu, Levent Toppare, Ali Cirpan, Multipurpose Selenophene Containing Conjugated Polymers for Optoelectronic Applications, Journal of Macromolecular Science, Part A, 2017, 54, 133.

17. Serife Hacioglu, Naime A. Unlu, Ece Aktas, Gonul Hizalan, D. Esra Yildiz, Ali Cirpan, Levent Toppare, A triazoloquinoxaline and benzodithiophene bearing low band gap copolymer for electrochromic and organic photovoltaic applications, Synthetic Metals, 2017, 228, 111.

18. Naime A. Unlu, Serife Hacioglu, Gonul Hizalan, D. Esra Yildiz, Ali Cirpan, Levent Toppare, Benzodithiophene and Benzotriazole Bearing Conjugated Polymers for Electrochromic and Organic Solar Cell Applications, Journal of the Electrochemical Society, 2017, 164, G71.

SELECTED WORKSHOPS – CONFERENCES

1. World Polymer Congress, MACRO 2016

17-21 July 2016, İstanbul /Turkey

Oral presentation, Solution Processed Orange Light Emitting Diodes Using Polyfluorene Derivative

2. International Workshop on Advanced Materials and Processes for Energy Applications

20-24 April 2016, İstanbul /Turkey

Oral presentation

3. LED Conference

1-4 October 2015, İstanbul /Turkey

Oral presentation, Conjugated Polymer Based Light Emitting Diodes

4. 1st International Conference on Perovskite Solar Cells and Optoelectronics,

27-29 September 2015, Lausanne, Switzerland

Poster presentation, Preparation and Characterization of Perovskite Layers

5. Faraday Discussion, Organics, Photonics and Electronics

8-10 September 2014, Glasgow, Scotland

Poster Presentation, Photovoltaic Properties of Silafluorene Bearing Polymer: Effect of Processing Conditions on Morphology

6. 5th EuChemMS

31 August- 4 September 2014, İstanbul, Turkey

Oral Presentation, Conducting Polymers and Their Applications

7. Solar Energy for World Peace

17-19 August 2013, İstanbul, Turkey

Poster Presentation, Effect of Active Layer Thickness on Solar Cell Parameters and Mobility

8. Fraunhofer Institute OLED, Advanced Course-Workshop

6-7 March 2013, Dresden, Germany

INSTRUMENTAL & EXPERIMENTAL SKILLS

1. Fabrication and characterization of organic photovoltaic devices and OLEDs (equipments used and tests performed)

Substrate preparation in clean room, using spin coater, spray coater, doctor blade, thermal evaporator. I-V measurement using LabTracer and Keithley sourcemeter, OLED testing using Spectrasuit and integrating sphere and IPCE measurement.

2. Other instruments

Cyclic voltammetry, Uv-Vis, AFM, IR, Fluorescence spectroscopy

SCHOLARSHIPS & HONORS

1. TUBİTAK (Turkish Scientific and Technical Research Council) National Scholarship Program for PhD Students
2. TUBİTAK (Turkish Scientific and Technical Research Council) National Scholarship Program for MSc Students
3. Graduated as the 1st ranking student from the department of Chemistry Education
4. Dean's High Honor List
   2008 -2009 (fall), 2008 -2009 (spring), 2009 -2010 (fall)
5. Dean's Honor List
   2006 -2007 (fall), 2006- 2007 (spring), 2007 -2008 (spring)
6. Run first place in the exam which was organized by Tekirdağ National Education Headship in 2003

LANGUAGES & SKILLS

Turkish (Native)
English (Advanced)
German (Elementary)

INTERESTS

Pilates, skiing

REFERENCES

Prof. Dr. Levent Toppare
Prof. Dr. Ali Çırpan